Università degli Studi di Cagliari

DOTTORATO DI RICERCA

Scienze e Tecnologie Chimiche

Ciclo XXVIII

TITOLO TESI

SOLID ACID CATALYSTS FOR BIOREFINERY PROCESSES

Settore/i scientifico disciplinari di afferenza

CHIM/04

Presentata da: Danio Perra

Coordinatore Dottorato: Prof. Mariano Casu

Tutor: Dott.ssa M. Giorgia Cutrufello

Esame finale anno accademico 2014 – 2015

University of Cagliari

PhD Thesis

Cycle XXVIII

Title of the Thesis

SOLID ACID CATALYSTS FOR BIOREFINERY PROCESSES

Scientific area

CHIM/04

Presented by: Danio Perra

PhD Coordinator: Prof. Mariano Casu

Supervisor: Dr. M. Giorgia Cutrufello

Final exam academic year 2014 – 2015

Acknowledgments

The development of this work has been possible thanks to the contribution of various people.
Firstly, I have to thank Dr. M. Giorgia Cutrufello for having supervised my research work in these three years.
A very special thanks goes to Dr. Daniela Meloni for helpful advices and for conveying to me passion and enthusiasm.
I would like to thank Prof. Italo Ferino for fruitful and enlightening discussions.
An important thanks goes to the whole group of Industrial Chemistry for the precious advices and the pleasant company.
I would like to express my gratitude to Prof. Konstantin Hadjiivanov for his patience, kindness and the precious teachings.
Another special thank goes to Prof. Kristina Chakarova and the whole group of Inorganic Chemistry at the Bulgarian Academy of Sciences.
For the financial support I gratefully acknowledge Sardinia Regional Government, for the PhD scholarship (P.O.R. Sardegna F.S.E. Operational Programme of the Autonomous Region of Sardinia, European Social Fund 2007-2013 - Axis IV Human Resources, Objective l.3, Line of Activity l.3.1.), MIUR (Ministero dell'Istruzione dell'Università e della Ricerca).
Finally, I want to thank my family and my wife for supporting and encouraging me in everything that I did.

Foreword

The present work regards the study of alternative synthetic routes for biofuels and biochemicals. Biofuels and biochemicals constitute the two main classes of biorefinery products. Biofuels are obtained from biomass and have many environmental advantages over the traditional fuels. In this work particular attention has been given to biodiesel, one of the most widely used biofuels. Biodiesel is a safe, non-toxic, and biodegradable alternative diesel fuel. The development of active acid catalysts for biodiesel synthesis could reduce the production costs, in particular because the acid catalysts permit the use of low value feedstocks such as waste and non-edible oils. Biodiesel production occurs with co-production of glycerol, which is co-product also in other industrial productions such as the production of fatty acids and soaps. Because of its large production the market demand is largely less than the supply. For this reason glycerol is considered a problematic product. Possible solution to its disposal is the use as platform chemical in the production of high value bioproducts. Among them are particularly interesting the trioses dihydroxyacetone and glyceraldehyde. They could be feedstocks for an alternative synthetic way for lactic acid and its esters. Lactic acid and lactates are, nowadays, considerably important because they are used as building blocks in the production of biodegradable polymers (the polylactic acids), which are potential substitute for petroleum derived polymers. Lactic acid is also one of the most promising bio-based platform molecules. The high costs of the conventional production process hinder the use of lactic acid and lactates in many applications. So it is essential to develop cheaper and greener synthetic routes.

In this work catalysts synthesis, characterization of the materials, and catalytic testing have been carried out mainly at the Laboratory of Industrial Chemistry in the Department of Chemical and Geological Sciences of the University of Cagliari.

The study involved the use of several techniques for the characterization of the materials. All the catalytic results have been related to the acid properties of the tested materials. For this reason the measurements of adsorption microcalorimetry and adsorption FTIR using basic probe molecules have been the most important used techniques in this work. The measurements of adsorption microcalorimetry were carried out at the Laboratory of Industrial Chemistry in Cagliari while the measurements of adsorption FTIR were carried out under the supervision of Prof. Konstantin Hadjiivanov at the Institute of General and Inorganic Chemistry of the Bulgarian Academy of Sciences.

This work is divided in five chapters. The first chapter is an introduction of the fundamentals of sustainable chemistry, biorefinery and acid-base heterogeneous catalysis. The

second chapter is a description of the most important techniques for the characterization of acid-base properties of solid materials. In the third chapter are listed the used materials, the experimental procedures and apparatus. The chapter four is the study of the acid catalyzed transesterification of tryglicerides for the production of biodiesel and glycerol. In chapter five is described the work on the conversion of dihydroxyacetone to methyl lactate.

SUMMARY

Chapter I

Introduction

1.1. An overview

The vast majority of raw materials used in the manufacture production prior to the nineteenth century were bio-based products and inorganic materials (stones, metals, etc.). From the first industrial revolution in the 18th century and with the massive use of coal since the beginning of nineteenth century, the society became dependent on fossil fuels. Following the diffusion of the combustion engine and the outbreak of the First World War the need for fossil fuels, mainly in the form of petroleum oil, has grown more and more until becoming a strong dependence. Today fossil resources are widely used to produce electricity, heat, and transportation fuels, as well as the vast majority of the many chemicals that are required by contemporary society. The scientific and technological development related to the exploitation of fossil resources has made available a vast array of materials, medicines, fertilizers, and fuels. The resulting benefits have been the improvement of the quality of life, that has permitted the considerable global population growth during the twentieth century.

On the other side, the unsustainable and uncontrolled industrial development, which began after the Second World War, caused an enormous environmental pollution (air pollution, acid precipitations, ozone depletion, forests destructions, and emission of radioactive substances), by stimulating global climate change and potentially disastrous global warming. Simultaneously to the environmental impact, the fossil resources depletion has begun to warn the global scientific community about the need of returning to the exploitation of renewable resources, albeit following a more rational and thorough strategy. In this contest, governments, industry, and the public have developed the need of a sustainable development for achieving societal, economical, and environmental objectives [1].

1.2. The sustainable development

The most widely accepted definition of “sustainable development” was coined by the World Commission on Environment and Development (also known as Brundtland commission) in 1987 as “development that meets the needs of the present without compromising the ability of future generations to meet their own needs” [2]. The only way to have a better quality of life for everyone and for the generations to come is to live in harmony with the planet. The sustainable development needs immediate and long term objectives and

regards social, economic, and environmental issues as inseparable and interdependent components of progress. The environment is the most important issue because the society and the economy are dependent from the environmental health as it is shown in Fig. 1.1. For this reason it is crucial to focus all the attention on the environmental concerns.

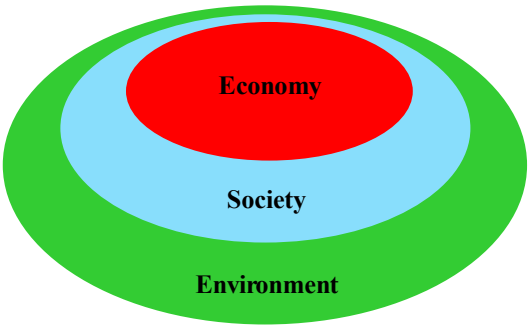

Figure 1.1. The three main elements of the sustainable development.

Up to now chemistry has played a central role in the industrial development. Today this role is different and much more difficult because chemistry is central to many of the environmental and resources use issues at the heart of the sustainable development. For example, finding alternatives to non-renewable resources such as oil, gas, and coal, contributing to waste minimisation and improved waste treatment and disposal, understanding the effects of toxic materials on both humans and the environment.

1.2.1. Green Chemistry

The concept of "Green Chemistry" was born in order to integrate the sustainable development model into chemistry. It was defined for the first time in 1991 by Anastas as "the invention, design and application of chemical products and processes to reduce or eliminate the use and generation of hazardous substances" [3]. The design of environmentally benign products and processes may be guided by the 12 Principles of Green Chemistry (generated by Anastas and Warner in 1998) [3]:

I. It is better to prevent waste than to treat or clean up waste after it is formed.

II. Synthetic methods should be designed to maximize the incorporation of all materials used in the process into the final product.

III. Wherever practicable, synthetic methodologies should be designed to use and generate substances that possess little or no toxicity to human health and the environment.

IV. Chemical products should be designed to preserve efficacy of function while reducing toxicity.

V. The use of auxiliary substances (e.g. solvents, separation agents, etc.) should be made unnecessary wherever possible and innocuous when used.

VI. Energy requirements should be recognized for their environmental and economic impacts and should be minimized. Synthetic methods should be conducted at ambient temperature and pressure.

VII. A raw material or feedstock should be renewable rather than depleting whenever technically and economically practicable.

VIII. Unnecessary derivatization (blocking group, protection/deprotection, temporary modification of physical/chemical processes) should be avoided whenever possible.

IX. Catalytic reagents (as selective as possible) are superior to stoichiometric reagents.

X. Chemical products should be designed so that at the end of their function they do not persist in the environment and break down into innocuous degradation products.

XI. Analytical methodologies need to be further developed to allow for real-time, in-process monitoring and control prior to the formation of hazardous substances.

XII. Substances and the form of a substance used in a chemical process should be chosen so as to minimize the potential for chemical accidents, including releases, explosions, and fires.

1.3. The role of catalysis

The application of catalysis is ubiquitous in the chemical industry, in areas ranging from pharmaceuticals to polymers to petroleum processing. More than 90 % of all industrial chemical processes are based on catalysis. Catalysis has a direct impact on the global economy, representing one of the key elements of our industrialized society. Catalysis is one the most important instrument for the actuation of a sustainable production. The IX principle of Green Chemistry is dedicated to the catalysis but catalysis is correlated with all the other principles [4,5]. The use of catalysts permits an energy requirement reduction (principle VI),

an increase in selectivity (principle II), a decrease in the use of processing and separation agents (principle V), and allows the use of less toxic materials (principle III). Heterogeneous catalysis is usually preferred to homogeneous mainly for the ease of catalyst separation after the reaction. Separation processes represent more than half of the total investment in equipment for the chemical and fuel industries [6]. It is a crucial advantage for the heterogeneous catalysis, however it is important that the solid catalysts are highly selective to guarantee the cost effectiveness of the process.

1.3.1. Acid-base solid catalysts

The heterogeneous catalysis is based mainly on porous solid materials. Their main advantage is the ability to interact with atoms, ions, and molecules not only at their external surface, but mainly at the internal surface which constitutes the most part of the solid surface [7]. The internal surface area is defined as the area of micropore (pore of internal width less than 2 nm) and mesopore (pore of internal width between 2 and 50 nm) walls while the external surface area is the area of a rough or macroporous surface [8]. In this contest zeolites are without any doubt the best known and most applied microporous materials. Zeolites consist of a crystalline framework of TO_4 tetrahedra (T is a tetrahedral atom such as Si or Al) which forms an ordered network of micropores ranging from 0.3 to over 1 nm [9]. The great advantages of zeolites are their uniform pore sizes with molecular dimensions, good stability, high selectivity, and high activity, the possibility to incorporate heteroelements in the structure, and their ion exchange capacities. Up to now more than 150 different zeolite structures are known [10]. Some of them are natural minerals originated in a hydrothermal environment from late-stage magmatic solutions [8]. The most of the known framework types have never been found in nature. They are prepared synthetically by the so-called “hydrothermal synthesis”, in which amorphous reactants containing silicon and aluminium are mixed with a cation source, usually at high pH, and heated at above 100 °C in a sealed autoclave [11]. Among the most important zeolites, in terms of commercial development, there are the X and Y zeolites, which are used in a large number of catalytic cracking applications [12]. These zeolites have the structure of the natural zeolite faujasite with the largest cavities and cavity entrance of any other known zeolite [13]. The biggest cavities (called supercages) with a diameter of 1.2 nm, are accessible through rings of 12 silicon and

aluminium atoms (each silicon or aluminium atom is called also “member ring”, MR) with a diameter of 0.9 nm. There are also other smaller cavities, the sodalite cages, with a free diameter of 0.7 nm, which are connected to the biggest cages by rings having a free diameter of 0.25 nm [14]. Many other zeolites were subsequently discovered introducing quaternary ammonium cations into zeolite synthesis. During their hydrothermal synthesis, the beginning of the crystallization occurs with the oligomerization of aluminosilicate species around organic compound, that play a role of structure-directing agent. They are successively removed by calcination and the space so released correspond to the uniform micropores of zeolites. In fact these organic compounds are also called “templates” [11]. Among the zeolites synthesized by using organic templates there is the Beta zeolite. The architecture of the micropores is tridimensional, being characterized by three mutually intersecting 12-member ring channel systems. Two topological identical linear channel systems, with pore openings of 0.64 nm × 0.76 nm, are mutually orthogonal and perpendicular to the (001) plane; the third 12-member ring channel system (openings 0.55 nm × 0.55 nm) is nonlinear and parallel to *c*-axis. At variance with the X and Y zeolites, no cages are present in the microporous channel system of Beta zeolite [15]. Another example of zeolite obtained through organic template is the MCM-22 zeolite. It has a particular structure constituted by layers linked together along the *c*-axis by oxygen bridge and contains two independent pore systems. Inside each layer there is a bidimensional sinusoidal 10 MR channel system (0.41 nm × 0.51 nm) and between the layers there are large cylindrical supercages (0.71 nm × 0.71 nm × 1.84 nm) interconnected to each other by 10 MR apertures (0.40 nm × 0.55 nm) [16].

In the structure of zeolites, with respect to pure silica, a silicon atom is replaced by a tetrahedral aluminium atom, leading to an electrostatic charge imbalance with a negative charge for each aluminium atom. So the electrical neutrality needs the addition of a cation such as a proton, that is bonded to the oxygen atom connected to neighbour silicon and aluminium atoms, resulting in the so-called bridged hydroxyl group, represented in Fig. 1.2, which is a Brønsted acid site. The guest cation can also be different from the proton, e.g. an alkaline cation or ammonium ion, giving different acid or basic properties [12]. The lattice has also structural defects that are in the form of silanols characterized by a weak Brønsted acidity (some example are reported in Fig. 1.2). Other sites are in the form of extraframework aluminium species that usually can be associated with weak Brønsted acid sites or Lewis acid

sites when they are coordinatively unsatured cations. The zeolite acidity is influenced by the zeolite geometry because of the long-range effects as well as the local structure of the acid sites [17].

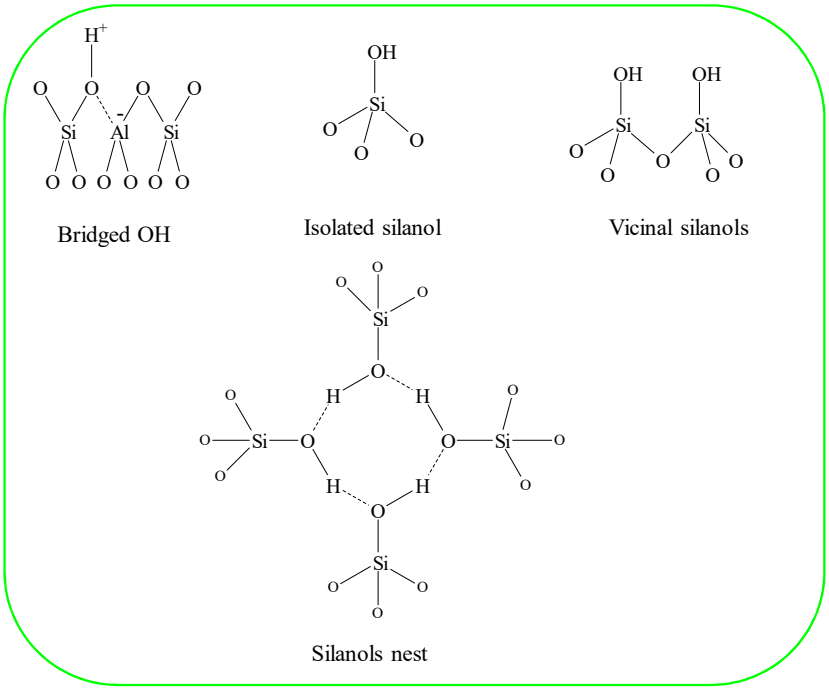

Figure 1.2. Some Brønsted acid species in zeolites.

Although zeolites are usually considered as acidic materials, actually they are Lewis acid-base pairs (Fig. 1.3) [18]. The exchangeable cations are the acid sites while the oxygens of the lattice, where the negative charge is delocalized, are the basic sites (Fig. 1.3). In the acidic form of zeolites, the protons are covalently bound to the oxygen atoms of the framework. When instead of the protons there are exchangeable metal cations, such as alkaline and alkaline earth atoms, the metal-oxygen bonds become more ionic with the increasing in the electropositivity of the cations. The negative charge, originally largely delocalized in the cluster, gets more localized on the oxygen of the Si–O–Al group next to the cation M^{n+}. So the anionic framework has to be considered as a weak base. This effect is particularly accentuated when the exchangeable cations are alkaline, which are the most electropositive elements in the periodic table. The negative charge and consequently the basic strength vary in the opposite way with respect to the electronegativity, i.e. they increase with

the increase in the cation size along the alkaline metal group [19]. The concentration of base sites increases with the aluminium content making the cationic faujasite X and Y with the highest aluminium content the most basic zeolites [20].

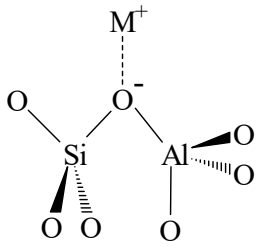

Figure 1.3. The acid-base pairs of the metal exchanged zeolites.

The microporous nature of zeolites limits their use in some applications where large bulky molecules are involved, which exceed the size of the pores and cages of the zeolites. Moreover, often liquid-phase systems are applied in these processes, which cause serious mass-transfer limitations for microporous materials. Diffusion limitations not only lead to a negative influence on catalytic activity but can also cause a loss in selectivity and a reduction in the lifetime of the catalyst. Due to this drawbacks, during the last decades a lot of research has come into effect on the synthesis of materials with larger porosity [21,22].

The introduction of structure-directing agents allows the synthesis of siliceous mesoporous materials designated as M41S with pore sizes in the range from 2 to 10 nm. These materials are amorphous and are characterized by ordered arrangements of mesopores with a narrow pore distribution. The most prominent component of this class is the MCM-41 which has a uniform hexagonal porous system. These materials may incorporate alluminium and are prepared similarly zeolites by hydrothermal treatment of a gel, for these reasons they are often referred to as “mesoporous zeolites”. However, at variance with zeolites, pore walls are amorphous [23,24]. These materials constitute an alternative to zeolites in reaction where large molecules are involved but, unfortunately, their industrial applications are limited mainly because of the low hydrothermal stability when compared to zeolites [25].

Another class of mesoporous materials with a mesopore organization similar to that of MCM-41 is called SBA-15. They have uniform and adjustable mesopores, high surface area, large pore volume, and versatile mesoporous walls [26]. SBA-15 shows large pore diameter

and wall thickness and the mesopores are connected by micropores. The thickness of the framework walls provides a higher hydrothermal and mechanical stability than the MCM-41 [25]. The material is synthesized by a cooperative self-assembly process in an acidic medium using the biodegradable and non-toxic triblock copolymer Pluronic 123 as structure directing agent [27]. The introduction of aluminium in the framework provides an acid concentration similar to that of zeolites, but because of the amorphous nature of their pore walls, these materials have lower acid strength than zeolites [24,28-31].

Besides aluminium, other heteroatoms may be incorporated into the framework of zeolites and mesostructured materials, partially substituting the lattice Si atoms, in order to provide different acidity. Metals such as Ti, Zr, Sn, Ta, Nb, Ga, etc. have been successfully incorporated [32]. Atoms such as Ti, Zr, Ta, Nb, and Sn introduce well defined Lewis acid sites inside the pores of these materials. They are tetrahedrally coordinated and thus do not create any Brønsted acid sites because they do not introduce a charge imbalance. Their Lewis acidity is related to the lowest unoccupied molecular orbital (LUMO) energy and to their ability to form an adduct with a Lewis base. The more stable the LUMO, the easier the overlapping among the orbitals involved, and consequently, the higher the acid strength of the site [33]. These active tetravalent metals are capable of enlarging their coordination sphere by moving from the original framework position to another more accessible position without becoming separated from the zeolite framework. At variance with Si^{4+} atoms in the centre of [SiO_4] tetrahedrons, ions such as Ti^{4+}, Zr^{4+}, and Sn^{4+} have larger radii and exhibited higher flexibility in their coordination geometry [34]. For these reasons they introduce Lewis acidity. Sn-, Zr-, Ta-, and Nb-Beta zeolites are active in MPV (Meerwein-Ponndorf-Verley) reduction of aldehydes to ketones and in the etherification of alcohols, that are typical reactions catalysed by Lewis acids [35-37].

Novel routes have been developed for the formation of a new generation of materials with at least two levels of pore size, the so-called hierarchical materials. Among them are particularly interesting the hierarchical zeolites. They have, in addition to the uniform zeolitic micropores, a secondary porosity. This secondary porosity consists of pores usually within the size range of mesopores, but they can also be within a wider range, from micropores to macropores [38]. The secondary porosity opens for zeolites the possibility of extending the use to reactions involving bulky molecules. A wide variety of synthetic strategies have been

developed for generating the secondary porosity in zeolites (the removal of framework atoms, surfactant-assisted procedures, hard-templating, and so on). Among them the dual templating strategy is one of the most developed. It is based on the combined use of a structure-directing agent for the synthesis of the zeolite and a surfactant template for the preparation of the mesophase, both added at the beginning of the synthesis in the reaction medium [21,38,39]. For example, the hierarchical Beta zeolite is prepared using the tetraethylammoniumhydroxide (TEAOH) as structure-directing agent for the zeolite microporous framework, while polydiallyldimethylammononium chloride (PDADMAC) is used as mesoscale cation polymer [40].

1.4. Biomass and biorefinery

The VII principle of Green Chemistry concerns one of the major challenges of our society: the "resource depletion". The current industrial economy has to be revolutionized because it is based on petroleum a non-renewable fossil resource.

In order to reduce the dependence on fossil feedstocks and also mitigate climate changes, alternative production chains are necessary. It is globally recognized that the so-called vegetal biomass, coming from dedicated crops and residues from agriculture, forestry, and industrial activities, have the potential to replace fossil resources as feedstock for industrial production. Unlike fossil fuel deposits, biomass is renewable in the sense that only a short period of time is needed to replace what is used as feedstock. Vegetal biomass is synthesized *via* the photosynthetic process that converts atmospheric carbon dioxide and water into sugars. Plants use the sugar to synthesize the complex materials that are generically named biomass. Carbohydrates and lignin are the primary organic products in the biomass and are followed by triglycerides and mixed organic residues [41].

The global energy potential of virgin biomass is very large. It is estimated that the world's standing terrestrial biomass (i.e., the renewable, above-ground biomass that could be harvested and used as an energy resource) is approximately 100 times the world's total annual energy consumption [42].

The industry where the biomass is converted to a range of useful products (chemicals, fuels, energy, and materials) is named biorefinery. The biorefinery concept is analogous to

petroleum refinery, which produces multiple fuels and chemicals from petroleum as represented in Fig. 1.4. The oil industry processes crude oil into a limited number of base fractions. The naphtha fraction is subsequently used by the chemical industry as a feedstock for the production of just a few platform chemicals from which all the major bulk chemicals are subsequently derived [41]. In the biorefinery the major platform chemicals will be different from those currently used by petrochemical industry. Although all oil refinery platform chemicals can be derived from biomass, the higher costs and lower yields make it necessary to look for other platform chemicals [41].

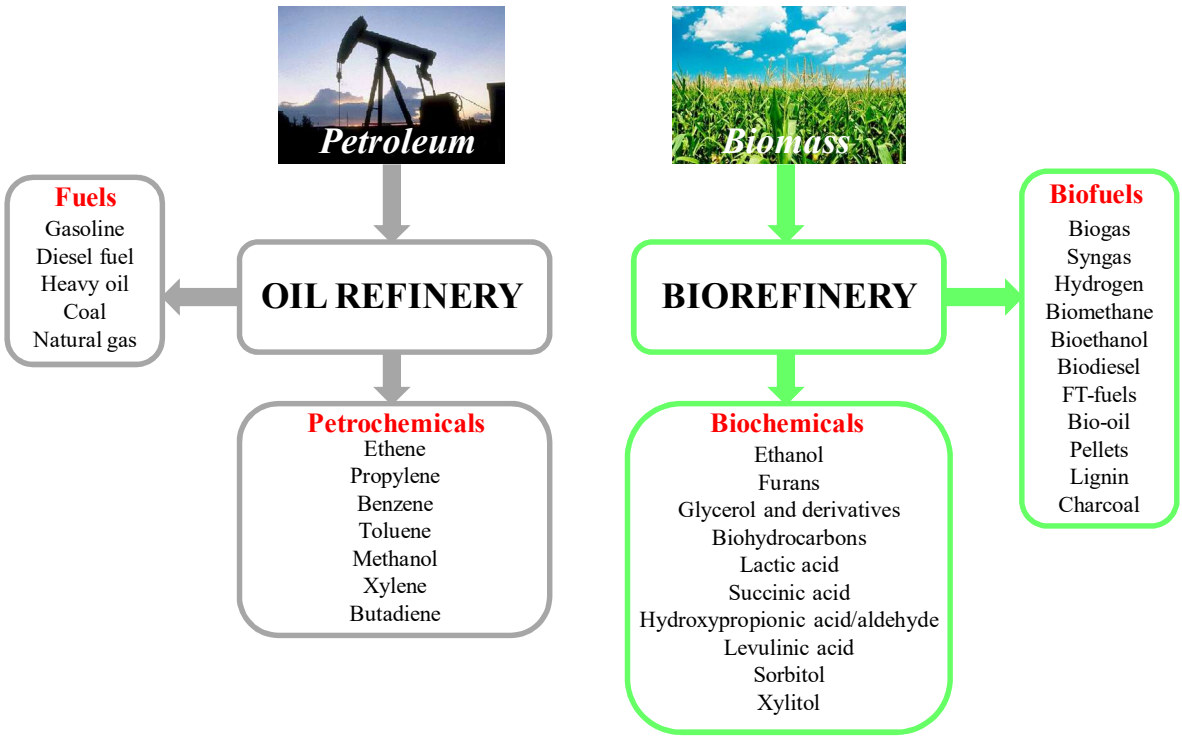

Figure 1.4. Schematic representation of a petroleum refinery and a biorefinery.

1.4.1. Biofuels

The term biofuels refers to solid or liquid or gaseous fuels for the transport sector that are obtained from biomass. They are easily available from common biomass sources, have a considerable environmentally friendly potential, and provide many economic and social benefits as reported in Table 1.1. Liquid biofuels provide one of the few options for fossil fuels replacement in the short- to medium-term [43]. Alcohol fuels can substitute for gasoline

in spark-ignition engines, while biodiesel, green diesel, and dimethyl ether (DME) are suitable for use in compression ignition engines [44].

Table 1.1. Potential benefits and challenges of biofuels [44].

Benefits	**Challenges**
Energy security	***Feedstok***
Domestic energy source	Collection network
Locally distributed	Storage facilities
Well connected supply demand chain	Food-fuel competition
Higher reliability	
	Technology
Economic stability	
	Pretreatment
Price stability	Enzyme production
Employment generation	Efficiency improvement
Rural development	Technology cost
Reduce inter-fuel competition	Production of value added co-products
Reduce demand supply gap	
Open new industrial dimensions	***Policy***
Control on monopoly of fossil rich states	
	Land use change
Environmental gains	Fund for research and development
	Pilot scale demonstration
Better waste utilisation	Commercial scale deployment
Reduce local pollution	Policy for biofuels
Reduce GHGs emission from energy consumption	Procurement of subcidies on biofuels prodution
Reduction in landfill sites	Tax credits on production and utilization of biofuels

In Europe there are current regulations regarding the substitution of unrenewable resources by biomass in the area of biofuels for transportation (European Parliament and Council directive 2009/28/EC and 2009/30/EC). According to the European Community Directive 2003/30/EC "on the promotion of the use of biofuels" the following products are considered biofuels: bioethanol, biodiesel, biogas, biomethanol, biodimethylether, bioethyltertiarybuthylether based on bioethanol, bioethyltertiarybuthylether based on biomethanol, synthetic biofuels, biohydrogen, and pure vegetable oil.

First generation biofuels are produced directly from food crops or animal fats. They have attained commercial level production using conventional technology. The most well known first generation biofuels are bioethanol and biodiesel [45]. Bioethanol is made from crop plants and starch contained in maize kernels or other starchy crops, by sugar

fermentation. Biodiesel is made from oil produced from oleaginous plants by transesterification processes or cracking to convert the vegetal oils into alkyl esters. First generation biofuels are afflicted by some skepticism because they need arable lands, high water, and fertilizer requirements [45]. One of the issues most debated is the food-versus-fuel competition, in which the production of these fuels from edible crops could increase the food price [46]. Therefore, the use of non-edible biomass (e.g. agricultural residues, industrial and municipal organic wastes) is favoured. Biofuels derived from non-edible crops are named second generation biofuels. They include by-products (cereal straw, sugar cane bagasse, forest residues), wastes (organic components of municipal solid wastes), and dedicated feedstocks (purpose-grown vegetative grasses, short rotation forests and other energy crops). The second generation feedstocks are processed differently than first generation biofuels and the process technologies are not yet commercial although pilot and demonstration facilities are being developed [47].

1.4.2. Platform biochemicals

In 2004 the US department of energy made a list of the most promising bio-based platform molecules [48], that was updated in 2010 [49]. In Fig. 1.4. is reported the complete list. The choice of these compounds has been made using specific criteria [49]. Each chosen compound has received considerable attention in literature and the developed technology permits the substitution of existing petrochemicals. It is also considered that the existing technology is applicable to high volume products and the commercial production from renewable carbon has to be well established [49]. All of them have available several and reactive functional groups, offering a big choice of potential reactions and products. These molecules can be synthesized biologically or chemically from sugars and triglycerides, and subsequently converted in a multitude of high value products. In comparison to oil derived platform molecules (ethene, propylene, etc.) the biomass platform molecules have much higher oxygen content, resulting in a shift in chemistry from the environmentally damaging oxidation procedures to largely greener reduction chemistry [41]. The oxygen content also gives them low volatility, high solubility in water, high reactivity, and low thermal stability, properties favoring catalytic processing by catalytic aqueous-phase technologies at moderate temperatures (so the principle VI is also involved) [50].

1.5. A biorefinery process

The transesterification of tryglicerides of vegetable oils is a typical process of biorefinery because it permits to obtain a biofuel (fatty acid methyl esters or biodiesel) and a platform biochemical (glycerol) [51-53]. Nowadays glycerol production exceeds the market demand, because it is the main co-product of biodiesel, fatty acids and soaps production. A possible solution to the disposal for glycerol, is its use as bio-based chemical platform in the production of value added chemicals. One of these possible applications could be the production of treoses, dihydroxyacetone and glyceraldehyde, by selective oxidation of glycerol [54]. Treoses are important building blocks in an alternative synthetic way for lactic acid and its esters, which are in the list of the most important platform biochemicals (Fig. 1.4) [55-57]. These steps constitute the reaction chain represented in Fig. 1.5, which is a typical example of process in biorefinery.

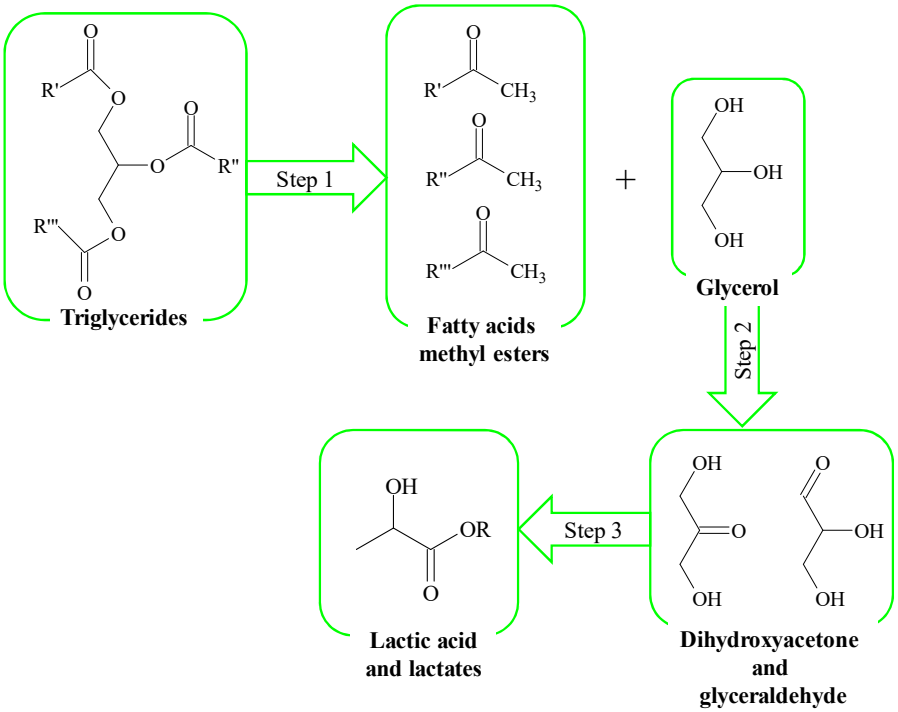

Figure 1.5. Scheme of the production steps of potential biorefinery process.

In all these production steps the role of the catalysts is essential. The first and the third step are acid-base catalyzed, while the second one is an oxidation process. The development

of efficient catalysts for these steps could make them a greener alternative to the current production processes.

References

[1] M.N. Belgacem, A. Gandini, *Monomers, Polymers and Composites from Renewable Resources*, Elsevier (Amsterdam), 2008.

[2] *World Commission on Environment and Development. Our Common Future*, Oxford University Press (New York), 1987.

[3] P.T. Anastas, J.C. Warner, *Green Chemistry: Theory and Practice*, Oxford University Press (New York), 1998.

[4] P.T. Anastas, M.M. Kirchhoff, T.C. Williamson, *Appl. Catal. A Gen*. 221 (2001) 3.

[5] P.T. Anastas, L.B. Bartlett, M.M. Kirchhoff, T.C. Williamson, *Catal. Today* 55 (2000) 11.

[6] R. Rinaldi, F. Schüth, *Energy Environ. Sci.* 2 (2009) 610.

[7] M.E. Davis, *Nature* 417 (2002) 813.

[8] G. Ertl, H. Knözinger, F. Schüth, J. Weitkamp, *Handbook of Heterogeneous Catalysis. Second Completely Revised and Enlarged Edition* Volume 1, Wiley-VCH (Weinheim), 2008.

[9] C. Perego, R. Bagatin, M. Tagliabue, R. Vignola, *Micropor. Mesopor. Mater*. 166 (2013) 37.

[10] C. Baerlocher, L.B. McCusker, D.H. Olson, *Atlas of Zeolite Framework Types*, Elsevier (Amsterdam), 2007.

[11] C.S. Cundy, P.A. Cox, *Micropor. Mesopor. Mater.* 82 (2005) 1.

[12] A.W. Chester, E.G. Derouane, *Zeolite Characterization and Catalysis*, Springer (Dordrecht), 2009.

[13] H.S. Sherry, *J. Phys. Chem.* 70 (1966) 1158.

[14] L. Broussard, D. Shoemaker, *J. Am. Chem. Soc.* 1074 (1960) 1041.

[15] I. Ferino, D. Meloni, R. Monaci, D. Perra, M.G. Cutrufello, E. Rombi, I. Ferino, *J. Therm. Anal. Calorim.* 121 (2015) 1139.

[16] M.E. Leonowicz, J.A. Lawton, S.L. Lawton, M.K. Rubin, *Science* 264 (1994) 1910.

[17] A. Corma, *Chem. Rev.* 95 (1995) 559.

[18] R.A. Schoonheydt, P. Geerlings, E.A. Pidko, R.A. van Santen, *J. Mater. Chem.* 22 (2012) 18705.

[19] D. Barthomeuf, G. Coudurier, J. Vedrine, *Mater. Chem. Phys.* 18 (1988) 553.

[20] D. Barthomeuf, *Micropor. Mesopor. Mater.* 66 (2003) 1.

[21] V. Meynen, P. Cool, E.F. Vansant, *Micropor. Mesopor. Mater.* 104 (2007) 26.

[22] L.H. Chen, X.Y. Li, J.C. Rooke, Y.H. Zhang, X.Y. Yang, Y. Tang, F.S. Xiao, B.L. Su, *J. Mater. Chem.* 22 (2012) 17381.

[23] J. Weitkamp, *Solid State Ionics* 131 (2000) 175.

[24] H. Chon, S.I. Woo, S.E. Park, *Recent Advances and New Horizons in Zeolite Science and Technology*, Studies in Surface Science and Catalysis, Vol. 102, Elsevier (Amsterdam), 1996.

[25] J.M.R. Gallo, C. Bisio, G. Gatti, L. Marchese, H.O. Pastore, *Langmuir* 26 (2010) 5791.

[26] X. Meng, F. Nawaz, F.S. Xiao, *Nano Today* 4 (2009) 292.

[27] J.P. Thielemann, F. Girgsdies, R. Schlögl, C. Hess, *Beilstein J. Nanotechnol*. 2 (2011) 110.

[28] F. Leydier, C. Chizallet, A. Chaumonnot, M. Digne, E. Soyer, A.A. Quoineaud, D. Costa, P. Raybaud, J. Catal. 284 (2011) 215.

[29] G. Crépeau, V. Montouillout, A. Vimont, L. Mariey, T. Cseri, F. Maugé, *J. Phys. Chem. B* 110 (2006) 15172.

[30] W. Daniell, U. Schubert, R. Glöckler, a Meyer, K. Noweck, H. Knözinger, *Appl. Catal. A Gen.* 196 (2000) 247.

[31] A. Taguchi, F. Schüth, *Micropor. Mesopor. Mater.* 77 (2005) 1.

[32] G. Yang, E.A. Pidko, E.J.M. Hensen, *J. Phys. Chem. C* 117 (2013) 3976.

[33] R.A. Schoonheydt, B.M. Weckhuysen, *Phys. Chem. Chem. Phys.* 11 (2009) 2794.

[34] Y. Román-Leshkov, M.E. Davis, *ACS Catal.* 1 (2011) 1566.

[35] G. Sankar, J.M. Thomas, C.R.A. Catlow, C.M. Barker, D. Gleeson, N. Kaltsoyannis, *J. Phys. Chem. B* 105 (2001) 9028.

[36] A. Corma, F.X. Llabrés I Xamena, C. Prestipino, M. Renz, S. Valencia, *J. Phys. Chem. C* 113 (2009) 11306.

[37] A. Corma, M.E. Domine, L. Nemeth, S. Valencia, *J. Am. Chem. Soc.* 124 (2002) 3194.

[38] D.P. Serrano, J.M. Escola, P. Pizarro, *Chem. Soc. Rev.* 42 (2013) 4004.

[39] A. Corma, *Chem. Rev.* 97 (1997) 2373.

[40] F.S. Xiao, L. Wang, C. Yin, K. Lin, Y. Di, J. Li, R. Xu, D.S. Su, R. Schlögl, T. Yokoi, T. Tatsumi, *Angew. Chem. Int. Ed.* 45 (2006) 3090.

[41] F. Cherubini, *Energy Convers. Manag.* 51 (2010) 1412.

[42] B. Kamm, Angew. *Chem. Int. Ed.* 46 (2007) 5056.

[43] G. Taylor, *Energy Policy* 36 (2008) 4406.

[44] P.S. Nigam, A. Singh, *Prog. Energy Combust. Sci.* 37 (2011) 52.

[45] A. Singh, S.I. Olsen, P.S. Nigam, *J. Chem. Technol. Biotechnol.* 86 (2011) 1349.

[46] S.N. Naik, V. V. Goud, P.K. Rout, A.K. Dalai, Renew. *Sustain. Energy Rev.* 14 (2010) 578.

[47] R.E.H. Sims, W. Mabee, J.N. Saddler, M. Taylor, *Bioresour. Technol.* 101 (2010) 1570.

[48] T. Werpy, G. Petersen, *Top Value Added Chemicals from Biomass.* Vol. I-Results of Screening for Potential Candidates from Sugars and Synthesis Gas, 2004.

[49] J.J. Bozell, G.R. Petersen, *Green Chem.* 12 (2010) 539.

[50] P.A. Jacobs, M. Dusselier, B.F. Sels, *Angew. Chem. Int. Ed*. 53 (2014) 8621.

[51] A. Islam, Y.H. Taufiq-Yap, E.S. Chan, M. Moniruzzaman, S. Islam, M.N. Nabi, *Energy Convers. Manag.* 88 (2014) 1200.

[52] M. Canakci, J. Van Gerpen, *Trans. ASAE* 44 (2001) 1429.

[53] B.R. Moser, *Vitr. Cell. Dev. Biol*. 45 (2009) 229.

[54] L. Li, C. Stroobants, K. Lin, P. a. Jacobs, B.F. Sels, P.P. Pescarmona, *Green Chem*. 13 (2011) 1175.

[55] M.A. Abdel-Rahman, Y. Tashiro, K. Sonomoto, *Biotechnol. Adv.* 31 (2013) 877.

[56] R. Datta, M. Henry, *J. Chem. Technol. Biotechnol.* 81 (2006) 1119.

[57] M. Dusselier, P. Van Wouwe, A. Dewaele, E. Makshina, B.F. Sels, *Energy Environ. Sci*. 6 (2013) 1415.

[58] Y. Fan, C. Zhou, X. Zhu, *Catal. Rev*. 51 (2009) 293.

[59] Z. Xu, L. Zhu, H. Chen, *Compr. Biotechnol.* (2011) 201.

Chapter II

Acid-base properties of zeolites and mesostructured silica-aluminas

2.1. Acidity and basicity

There are numerous solid materials which can be used as catalysts (zeolites, polymers, carbon based solids, hydroxyapatites, etc.) for many important reactions. The surface acid-base properties are decisive for the catalytic performances of a solid. So they can be described in terms of their Brønsted or Lewis acidity or basicity. Some types of solids show predominantly Brønsted species while other types show mainly Lewis species. In general these concepts are superimposable, because a proton is an electron pair acceptor. However when the proton is absent the acid-base interaction can be explained by the Lewis definition.

Acidity and basicity of solid materials are not expressed by the values of the negative logarithm of the acid dissociation constants, the pK_a and the pK_b values, because these value are defined only for aqueous solutions, where the solvent participates to the acid-base equilibrium. Usually the acid-base properties of the isolated species on the surface of solid acids or bases are represented by the proton affinity (PA) which is a property of a molecule in the absence of the solvent. The proton affinity is the negative enthalpy of a proton addition reaction [1]. For an acidic species it is related to the reaction:

$$BH \rightarrow B^- + H^+ \quad \Delta H = PA$$

While for a basic species:

$$BH^+ \rightarrow B + H^+ \quad \Delta H = PA$$

The strength of the interaction between a base or an acid and a surface acid or base site is determined by the relative proton affinities [2].

2.2. Techniques used to evaluate acidity and basicity of porous solids

The acid-base chemistry of solid surfaces differs in some important aspects from that of solutions. Spatial separation and lack in mobility are characteristic of acid/base sites on solid surfaces that are not present among species in aqueous solutions. So it is possible the coexistence of acid and base sites in the same surface without any

equilibrium [3]. The existence of a heterogeneous distribution of active sites with a wide range of strength distribution is a peculiarity of solid surfaces. Another important feature, unique to porous solid surfaces, is the accessibility of sites; because of it not all the sites are involved to a specific reaction because some of them are not available for some molecule. So, while for homogeneous phases the acid/base properties are expressed by a single parameter (for example the pH), for solid surfaces there are five properties that need to be considered [3]:

- Nature of the sites (acidic or basic);
- Type of sites (Lewis or Brønsted);
- Concentration of each type of site;
- Strength of the sites;
- Accessibility of the sites.

For these reasons, the methods for the evaluation of acid-base properties in solutions are not directly usable for solid surfaces and it is necessary to use two or more techniques for a complete evaluation of acid/base properties.

The standard procedure to investigate these properties is by studying the adsorption of suitable gas-phase probe molecules on the surface [4]. The choice of the probe molecule depends on the used technique but in general there are some criteria that must be respected [3]. The nature of the sites, acidic or basic, is verified by adsorption of a chosen complementary probe molecule that is basic for acid sites or acidic for basic sites. The type of sites, Brønsted or Lewis, can be identified by three methods: *i*) the selective adsorption of a probe molecule for only one type of sites, *ii*) the production of a distinct spectroscopic signature for each type of site with the probe molecule, *iii*) the conversion of the probe molecule *via* different reaction pathways on Brønsted or Lewis sites. The acidic/basic sites strength is assessed by heats of adsorption, temperatures of desorption, spectroscopic parameter or indicator colour changes. The accessibility can be monitored by varying the bulkiness of the probes [3,5].

Titration using an indicator and an aprotic solvent is the oldest method used for the investigation of acid-base properties of solids. The colour taken by an appropriate

indicator, adsorbed on the solid surface, permits a qualitatively estimate of the acid or base strength of the surface sites. A suitable titrator enables the determination of the concentration of the surface acid or base sites [5,6]. The titration method has almost been abandoned because of the many limitations. The indicators usually are really selective for either Brønsted or Lewis acid or base centers, failing when both types are simultaneously present [5]. The use of aprotic media is not compatible with the pK_a values of the indicators that are defined only for aqueous solutions. The bulky indicator molecules are hindered into the interior of the zeolite crystallites, restricting the titration to the outer surface. Another drawback is that, in many cases, the time of the experiment become very long, mainly because of the competition between the molecules of the solvent and the molecules of the titrator for the adsorption on the surface sites [5].

Among the spectroscopic techniques, FTIR and NMR spectroscopies are the most widely used for the characterization of acidity and basicity of solid materials. Basicity and Lewis acidity are usually investigated through use of probe molecules. Unfortunately the basicity has been much less studied than acidity, because only a few industrial processes are catalyzed by bases, so to date only a few acidic probes can be used successfully [5,7]. FTIR spectroscopy, in particular with probe molecules adsorption, is one of the most powerful techniques for identifying the nature and quantifying the strength and the concentration of the acid or base sites of solids [5]. The application of the Lambert-Beer Law permits the estimation of the number of acid and base sites [5,8,9]. The use of appropriate probe molecules enables the easily distinction between Brønsted and Lewis active sites. The acid and base strength can be estimated from peak shift values of adsorbed probe molecules or from the profile of absorbance *versus* desorption temperature [8,10]. Nuclear magnetic resonance (NMR) spectroscopy is a suitable method for characterizing Brønsted acid sites on solids. ^{1}H MAS NMR allows the access to the intrinsic properties of the proton but does not permit the evaluation of the acid strength. It was believed that the acid strength is related to the chemical shift, but in NMR spectroscopy too much parameters affect the chemical shift [3]. Quantification of the protons of a specific type is possible by signal integration and a simple calibration with a suitable external standard [3]. The ^{27}Al MAS NMR is useful with aluminosilicates. The signal at δ = 60 ppm, ascribable to tetrahedrally coordinated framework alluminium, can be integrated, allowing the

determination of the Brønsted acid sites number [5]. The use of probe molecules also in NMR enriches the techniques, allowing the collection of information similar to that provided by IR spectroscopy. However, in comparison to IR spectroscopy, the quantification is easier but the instrumentation is much more expensive and it is necessary to use molecules enriches with suitable isotopes [11].

Temperature programmed desorption (TPD) is utilized to determine both the density and strength of acid base sites in solid materials. The technique is based on the desorption of a gaseous base or acid probe by heating the sample with a temperature program. The amount of base desorbed is detected gravimetrically, volumetrically, by gas-chromatography, or by mass-spectrometry [12]. The temperature of the desorption peak is related to the acid or base strength, while the area under the desorption peak is related to the number of the acid or base sites. Some limitations have to be considered: the difficult distinction between Brønsted and Lewis, the corrupted results by readsorption of the species desorbed from the active sites, and the dependence of the results on the temperature program which makes difficult to compare results obtained with different programs [5,7]. However these limitation can be overcome using complementary techniques.

Adsorption microcalorimetry is based on the measure of the heat of adsorption of an appropriate gaseous probe molecule with the surface active sites. The technique provides a direct measure of the strength of interaction and a quantitative analysis of the sites strength distribution. The fundamental disadvantage of this technique is the impossibility of understanding the nature of the sites where the adsorption occurs. For this reason, in the same way of TPD, the microcalorimetry can be associated with a complementary techniques such as FTIR or NMR [3,13].

2.2.1. Adsorption microcalorimetry

Generally the adsorption is an exothermic phenomena ($\Delta H < 0$), in which the evolved energy is proportional to the strength of the interaction between the active site and the adsorbed molecule. The pairing of a microcalorimeter with a volumetric system allows the simultaneous measure of the heat evolved and the amount adsorbed [14].

2.2.1.1. The adsorption microcalorimeter apparatus

The whole apparatus consists of two main parts: the calorimeter and the volumetric system. The calorimeter is a container in which the thermal phenomena are carried out and studied. It consists of a thermostat which surrounds the sample cell that is in thermal contact with the thermostat through a resistance. The most widely used calorimeter is the Tian-Calvet heat-flow microcalorimeter which was developed by Calvet and later improved by Tian. It is based on the heat exchange between the sample and the thermostat, and the heat is measured through a heat-flowmeter [14]. The heart of the Tian-Calvet calorimeter is a cylindrical container (where the sample is located), showed schematically in Fig. 2.1, surrounded by a large number of thermocouples which constitute a thermoelectric pile. A galvanometer measures the electromotive force generated by the thermopile, that is proportional to the total heat flow from the internal boundary on the calorimetric wall. In this way very small temperature differences can be detected (≈ 10^{-6} °C).

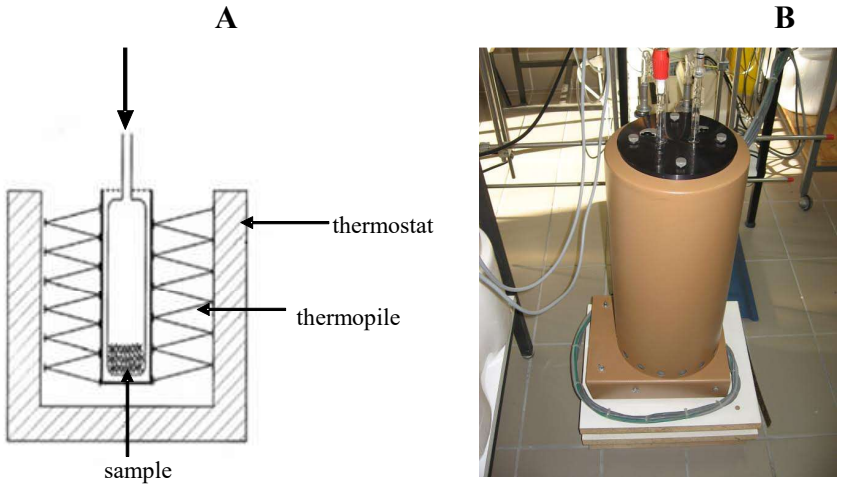

Figure 2.1. Scheme of the gas adsorption bulb in a Tian-Calvet thermopile [14] **(A)** and a picture of the microcalorimeter **(B)**.

The calorimeter has two twin calorimeter containers with their thermoelectric piles connected in opposition. The thermal process is carried out in one of them while the other has a function of reference [15]. The presence of two containers with two heat flow-meters is due to the need of compensating parasitic phenomena such as external connection and probe gas introduction heat [16]. The calorimeter needs to be associated

with a sensitive volumetric system for determining the adsorbed amount. The whole apparatus is schematically represented in Fig. 2.2. Solenoid valves permit the dosing of the probe. A high vacuum pump is also fundamental because the sample needs to be evacuated before each experiment with the aim of eliminating the species physisorbed (such as water and carbon dioxide) during the storage of the sample.

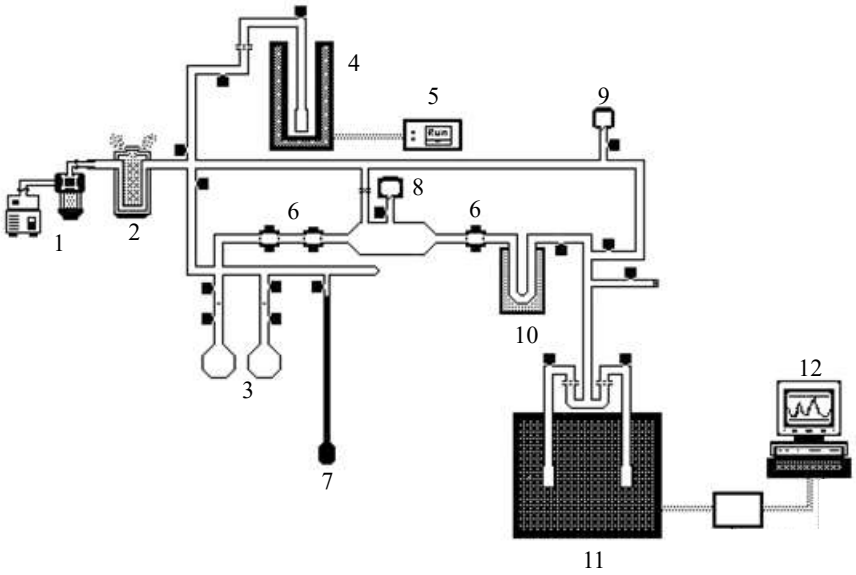

Figure 2.2. Schematic representation of the whole microcalorimetry apparatus: (1) pumps, (2) liquid nitrogen trap, (3) probe balloons, (4) oven, (5) temperature programmer, (6) valves, (7) Hg manometer, (8) capacitance manometer, (9) penning, (10) cold trap, (11) calorimeter, (12) computer.

2.2.1.2. Experimental procedure and calorimetric results

The experiment is carried out by sending stepwise small doses of probe gas inside the volumetric system previously evacuated at 10^{-4} Pa. For each dose, thermal equilibrium must be reached before pressure, adsorbed amount, and integral heat are measured. The equilibrium pressure is measured by a capacitance manometer while the adsorbed amount is determined through the pressure drop. In this way a curve representing the adsorbed amount *versus* the pressure is obtained (Fig. 2.3). For each dose of probe gas the heat produced is given by the area under the corrisponding thermogram peak. The adsorption experiment is concluded when a relatively high pressure (≈ 100 Pa) is reached without significant evolution of heat and the adsorbed amount becomes negligible [17].

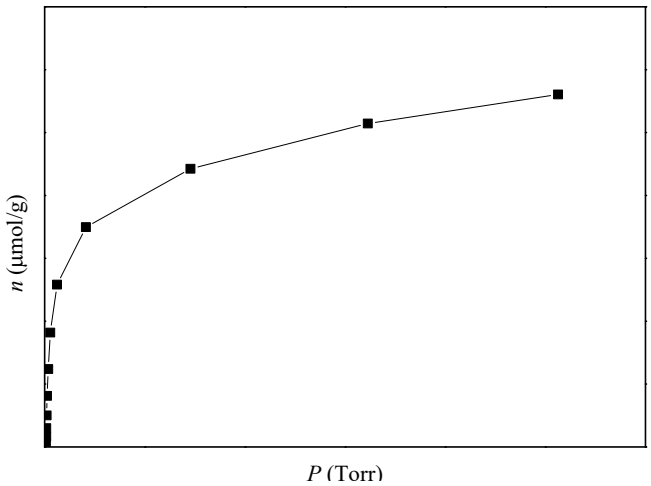

Figure 2.3. The volumetric isotherm: adsorbed amount *vs*. pressure.

The integral heat of adsorption is defined as the amount of heat evolved by the system when *n* moles of probe molecule are adsorbed at constant temperature and volume [16]:

$$Q_{int} = K \int Edt$$

Where *K* is an instrument constant and *E* is the voltage signal generated by the thermocouples and recorded over the duration of the thermal event. The integral heat is often plotted *versus* the adsorbed amount *n*, as reported in Fig. 2.4.

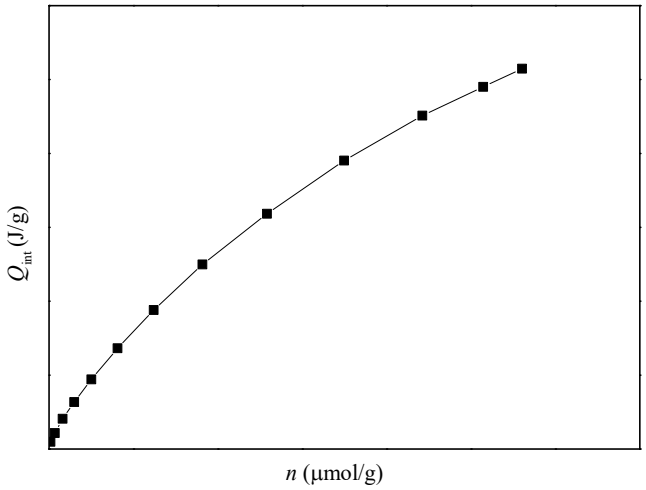

Figure 2.4. The integral heat as a function of the adsorbed amount.

However the integral heat of adsorption is not very useful because it does not give information about the sites distribution is preferred the value of the differential heat of adsorption, Q_{diff}, which is related to the integral heat of adsorption by:

$$Q_{diff} = \left[\frac{\delta Q_{int}}{\delta n}\right]_{T,m}$$

The differential heat is commonly plotted as a function of n, the adsorbed amount (Fig. 2.5).

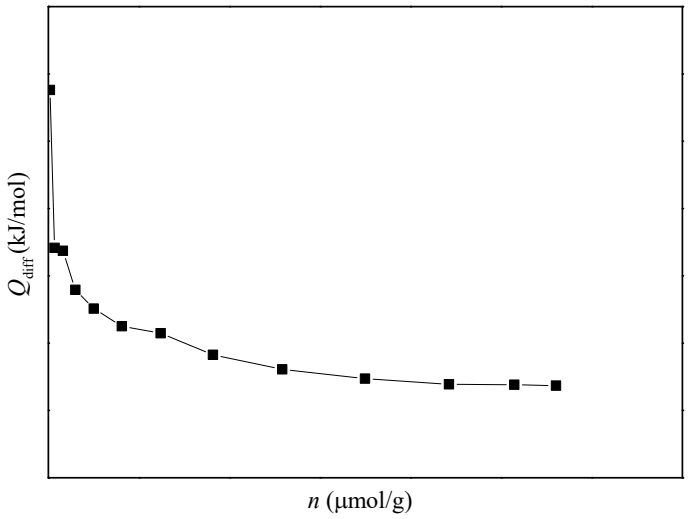

Figure 2.5. The differential heat as a function of the adsorbed amount.

The variation of the differential heat of adsorption as a function of the adsorbed amount gives information of the homogeneity or heterogeneity of the surface active sites. The differential heat decreases with the adsorbed amount because of the heterogeneity of the surface sites. The adsorption involves first the strongest sites which are characterized by the highest Q_{diff}. The presence of well defined steps is an indication of families of active sites, with characteristic values of differential heat.

Useful representation of the sites families is based on the plot of the site energy distribution function versus Q_{diff}. The function is the negative inverse of the first derivative of the differential heat with respect to the amount adsorbed, $-\delta n/\delta Q_{diff}$. Peaks of this plot correspond to the steps of the Q_{diff} *vs*. n curve and the area is proportional to

the adsorbed amount on the family of sites whose strength corresponds to the abscissas range of the peak [17].

A method used for the evaluation of the strong acid/base sites concentration is based on the volumetric isotherms (*n vs. P*), represented in Fig. 2.6. The procedure involves a first adsorption in which the probe molecules are either irreversibly or reversibly adsorbed and the overall adsorption isotherm is registered. Then the weakly adsorbed moiety is removed by outgassing at the same temperature of the previous adsorption, after which a new adsorption step is carried out in order to obtain a second isotherm due to only the physical adsorption. The difference among the two isotherms is the irreversibly adsorbed amount that represents the amount of the strong acid/base sites [18].

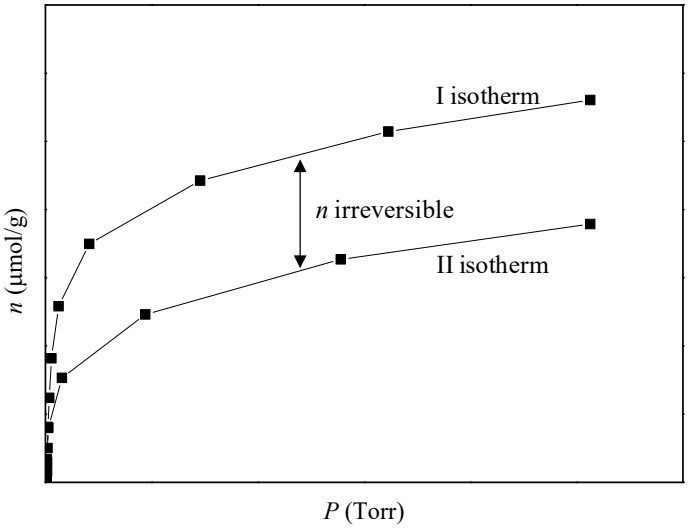

Figure. 2.6. The volumetric isotherms of the overall adsorbed gas (I isotherm) and the reversibly adsorbed amount (II isotherm).

The adsorption of a probe molecule on the surface of a material usually is the contribution of the chemical and physical adsorption. Chemical adsorption is defined as the formation of a chemical bond between the sorbate and the active sites on the surface. The corresponding evolved heat is of the same magnitude of the chemical reaction energy. This interaction is strong and specific. Physical adsorption is based on weaker and aspecific interactions (van der Walls interactions). The difference between chemical and physical adsorption, in first approximation, is in the magnitude of the heat of

adsorption, because the physisorption evolved heat is generally not much larger than the energy of condensation of adsorptive [14]. The amount of physisorbed probe gas can be determined through the following evaluations: *i*) low values of Q_{diff} are related to the physisorption, in particular when the values are associated with the reversible adsorption, *ii*) the presence of a plateau in the curves of the Q_{int} *versus* the adsorbed amount and the simultaneous upward deviation of the adsorption isotherms, *iii*) the decrease of the time required for reaching the equilibrium after sending a dose.

A good probe molecule for the overall acidity or basicity is a strong basic or acidic molecule because the calorimetric method is based on the neutralization of the surface active sites by the formation of a real chemical bond. Ammonia (PA = 857.7 kJ/mol) and pyridine (PA = 922.2 kJ/mol) are the most used molecules to probe the overall acidity, both Brønsted and Lewis acidity. The smaller molecular dimensions of ammonia make its diffusion not affected through pores, channels or windows greater than about 0.4 nm, while the strong basicity in gas phase permits the adsorption even on the weakest acid sites. Bulky probe molecules such as substituted pyridines, which cannot penetrate into the zeolite channels and cavities, are useful to determine the external acidity [19,20]. For basicity measurements carbon dioxide is one of the most used but can be adsorbed on cations and can react with hydroxyls and framework oxide ions to give carbonated species. Another used molecule is the sulfur dioxide that is more acidic than carbon dioxide and more suitable to quantify the total basicity of a sample [18].

2.2.2. Probe molecules adsorption FTIR spectroscopy

Infrared spectroscopy is one of the most used and valuable techniques to investigate the acid-base properties of materials. It provides direct information about the chemical nature and the strength of the chemical bonds of surface active sites. However the infrared spectroscopy cannot see *c.u.s.* (coordinatively unsatured) ions, which are important Lewis species, and gives very poor information on the acidity and basicity of the surface hydroxyls groups, which have a relevant role in many important reactions. These problems can be solved by using appropriate probe molecules [10]. There are several well-known probe molecules for the IR investigations. Each molecule must

fullfil some important criteria, which include the knowledge of the interactions of the functional group, the stability of the adsorption complexes, the high extinction coefficient, and the absence of other bands in the absorption region. In general the use of weakly interacting probe molecules is preferred because they are much more specific than strongly interacting probe molecules, so they permit the detection of interaction strength distributions [2].

2.2.2.1. CO as probe molecule

The most frequently used probe molecule for the acidity investigations is carbon monoxide. It is a weakly basic probe molecule. The adsorption of CO on the oxide surface can be either non-reactive or reactive. Adsorption is non-reactive when CO is coordinated to the cationic sites and forms carbonyls, while it is reactive when CO is chemically transformed on the surface. The use of CO as probe molecule is based only on the non-reactive adsorption. The vibrational spectrum of CO is very simple and most oxide samples are transparent in the C–O stretching region. The C–O stretching vibration frequency is very sensitive to the strength of the bond formed with the surface. The molecule is small and therefore its diffusion is not hindered. These are the reasons why CO is commonly used as probe molecule in acidity investigation. The only drawback related to the use of CO as probe molecule is the need to work at low temperatures because at room temperature only complexes of CO with the Brønsted acid sites can be detected [10].

The electronic structure of CO represented in Fig. 2.7 is useful for understanding the interactions of this molecule with the acid sites. The molecule has four full bonding orbitals (3σ, 4σ, $1\pi_x$ and $1\pi_y$), an occupied slightly antibonding orbital (5σ) and three empty antibonding orbitals ($2\pi_x$ *, $2\pi_y$* and 6σ*). So the bond order is 3. The 5σ orbital is the HOMO (highest occupied molecular orbital) while the LUMO (lowest unoccupied molecular orbital) is the 2π* orbital. The orbitals 4σ and 5σ are oriented away from the molecule along the molecular axis. The 4σ orbital energetically belongs to the oxygen while the 5σ belongs mainly to the carbon atom. The higher energy of the 5σ orbital makes the carbon atom a stronger Lewis base than the oxygen atom. The electro-donating properties of this orbital are important because they stabilize the entire molecule forming σ bonds when the symmetry of the corresponding orbitals fits. When

CO interacts with a transition metal having empty d orbitals, a π bond by π back-donation can also be formed. This interaction leads to weakening of the C–O bond because it fills the 2π* orbitals while reinforcing the σ bond because it increases the electron density of the CO molecule [10]. CO can participate in coordination bonds as weak Lewis base also *via* the oxygen atom using the much more stable 4σ orbital forming isocarbonyls, but this interaction is rarer than the previous. The electrostatic interaction without any electron transfer is another common interaction for CO molecule. CO has a charge separation with a negative charge located on the carbon end. This charge separation is very weak because of the strong electronegativity of the oxygen end and the dipole moment of CO is very small. The interaction between CO and hydroxyls groups is essentially electrostatic [1].

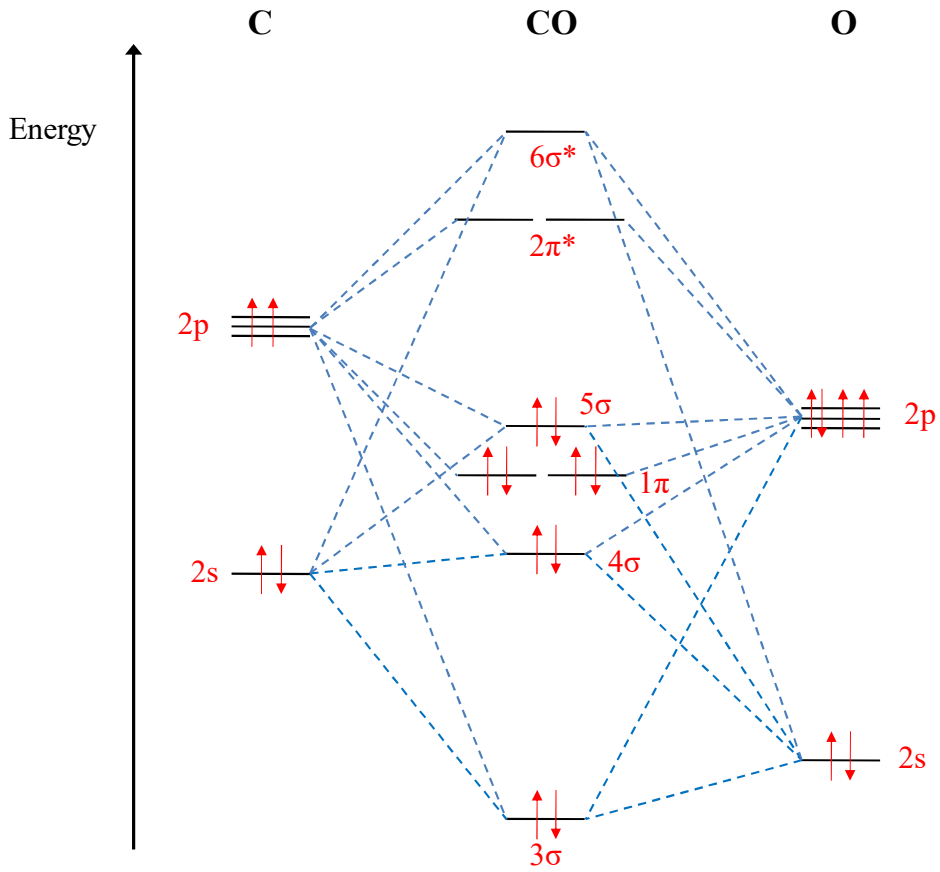

Figure 2.7. The electronic configuration of CO [21,22].

2.2.2.2. Methods for acidity characterization

Two methods are used to measure the acidity strength of hydroxyls groups in zeolites and in other oxidic materials by adsorption FTIR: the *ion-pair method* and the *H-bond method*. The ion-pair method is based on the protonation of strong bases as probe molecules such as ammonia and pyridines, while the so called H-bond method is based on the use of weak bases such as CO which are too weak to allow the proton transfer [1].

When a hydroxyl group interacts with a weak base by a hydrogen bond the O–H bond order decreases and the O–H stretching mode undergoes a red shift (to lower frequencies), Δν(OH), that is a measure of the acid strength of the OH group. The red shift is accompanied also by a large increase in the integral intensity and by a broadening of the band width at half maximum [1]. There is a direct relationship between the Δν(OH) and the enthalpy of formation of the H-bond, ΔH_B [2]:

$$|\Delta\upsilon(OH)|^{1/2} \approx \Delta H_B$$

The interaction affects also the stretching modes of the H-bonded probe molecule, and the stronger is the hydrogen bond, the higher is the CO stretching frequency. The carbonyl bands are detected in the region of 2183-2145 cm^{-1} as a function of the hydroxyls acidity. However the estimation of the hydroxyls acidity by the carbonyl band shift is much less accurate than that assessed by the shift for the O−H stretching frequency. Moreover a further complicating is due to the superimposition of the OH−CO bands with the bands of CO on the Lewis acid sites (metal ions).

The assessment of the Lewis acid strength is less accurate than that of Brønsted acidity. The aprotic species may only form an acid-base adduct with the CO molecules, modifying the bond energies and hence the force constants and normal mode frequencies of the CO probe molecule. Also in this case the stronger is the interaction, the more pronounced is the vibrational frequency shift the greater is the Lewis acidity [23].

In general it is also useful to record spectra at various CO coverages in order to distinguish between the different adsorption forms. The most acidic sites interact first with CO at lower coverage, while the weaker sites are successively occupied.

2.2.2.3. The apparatus system for adsorption FTIR measurements

The apparatus system to record the infrared spectra of adsorbed molecules, shown in Fig. 2.8, consists of two main elements connected to the spectrometer: the IR cell and the vacuum adsorption apparatus.

Figure 2.8. The whole apparatus for adsorption FTIR experiments.

The sample is introduced inside the IR cell (shown in Fig. 2.9) in the form of a wafer of about 1 cm^2 and it is held by a quartz support. The holder has a magnetic element by which the sample is moved inside the cell.

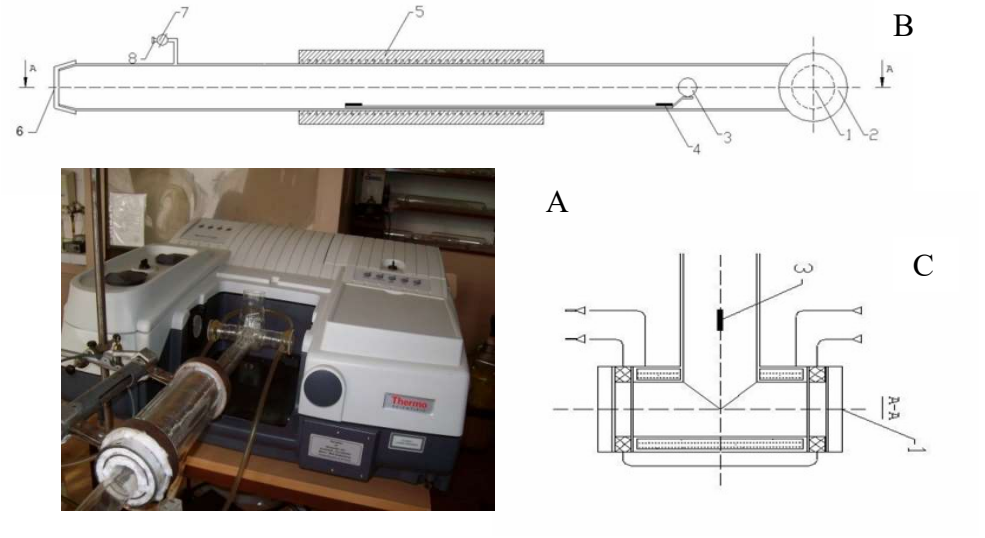

Figure 2.9. Picture of the IR cell and the spectrometer **(A)**; A section of the IR cell **(B)** and a section of the optical part of the IR cell **(C)**: (1) optic part, (2) CaF_2 window, (3) sample holder, (4) magnets, (5) oven, (6) place for introduction of the sample, (7) vacuum valve, (8) connection to the vacuum-adsorption apparatus.

A tubular oven (Fig. 2.9B) is able to heat up to 550 °C a part of the cell, permitting to treat the sample at various temperatures before the IR measures. The optic part of the cell has two calcium fluoride windows (Fig. 2.9B) transparent to the IR frequencies. The optic part (Fig. 2.9C) can be cooled to the liquid nitrogen temperature by pouring liquid nitrogen in a cooling jacket.

As represented in Fig. 2.10, the IR cell is connected to the vacuum system, which permits to maintain a high vacuum (up to 10^{-3} Pa), to adsorb/desorb probe molecules and vapours, and to record the spectra of adsorbed molecules without exposing the pellet to the air. The apparatus consists of two pumps, an oil vacuum pump and a turbo-molecular pump.

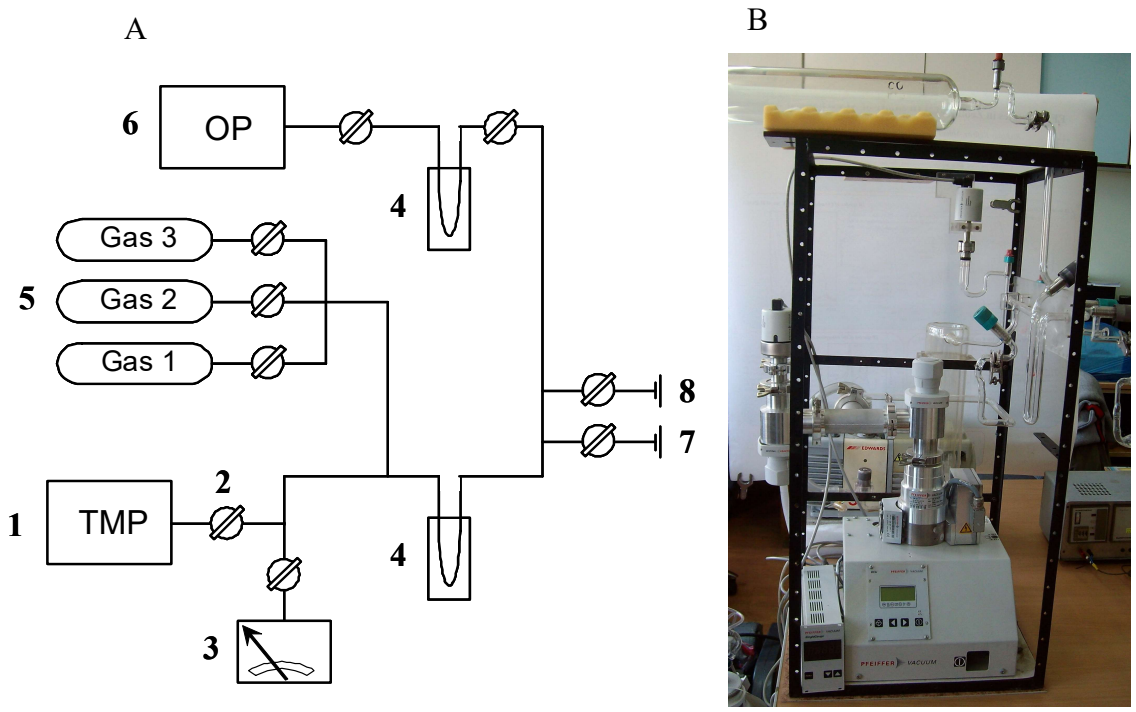

Figure 2.10. Schematic representation of the vacuum-adsorption apparatus **(A)**: (1) turbo-molecular pump, (2) vacuum valve, (3) pressure gauge, (4) liquid nitrogen trap, (5) balloons, (6) oil vacuum pump, (7) connection to the IR cell, (8) connection to the atmosphere or additional devices; a picture of the apparatus **(B)**.

References

[1] K. Hadjiivanov, *Adv. Catal.* 57 (2014) 99.

[2] H. Knözinger, S. Huber, *J. Chem. Soc. Faraday Trans.* 94 (1998) 2047.

[3] F.C. Jentoft, *Reference Module in Chemistry, Molecular Sciences and Chemical Engineering, Solid Acids and Bases*, Elsevier (Amsterdam), 2013.

[4] A. Auroux, *Top. Catal.* 19 (2002) 205.

[5] G. Ertl, H. Knözinger, F. Schüth, J. Weitkamp, *Handbook of Heterogeneous Catalysis. Second Completely Revised and Enlarged Edition Volume 1*, Wiley-VCH (Weinheim), 2008.

[6] K. Tanabe, M. Misono, Y. Ono, H. Hattori, *New Solid Acids and Bases, Studies in Surface Science and Catalysis*, Vol 51, Elsevier (Amsterdam), 1989.

[7] M. Hunger, *Zeolites and Catalysis: Synthesis, Reactions and Applications Catalytically*, *Chapter 17, Catalytically Active Sites: Generation and Characterization,* Wiley (Weinheim), 2010.

[8] M. Tamura, K. Shimizu, A. Satsuma, *Appl. Catal. A Gen.* 433-434 (2012) 135.

[9] W.E. Farneth, R.J. Gorte, *Chem. Rev.* 95 (1995) 615.

[10] K.I. Hadjiivanov, G.N. Vayssilov, *Adv. Catal*. 47 (2002) 307.

[11] Y. Jiang, J. Huang, W. Dai, M. Hunger, *Solid State Nucl. Magn. Reson.* 39 (2011) 116.

[12] R. Gorte, *J. Catal.* 75 (1982) 164.

[13] A. Auroux, *Top. Catal.* 4 (1997) 71.

[14] F. Rouquerol, J. Rouquerol, K.S.W. Sing, P. Llewellyn, G. Maurin, *Adsorption by Powders and Porous Solids, Principles, Methodology and Applications, Second Edition*, Elsevier (Amsterdam), 2014.

[15] E. Calvet, H. Prat, *Recent Progress in Microcalorimetry*, Pergamon (Oxford), 1963.

[16] N. Cardona-Martinez, A.J. Dumestic, *Adv. Catal.* 38 (1992).

[17] V. Solinas, I. Ferino, *Catal. Today* 41 (1998) 179.

[18] A. Auroux, *Molecular Sieves, Acidity and Basicity: Determination by Adsorption Microcalorimetry*, Springer (Berlin), 2008.

[19] C.E. Webster, R.S. Drago, M.C. Zerner, *J. Am. Chem. Soc*. 120 (1998) 5509.

[20] A.W. Chester, E.G. Derouane, *Zeolite Characterization and Catalysis*, Springer (Dordrecht), 2009.

[21] E. Wiberg, N. Wiberg, *Inorganic Chemistry*, Academic Press (Oxford), 2001.

[22] C.E. Housecroft, *Inorganic Chemistry: Solutions Manual*, Pearson (Upper Saddle River), 2007.

[23] G. Busca, *Phys. Chem. Chem. Phys*. 1 (1999) 723.

Chapter III

Experimental procedures and instrumentation

3.1. Materials

Tetraethylorthosilicate ($Si(OC_2H_5)_4$,TEOS, 98 %), Pluronic P123 triblock copolymer ($EO_{20}PO_{70}EO_{20}$), hexamethylenediamine (HMI, 99 %), tetraethylammonium hydroxide (TEAOH, 20 % in water), polydiallyl dimethyl ammonium chloride (PDADMAC, 20 % in water; typical Mw = 200,000-300,000 g/mol) aluminium nitrate ($Al(NO_3)_3 \cdot 9H_2O$, 98.5 wt%), silica (SiO_2 Aerosil, Degussa), tin (V) chloride pentahydrated (99 wt%), ammonium hydroxide solution (28 % in water, 99.99 %), methanol (99.8 %), diethyl ether (≥ 99.8 %), ethanol (99.8 %), *n*-eptane (anhydrous, 99 %), N-methyl-N-trimethylsilyltrifluoroacetamide (MSTFA, derivatization grade), 1,2,3-tridecanolylglycerol (tricaprin, 99 wt%), sodium hydroxide solution (0.1 M), nitric acid (70 %), hydrofluoric acid (40 %), dihydroxyacetone dimer (97 wt%), 1,1,2,2-tetramethoxypropane (99 wt%), and (-)-methyl L-lactate (98 wt% optical purity ee: 97 %) were purchased from Aldrich. Sodium aluminate ($NaAlO_2$: 56%Al_2O_3, 37%Na_2O) and sodium chloride (99.5 %) were provided by Carlo Erba, while HCl (37 %) was a Merck product. Pyruvaldehyde dimethyl acetal (> 97 %) was provided by Alfa Aesar. *Jatropha curcas* oil was supplied by Vero Energia Italia. Soybean oil was a supermarket shelf product.

3.2. Catalysts Synthesis

3.2.1. Al-SBA-15

Al-SBA-15 catalysts, with different Si/Al molar ratios, were prepared by a modified two-step "pH-adjusting" method [1] by using $Al(NO_3)_3 \cdot 9H_2O$ as aluminium source (instead of $NaAlO_2$) and a hydrothermal treatment of 48 h. Step 1: 4 g of Pluronic P123, 6.7 g of NaCl, and 126 mL of 1 M HCl aqueous solution were stirred at 40 °C until the complete dissolution of surfactant. The appropriate amount (8.5 g) of TEOS was then added drop-wise to the above solution and the mixture was kept under magnetic stirring at 40 °C for 24 h. The amount of $Al(NO_3)_3 \cdot 9H_2O$ required to obtain the desired Si/Al molar ratio was then added, followed by magnetic stirring for 24 h at 40 °C. The resulting gel was introduced into a 250 mL Teflon-lined stainless steel autoclave and submitted to a first hydrothermal treatment at 100 °C for 48 h. Step 2: the suspension resulting from step 1 was cooled to ambient temperature and then the pH value of the mother liquor was adjusted to 5 with ammonia under stirring. The mixture was submitted to a second hydrothermal treatment in autoclave at

100 °C for 48 h. The solid was separated by filtration, washed with distilled water, dried at 60 °C overnight, and calcined in oven at 550 °C for 5 h (heating rate 4 °C/min).

3.2.2. Beta zeolites

Two Beta zeolites, differing as to the Si/Al ratio, were synthesized in according to the Mobil Patent in Ref 2. 0.16 g of NaOH, the appropriated amount of $NaAlO_2$ (depending on the Si/Al molar ratio) and 20 g TEAOH (tetraethyl ammonium hydroxide, 35 wt%) were stirred at room temperature in a Teflon vessel until complete dissolution of the surfactants. Then 4.8 g of SiO_2 (Aerosil silica) were added step-wise with the help of a little amount of distilled water and the reaction mixture was stirred for 1 h. The obtained gel was transferred into a Teflon-lined stainless steel autoclave and submitted to a hydrothermal treatment at 140 °C for 20 h. The resulting solid was separated by filtration under vacuum, washed with distilled water, and dried at 60 °C overnight. The template TEAOH was removed by calcination at 550 °C for 5 h (heating rate, 2 °C/min). The samples were ion-exchanged with an aqueous solution of NH_4NO_3 (2 M) and stirred continuously at 80 °C for 1 h. The procedure was repeated for three times. After being filtered and dried, the catalysts were calcined at 500 °C for 5 h in air.

3.2.3. Hierarchical Beta zeolites

Hierarchical Beta zeolites were synthesized by using TEAOH (tetraethyl ammonium hydroxide) as template and polydiallyl dimethyl ammonium chloride (PDADMAC) as co-template, following the procedure reported in Ref 3. 0.16 g of NaOH, the appropriate amount of $NaAlO_2$ (depending on the Si/Al molar ratio) and 20 g TEAOH (tetraethyl ammonium hydroxide 35 wt%) were mixed under mechanical stirring at room temperature in a Teflon vessel until complete dissolution of the surfactants. Then 4.8 g of SiO_2 (Aerosil silica) were added step-wise with the help of a little amount of distilled water and the reaction mixture was stirred for 1 h. The appropriate amount of the cationic polymer polydiallyldimethyl ammonium chloride (PDADMAC) was added and the mixture was left under stirring at room temperature for 24 h. The final gel was transferred into a Teflon-lined stainless steel autoclave and submitted to a hydrothermal treatment at 140 °C for 168 h. The resulting solid was separated by filtration under vacuum, washed with distilled water and

dried at 60 °C overnight. TEAOH and PDADMAC templates were then removed by calcination at 550 °C for 5 h (heating rate, 2 °C/min). The samples were ion-exchanged with an aqueous solution of NH_4NO_3 (2 M) and stirred continuously at 80 °C for 1 h. The procedure was repeated for three times. After being filtered and dried, the catalysts were calcined at 500 °C for 5 h in air.

3.2.4. MCM-22 zeolites

MCM-22 samples with different Si/Al molar ratios were synthesized by the procedure reported in Ref 4. The appropriate amounts of all the reactants were calculated in accordance with the following molar composition: 0.5 Al_2O_3 : (x/11.11) Na_2O : (x/2) HMI : x SiO_2 : (x/0.022) H_2O. A sample with Si/Al = 15 was prepared as follows: 0.45 g of sodium aluminate and 0.4 g of sodium hydroxide were dissolved in 67.5 g of distilled water. 4.09 g of hexamethyleneimine were added drop-wise to the solution and it was left under stirring for 10 minutes. Then 4.95 g of silica were added stepwise under stirring. After 30 min under stirring the resulting gel was transferred in a Teflon-lined stainless-steel autoclave and then left under rotation at 150 °C for 220 h. The autoclave was cooled in water and the solid sample was filtered, washed with distilled water, and dried at 70 °C. The template was removed by calcination using the following program:

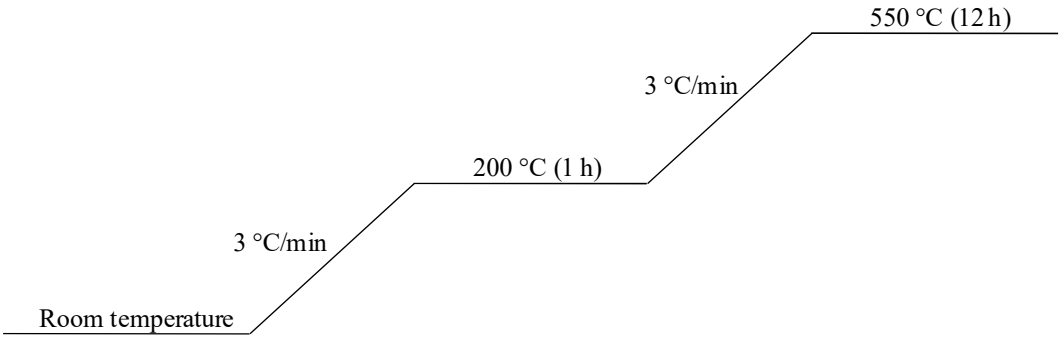

The samples were ion-exchanged with an aqueous solution of NH_4NO_3 (2 M) and stirred continuously at 80 °C for 1 h. The procedure was repeated for three times. After being filtered and dried, the catalysts were calcined at 500 °C for 5 h in air.

3.3. Characterization of the catalysts

3.3.1. Inductively coupled plasma atomic emission spectroscopy (ICP-AES)

ICP-AES analyses were performed on a Varian Liberty 200 vacuum unit inductively coupled plasma emission spectrometer to determine the chemical composition of the calcined catalysts. Before analysis, a HF solution (40 wt%) was added to a known amount of sample, and the mixture was then heated until the complete dissolution of the solid was achieved. The residue remaining after evaporation was solubilized with 2 mL of aqua regia and then diluted to a known volume with bidistilled water.

3.3.2. X-ray diffration (XRD)

Low-angle and wide-angle X-ray diffraction patterns were recorded on a Seifert X3000 diffractometer with a θ-θ Bragg Brentano geometry using Cu-Kα radiation and a graphite monochromator before the scintillation detector.

3.3.3. N_2 adsorption/desorption

Textural analysis was carried out with a Micromeritics ASAP 2020 apparatus by determining the nitrogen adsorption/desorption isotherms at -96 °C. Before analysis, the samples were pretreated overnight under vacuum (10^{-3} Pa) at 250 °C for 12 h. Specific surface area was determined by the Dubinin-Radushkevich and BET methods for microporous and mesoporous materials, respectively. Micropore volumes were calculated from the t-plot method through the use of the Harkins–Jura equation, while the BJH method was used for assessing the mesopore volume. From the desorption branch of each isotherm, the pore size distribution was also obtained (Horvath-Kawazoe method for microporous materials and the BJH model for mesoporous materials) [3 (and literature therein)].

3.3.4. ^{27}Al Magic Angle Spinning Nuclear Magnetic Resonace (^{27}Al MAS NMR)

High resolution ^{27}Al MAS NMR spectra were collected using a Varian UNITY INOVA Spectrometer with a 9.39 T wide-bore Oxford magnet equipped with a 4 mm probe. The experiments were performed by packing 100 mg of sample in a 4 mm Si_3N_4 rotor at a spinning rate of 7 KHz. Each experiment was run with a recycle time of 500 us, 90° pulse

lengths (6.6 ms), and 5000 scans. ^{27}Al chemical shifts were referenced to $Al(NO_3)_3$ aqueous solution. Quantitative information on the ^{27}Al atom environments was obtained by fitting the signals with Gaussian curves using the software package Origin 9 from OriginLab Corporation.

3.3.5. NH_3 adsorption microcalorimetry

A Tian-Calvet heat flow microcalorimeter (Setaram) equipped with a volumetric vacuum line was used for microcalorimetric measurements. Each sample (0.1 g) was thermally pre-treated at 250 °C for 12 h under vacuum ($5 \cdot 10^{-3}$ Pa). The H-MCM-22 samples were also investigated after pre-treatments at 80 and 400 °C under vacuum. Adsorption was carried out at 80 °C by admitting successive doses of the probe gas (ammonia) and recording the thermal effect. The equilibrium pressure relative to each adsorbed amount was measured by means of a differential pressure gauge (Datametrics) and the thermal effect was recorded. The run was stopped at a final equilibrium pressure of about 130 Pa. The adsorption temperature was maintained at 80 °C, in order to limit physisorption. The adsorption isotherm (relating the amount of probe gas with the corresponding equilibrium pressure) and the calorimetric isotherm (relating the integral heat of adsorption with the corresponding equilibrium pressure) were obtained from each adsorption run. Combining the two sets of data, a plot of the differential heat of adsorption as a function of the adsorbed amount was drawn, which gives information on the influence of the surface adsorbed amount on the energetics of the adsorption.

3.3.6. Fourier Transform Infrared (FTIR) spectroscopy and CO adsorption FTIR spectroscopy

FTIR spectra of the H-MCM-22 samples were registered with a Nicolet Avatar 360 spectrometer. The spectra were recorded accumulating 64 scans at a spectral resolution of 2 cm^{-1}. Self-supporting wafers (*ca.* 10 mg/cm^2) were prepared from the sample powders and treated directly in a purpose-made IR cell. The cell was connected to a vacuum-adsorption apparatus allowing a residual pressure below 10^{-3} Pa. The samples were pretreated by evacuation at different temperatures ranging from 100 to 480 °C. The measures were performed after cooling the samples at room temperature. The CO adsorption FTIR measures

were carried out cooling the sample to liquid nitrogen temperature after preliminary treatment at 100 °C and 450 °C. CO was sent to the sample cell until the pressure was about 200 Pa. The spectra were registered until no spectral changes were observed. The adsorption was followed by slow evacuation in order to desorb the CO adsorbed on the surface of the sample. FTIR measures were carried out also during the desorption of CO in order to get information on the band stabilities.

3.4. Characterization of the oils

The fatty acid distribution in soybean and *Jatropha curcas* oils was determined as follows: 0.5 g of oil and 2 mL of 5 wt% KOH in methanol were mixed in a screw capped vial. The vial was shaken for 30 min at room temperature and the formed methyl esters extracted by adding 2 mL of hexane. The upper phase was dried with sodium sulfate and the methyl esters were analyzed with a Gas Chromatograph Agilent 6890 equipped with a FID. A capillary column (length 30 m, internal diameter 0.25 mm, film thickness 0.25 μm) Supelcowax^{TM} 10 was used, with nitrogen as the carrier gas. The column oven temperature was set at constant temperature (190 °C) for the whole analysis duration (15 min). The injector and detector temperatures were set at 250 °C and 260 °C, respectively. FAMEs were quantified by means of the internal normalization method. For the determination of the FFAs content, oleic acid was used in the analysis calibration as a molecule representative of the free fatty acid. The FFA content expressed as mg of KOH required to neutralize the free fatty acids in 1 g of oil (acid number), was determined according to the standard ASTM D 974 procedure.

3.5. Catalytic testing

3.5.1. Transesterification of vegetable oils

The transesterification reaction was carried out in a 100 mL stainless steel batch reactor (Parr 4843), equipped with intake and exhaust valves for N_2, liquid sampling valve, pressure gauge, internal thermocouple, and stirrer. The reactor was fitted with a heating

mantle, which allowed the achievement of a uniform temperature. A reaction temperature of 180 °C was considered a balanced choice, in order to ensure the occurrence of the transesterification reaction to a significant extent while limiting the possibility that undesired reactions take simultaneously place. Because of the methanol volatility at such temperature, the runs were carried out under a pressure of 4 MPa.

In a typical run, $1.25 \cdot 10^{-2}$ mol of oil and $1.50 \cdot 10^{-1}$ mol of methanol were charged into the reactor and contacted with 1 g of freshly calcined (12 h at 500 °C) catalyst. No differences in the FAMEs yield (as defined in equation below) were observed in preliminary runs carried out with a stirring speed of 200, 400, and 600 rpm, which indicated the absence of mass transfer limitations. It was however considered safer to work at a stirring speed of 400 rpm instead of 200 rpm. Such stirring speed seemed also more appropriate than 600 rpm, in order to avoid any possible risk of spreading of the reaction mixture onto the walls of the reaction vessel. After a given reaction time, the reactor was cooled down to room temperature by immersion into an ice-bath and the sample collected in a closed vial for analysis. An Agilent 6890 Series on-column gas-chromatograph equipped with a capillary column (MXT-Biodiesel TG from Superchrom, 15 m length, 0.32 mm ID, 0.10 μm film thickness with 2 m of 0.53 mm ID Guard) and a FID was used. Helium was the carrier gas. The temperature programme of the oven was as follows: from 50 °C (hold 1 min) to 180 °C (heating rate 15 °C/min), from 180 °C to 230 °C (heating rate 7 °C/min) and from 230 °C to 380 °C (heating rate 30 °C/min), then hold for 10 min. The temperature of the detector was set at 380 °C. The reaction products were identified by GC-MS (7820A Agilent GC coupled with 5975 Agilent MSD). The measurements were carried out by working in electron impact at 70 eV with a source temperature of 100 °C. The GC details were as follows: carrier gas He, HP-5-MS capillary column (30 m length, 0.25 mm ID, 0.25 μm film thickness), oven temperature program from 150 °C to 270 °C (heating rate 15 °C/min).

Besides glycerol and methyl esters, monoglycerides, diglycerides, and FFAs were also produced. The evolution of the FAMEs and FFAs content as a function of the reaction time was determined. Methyl palmitate (MeP), methyl oleate (MeO), methyl linoleate (MeL), methyl linolenate (MeLn), and methyl stearate (MeS) were monitored in the reaction mixture. Tricapryn was used as an internal standard. Approximately 0.08 g of the reaction mixture was weighed in a vial and a sample of 500 μL of tricapryn solution (0.1 g of tricapryn diluted to

100 mL in *n*-heptane) was added. 5 µL of this solution were functionalized with 20 µL of MSTFA and set for 15 to 20 min at room temperature. For the GC analysis, 1 µL of the functionalized sample was injected on-column and the peak areas of the compounds were integrated. The FAMEs yield was calculated according to the following equation:

$$\text{yield}\,(\text{mol}\%) = \frac{\text{mass FAMEs produced}/\text{MM}_{\text{av}}\ \text{FAMEs}}{3 \times (\text{mass oil loaded}/\text{MM}_{\text{av}}\ \text{oil})} \times 100$$

where MM_{av} is the experimental average molar mass and the factor 3 takes into account that each triglyceride molecule yields three methyl ester molecules.

The nature of the organic material retained by the catalyst during the reaction was determined after dissolution of the spent catalyst in 40 wt% HF at room temperature, extraction in methylene chloride, and almost complete evaporation of the solvent by analysis with GC-MS (7820A Agilent GC coupled with 5975 Agilent MSD) with an oven temperature program from 40 °C (hold 3 min) to 260 °C (heating rate, 40 °C/min).

3.5.2. Conversion of dihydroxyacetone to methyl lactate

The catalytic reaction was performed in a sealed batch reactor (Ace pressure tube, volume 15 mL) under autogenous pressure with magnetic stirring. 4 g of a 0.25 M dihydroxyacetone solution in methanol and 0.08 g of catalyst were put into the reactor. After closing, the reactor was introduced and maintained in a hot oil bath in order to have a constant internal temperature of 115 °C. The reaction was stopped after the desired reaction time and the reaction mixture was cooled to room temperature and centrifuged, in order to separate the solid catalyst. The reaction solution was analysed with an Agilent 6890 Series GC System equipped with a capillary column (HP-5 Crosslinked 5 % PH ME Siloxane; length, 30 m; ID, 0.32 mm; film thickness, 0.25 µm) and a FID, using He as carrier gas. The main products (methyl lactate, pyruvaldehyde dimethyl acetal, and 1,1,2,2 tetramethoxypropane) were identified by comparison with the pure compounds and quantified using *n*-eptane as an internal standard. The results are expressed in terms of yields (mol%) and the conversions (mol%) were calculated as the sum of the yields of the main products.

References

[1] C. Li, Y. Wang, Y. Guo, X. Liu, Y. Guo, Z. Zhang, Y. Wang, G. Lu, *Chem. Mater.* 19 (2007) 173.

[2] R.L. Wadlinger, G.T. Kerr, E.J. Rosinski, *Catalytic Composition of a Crystalline Zeolite*, Mobil Oil corporation US Patent 3,308,069, 1967.

[3] F. Rouquerol, J. Rouquerol, K.S.W. Sing, P. Llewellyn, G. Maurin, *Adsorption by Powders and Porous Solids, Principles, Methodology and Applications*, Second Edition, Elsevier (Amsterdam) 2014.

[4] J.C.J. Bart, N. Palmeri, S. Cavallaro, *Biodiesel Science and Technology. From Soil to Oil*, CRC Press (Boca Raton) 2010.

[5] P. Magnoux, P. Roger, C. Canaff, V. Fouche, N.S. Gnep, M. Guisnet*, Stud. Surf. Sci. Catal*. 34 (1987) 317.

Chapter IV

Transesterification of vegetable oils

4.1. Introduction

4.1.1. Biodiesel and glycerol

Biodiesel is defined by ASTM as "a fuel comprised of mono-alkylesters of long-chain fatty acids derived from vegetable oils or animal fats, designated B100" [1]. It is an environmental friendly diesel fuel substitute made from renewable biological sources such as vegetable oils and animal fats by chemically reacting oil or fat with an alcohol (transesterification), in the presence of a basic or an acidic catalyst. The reaction is schematized in Fig. 4.1A. The products of the reaction are alkyl esters (fatty acid alkyl esters, FAAEs) and glycerol, which is a high value co-product. Alkyl esters are also obtained by esterification of free fatty acids contained in oils with an alcohol in the presence of an acidic catalyst, as schematized in Fig. 4.1B.

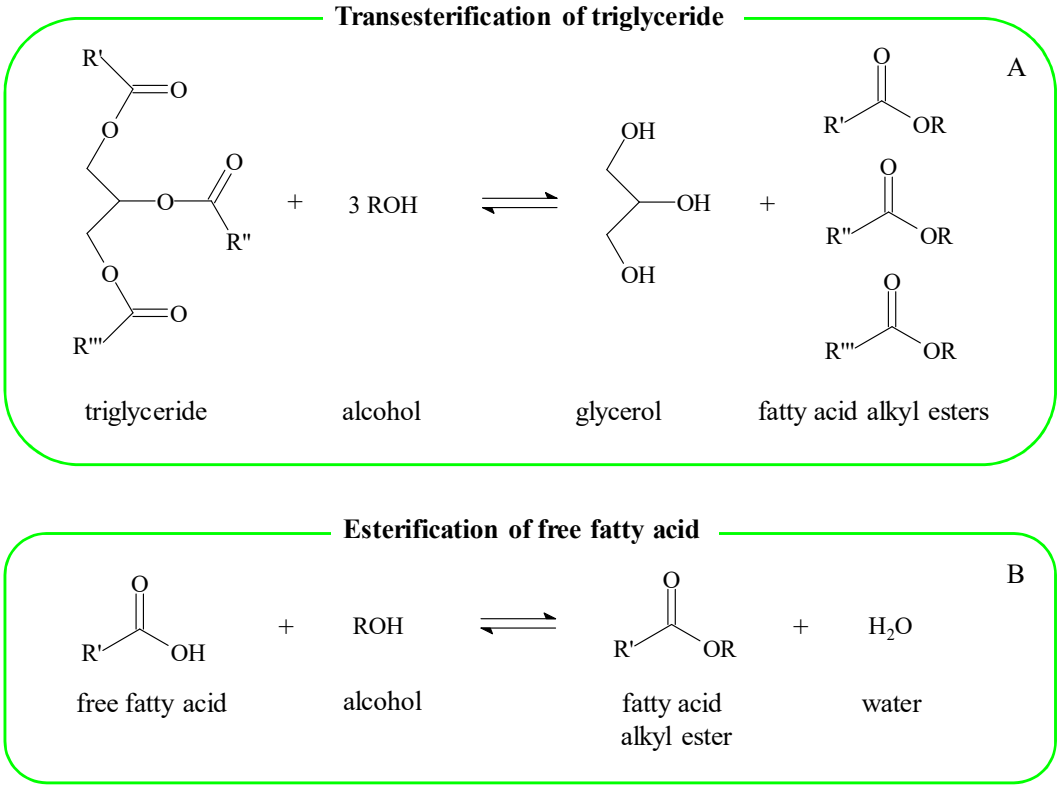

Figure 4.1. Scheme of reaction for transesterification of triglycerides (**A**) and for esterification of free fatty acids (**B**).

FAAEs are renewable, biodegradable and non-toxic [2]. Biodiesel makes a little contribution to global warming because this fuel is characterized by a closed carbon cycle where the CO_2 from its combustion is absorbed through photosynthetic ways. A life cycle analysis of biodiesel showed that overall CO_2 emissions were reduced by 78 % compared to petroleum-based diesel [3]. Biodiesel has a higher cetane number than diesel fuel, no aromatics, almost no sulphur, and contains 10-11 wt% oxygen [4]. These characteristics reduce exhaust emissions of carbon monoxide, unburned hydrocarbons, and particulate emissions compared to petroleum-diesel fuel [5]. Important disadvantages of biodiesel include high feedstock cost, inferior storage and oxidative stability, lower volumetric energy content, inferior low-exhaust temperature operability versus petrodiesel, and -in some cases- higher NO_x exhaust emissions [1].

Glycerol besides being a co-product in the production of biodiesel, is also a co-product of other important industrial productions such as oil/fats saponification and fatty acids production. Lately an intense debate has focused on the inevitable production of a surplus of glycerol as a by-product with a low commercial value in the production of biodiesel [6]. For this reason scientists are developing technologies to convert or use glycerol in order to improve the biodiesel business and drastically improve its economic viability [6].

Glycerol is most commonly used without modification, or very basic structural modifications, as an additive. Its uses, represented in Fig. 4.2, are in the manufacture of food and beverages, tobacco, pharmaceutical, personal care products, urethane foams, and synthetic resins [7]. However in the majority of products it is only used in small quantities [6].

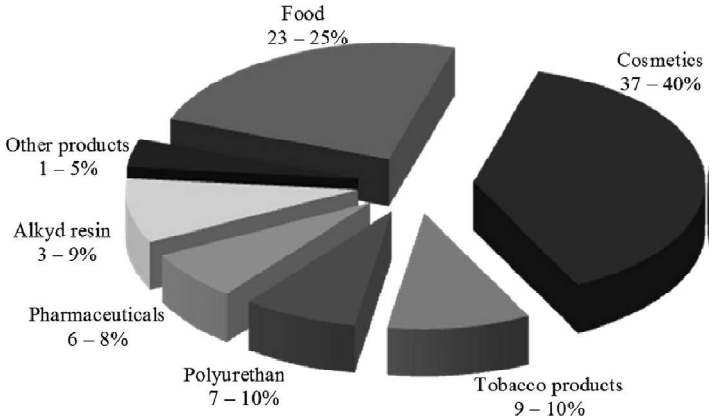

Figure 4.2. Scheme of the traditional uses of glycerol with average worldwide values [6].

Glycerol is a highly functionalized molecule compared to petro-chemically produced hydrocarbons, thus a large number of added value chemicals can be produced from glycerol *via* various type of chemical reactions, schematized in Fig. 4.3 [8]. The development of new applications could be the most constructive approach to utilize excess glycerol.

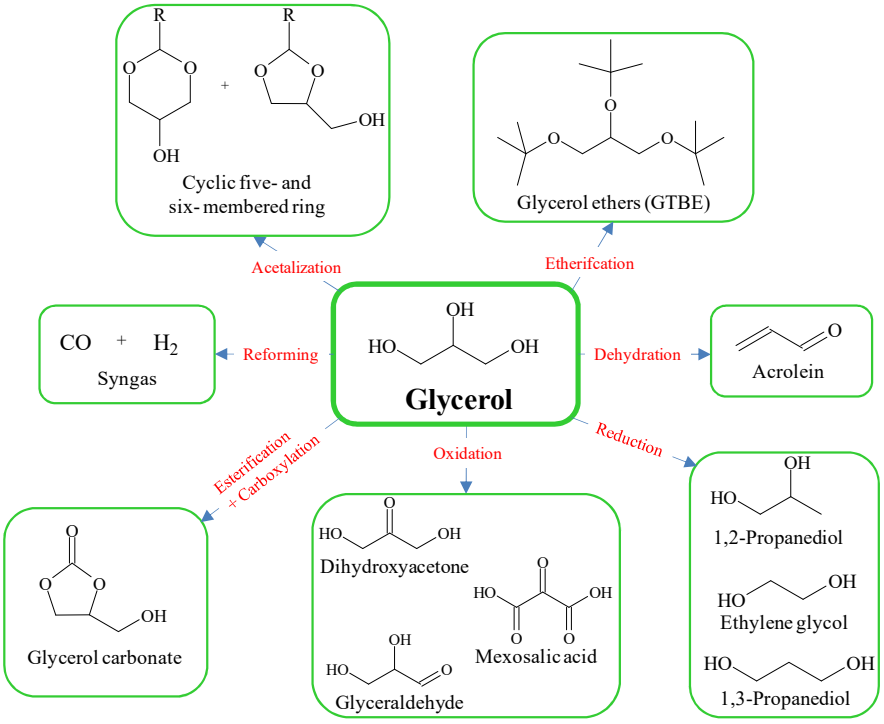

Figure 4.3. Scheme of the main reactions of glycerol to value-added chemicals [7,9].

4.1.2. Biodiesel production

The transesterification reaction is reversible, although the backward reaction is negligible largely because glycerol is not miscible with fatty acid alkyl esters. The reaction system is biphasic at the beginning and at the end of biodiesel production because alcohol (in particular methanol), vegetable oils, glycerol, and FAMEs are not miscible [1].

Most of commercial biodiesel is obtained from soybean or rapeseed oil and methanol by alkaline catalysis [10]. Methanol is most commonly used since it is generally less expensive than other alcohols, but ethanol prevails in regions such as Brazil where it is less expensive than methanol [1]. Homogeneous base alkaline catalysts such as sodium or potassium hydroxide or methoxide are typically used because they are inexpensive and very effective in the commercial production of biodiesel from refined or treated oils [11]. The

classic conditions for alkaline transesterification include triglycerides reacting with an excess of methanol (methanol/oil molar ratio 6) and 0.5 wt% of alkali catalyst (with respect to triglycerides) at 60 °C and atmospheric pressure for 1 h to produce FAMEs and glycerol [1,12].

However with feedstocks containing significant percentages of free fatty acids (FFAs), typical homogeneous alkaline base catalysts will not be effective as a result of the unwanted side reaction schematized in Fig. 4.4A, in which the catalyst reacts with FFAs to form soap and water, thus irreversibly quenching the catalyst and resulting in an undesirable mixture. In fact, base-catalyzed transesterification will not occur or will be significantly retarded if the FFAs content of the feedstock is 3 wt% or larger [1]. The undesirable soap production requires energy intensive separation operations that represent more than half of the total investment in equipment for the fuel industries [13]. A further complicating factor of high FFAs content is the production of water which is obtained either by esterification (Fig. 4.1B) or by saponification of FFAs, as shown in Fig. 4.4A. The produced water is particularly problematic because it can hydrolyze fatty acid alkyl esters obtained producing additional FFAs and methanol, as schematized in Fig. 4.4B [1].

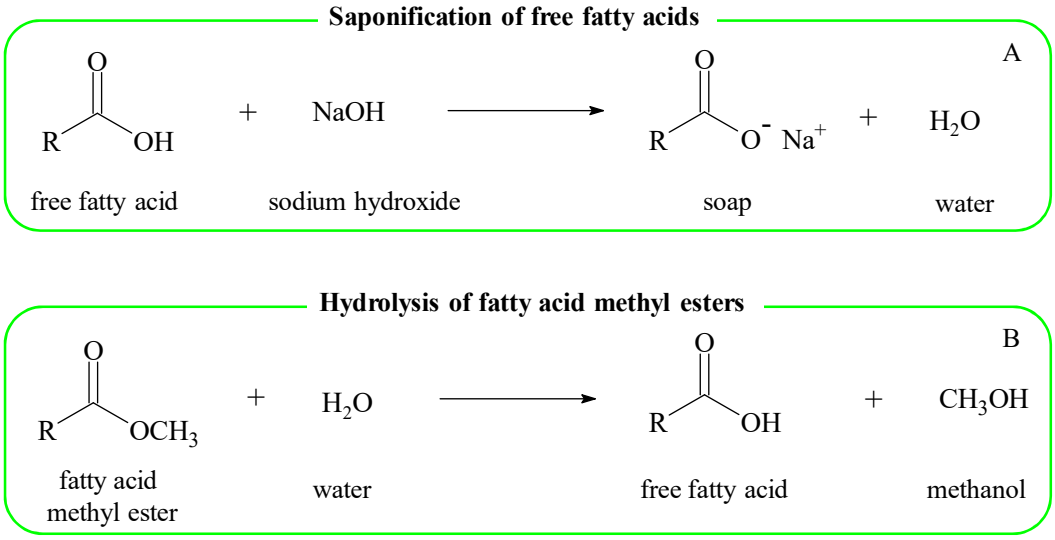

Figure 4.4. Scheme of reaction for the typical side reactions in alkaline transesterification of triglycerides: the saponification of free fatty acids (**A**) and the hydrolysis of fatty acid methyl esters (**B**).

The use of solid basic catalysts bring the advantages of the heterogeneous on the homogeneous catalysis, but does not permit, in any case, the overcoming of the problems related to the use of acidic feedsocks, because of the deactivation of the active sites.

The acid-catalyzed biodiesel production is about 4,000 times slower than the corresponding base-catalyzed process, needing higher temperatures and pressures. Nevertheless it is not adversely influenced by the presence of FFAs, indeed acid catalysts can simultaneously catalyze triglyceride transesterification and free fatty acids esterification [1]. This advantage permits the use of secondary and cheap raw materials such as waste oils and most of other non-food feedstock, which usually contain significant amount of free fatty acids [4]. Biodiesel production from low-cost raw materials can be carried out by two-step processes where the acid-catalyzed esterification of FFAs is combined with the base catalyzed transesterification of triglycerides [14]. However economic analysis has proven that the two-step process is less economical than the one-step acid-catalyzed process [2].

4.1.3. Heterogeneous acid catalysts for biodiesel production

Recently a lot of work has been carried out in relation to solid acids as catalysts for either transesterification or esterification or together. Compared with conventional homogeneous acids, heterogeneous acid catalysts are easily removable, reusable, and non-corrosive. Furthermore, the heterogeneous catalysts allow to be used in a continuous flow reactor. Continuous processes can minimize product separation and purification costs, making biodiesel economically viable and able to compete with commercial petroleum-based diesel fuel [2].

Solid acid catalysts that have been investigated as a potential alternative to mineral acids in the transesterification of several oils include Amberlyst® 15 [15] and Nafion® resins [16], sulphated zirconia [17], tungsten oxides [18], and La^{3+}exchanged Beta zeolites [19]. Besides the low surface area, a limit of the ion exchange resins is their thermal stability, which becomes a problem at the high temperatures needed to achieve a sufficiently high reaction rate. Sulfated zirconia, though active, selective, and thermally stable under the process conditions, undergoes leaching of sulfate species, which compromises the reusability of the catalyst. Remarkably high temperature and long reaction time are necessary for achieving a high conversion on zirconia and zirconia/alumina-supported WO_3. Over

La^{3+}exchanged zeolites the reaction is supposed to take place only at the external surface sites, as the diffusion of the cumbersome triglyceride molecules would be severely limited in the microporous channel system of such solids.

4.1.4. Feedstocks

First generation biodiesel is derived from edible vegetable oils such as soybean, palm, oilseed rape, and sunflower. These are food-grade oils significantly more expensive than petroleum used for diesel fuel. Currently the most of commercial production of biodiesel is of first generation and is dominated by United States, Europe Union, Brazil, and Malaysia [20,21]. The high cost of the common feedstocks and the rapid increase of the biodiesel production have made necessary the development of alternative feedstocks such as non-edible oilseed plants, microalgae, animal fats, and waste oils. Biodiesel derived from these feedstocks is named second generation biodiesel [21]. Waste cooking oil is far less expensive than refined vegetable oils and therefore has become a promising alternative feedstock to produce biodiesel. In fact, generation of waste cooking oil in any country in the world is huge, and may result to environmental contamination if no proper disposal method is implemented [2]. The overall production costs (70-95 % of the final costs) of biodiesel can be reduced by more than half compared to virgin vegetable oil [22,23]. Algal biomass has received considerable recent attention, since lipids from algae can be used for biodiesel production via conventional transesterification technologies. Microalgae are fast-growing and produce higher oil yields than plant counterparts on land unusable for plant cultivation and without fresh water [21]. However at the moment microalgae are not a feasible choice because of the extensive energy input due to the strong dependence on fertilizers and the complicated extraction of lipids due to the fact that physical extraction methods are not suitable [24,25]. Non-edible oils from terrestrial crops constitute another valid source for biodiesel production. They are easily available in many parts of the world and very cheap compared to edible oils. Some of these oilseed plants grow also in the so-called “marginal lands”, arid and poor lands near deserts and other inhospitable areas, reducing the competition with food crops for water, soil and energy [26]. *Jatropha curcas* is one of the most promising oilseed plant for biodiesel production. It is native to tropical America but now is diffused in tropical and subtropical regions of Africa and Asia. It has the capability to grow on marginal soils, adapts to wide

agro-climatic conditions, and is very resistant to drought. The extracted oil is not edible because it is poisonous. The *Jatropha curcas.* fruits have a high oil content, consisting of around 30-40 wt% seed oil against the 20 wt% of soybean seeds. *Jatropha* seed yields can vary from 0.5 tons per hectare under arid conditions to 12 tons per hectare under optimum conditions [27]. The oil has a high content of free fatty acids, ranging from 4 to 10 wt% (at variance with 1 wt% for soybean oil), so it is not suitable for base catalysts or it needs a preliminary esterification step [26]. The *Jatropha* biodiesel has good properties and only slightly worse cold-flow properties (cloud and pour point) compared to soybean biodiesel, but still a far better cold stability than biodiesel obtained from more saturated feedstocks such as palm oil or tallow [28].

4.2. Results and discussion

The transesterification of soybean oil was performed with methanol over acidic hierarchical Beta zeolites and Al-SBA-15 mesostructured materials. For comparison the transesterification behaviour of conventional microporous Beta and MCM-22 zeolites was also investigated. The samples of Al-SBA-15 were tested also in the transesterification of *Jatropha curcas* oil.

4.2.1. Characterization of the oils

The results of the analysis of the fatty acid distribution, carried out following the procedure described in Chapter 3, are reported in Table 4.1. From such distribution average molar masses of 872.90 g/mol and 292.32 g/mol for soybean oil, and 872.16 g/mol and 291.89 g/mol for *Jatropha* oil were calculated for the vegetable oils and the methyl esters, respectively. The FFAs content, determined according to the standard ASTM D 974 procedure and expressed by the acid number, was 0.20 mg_{KOH}/g_{oil} (0.10 wt% of FFAs) and 10.98 mg_{KOH}/g_{oil} (5.49 wt% of FFAs) for soybean oil and *Jatropha* oil, respectively. Besides the different fatty acid distribution, the total FFAs content of *Jatropha* oil was 50 times more acidic than soybean oil.

Table 4.1. The fatty acid distribution (expressed in wt%) for soybean and *Jatropha curcas* oils.

Oil	Palmitic	Palmitoleic	Stearic	Oleic	Linoleic	linolenic
Soybean	10.42	n.d.	3.66	28.08	52.78	5.06
Jatropha c.	15.70	0.85	6.57	46.07	30.81	n.d.

4.2.2. Structural and textural characterization of the catalysts

The ICP-AES results for all the samples gave total Si/Al molar ratio in agreement with the gel compositions, indicating the efficiency of the preparation procedures. Beta and MCM-22 zeolites samples were denoted writing in brackets, next to the name of the catalysts, the corresponding Si/Al molar ratio as Beta(23), Beta(43) and MCM-22(40). Similarly the hierarchical Beta zeolites were denoted as Beta-H(18) and Beta-H(30), while the three Al-SBA-15 samples were denoted as Al-SBA(3), Al-SBA(22) and Al-SBA(73).

The wide-angle X-ray diffraction patterns of the microporous MCM-22 and Beta and micro/mesoporous hierarchical Beta-H zeolites are shown in Fig. 4.5. The formation of crystalline MCM-22 is revealed by comparing the line positions and intensities of the MCM-22(40) pattern with those reported in the literature (Refs. 29-31). The patterns of both the microporous Beta and the hierarchical Beta-H samples show well-resolved peaks in the 5°-40° range, characteristic of the Beta zeolite structure [31-33].

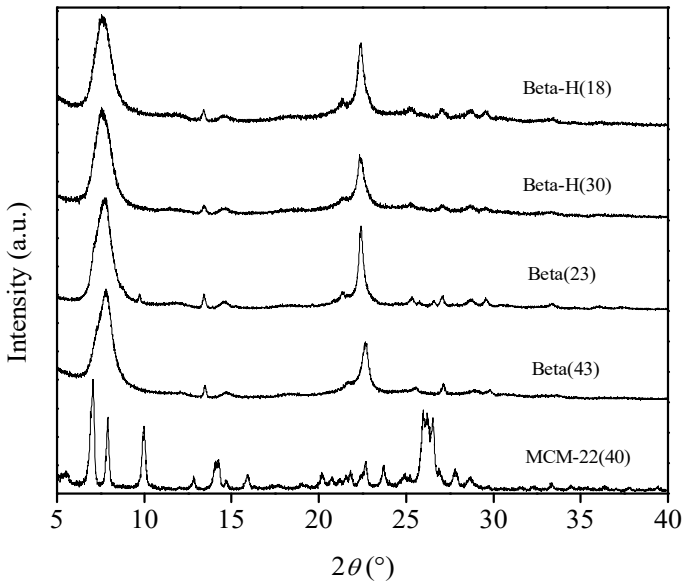

Figure 4.5. Wide angle X-ray patterns for MCM-22, Beta and Beta-H catalysts.

A typical wide angle pattern of an Al-SBA-15 sample, represented in Fig. 4.6, is a clear evidence of its amorphous structure.

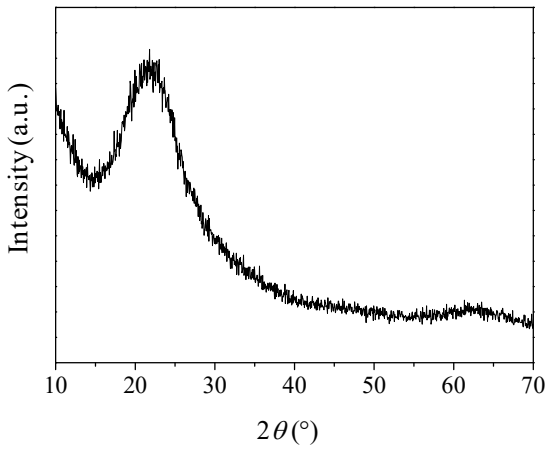

Figure 4.6. Typical wide-angle X-ray diffraction pattern of a sample of Al-SBA-15.

The low-angle X-ray diffraction patterns of the Al-SBA-15 samples, represented in Fig. 4.7, show three well-resolved peaks which can be indexed as the (100), (110), and (220) reflections associated with a hexagonal symmetry. These results are in agreement with the presence of a two-dimensional hexagonal P6 mm structure with a large unit-cell parameter and indicate that the structure is actually representative of a long-range order.

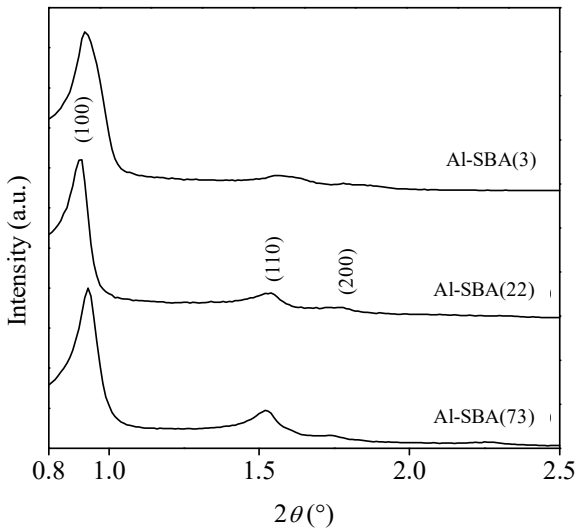

Figure 4.7. Low-angle X-ray diffraction patterns for Al-SBA-15 samples.

The ^{27}Al MAS NMR spectra of the Al-SBA-15 catalysts are shown in Fig. 4.8. Two resonance peaks are visible in each spectrum, at about 55 and 0 ppm, respectively. The resonance at *ca.* 55 ppm can be assigned to aluminium species in tetrahedral coordination $Al_{(IV)}$, whereas the resonance at 0 ppm can be assigned to octahedral aluminium species $Al_{(VI)}$ [34,35]. Comparison of the $Al_{(IV)}$ amount with the total aluminium content revealed that 90, 92 and 87 % of the Al atoms are incorporated in tetrahedral positions for Al-SBA(3), Al-SBA(22) and Al-SBA(73), respectively.

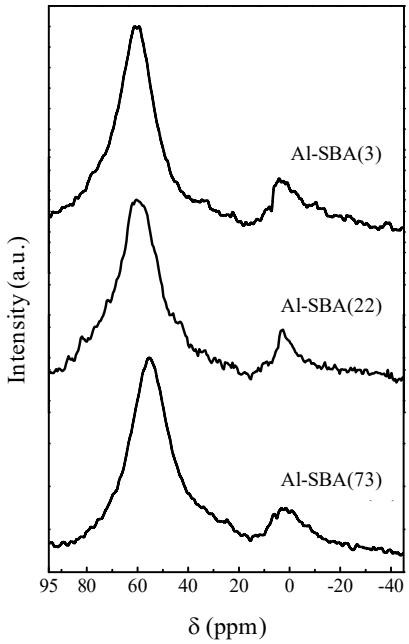

Figure 4.8. ^{27}Al MAS NMR spectra for Al-SBA-15 samples.

Nitrogen adsorption-desorption isotherms for all the samples are reported in Fig. 4.9. The corresponding textural data are given in Table 4.2. The microporous character of MCM-22(40), Beta(23), and Beta(43) is revealed by the steep rise of the adsorbed volume at very low (< 0.1) p/p_0 in their adsorption isotherms, followed by a long plateau extending up to the high p/p_0 values. The presence of a very narrow, vertical hysteresis loop confined in the region at p/p_0 very close to unity in the MCM-22(40) isotherm is taken as an indication [36] of the presence of some slit-shaped, wide mesopores (or narrow macropores), most probably originated by the aggregation of the lamellar particles characteristic of MCM-22 zeolites [29]. The surface area and micropore volume values for the microporous zeolite samples (Table

4.2) are in the range 537-837 m^2/g and 0.17-0.29 mL/g, respectively. The pore size distribution plot (Fig. 4.9F-H) was monomodal and narrow, centred at *ca.* 0.5 nm (Table 4.2).

The isotherms for the two Beta-H samples show the typical "rectangular" shape of microporous solids already observed for MCM-22(40), Beta(23), and Beta(43) associated with a hysteresis loop at relative pressures of 0.7-0.95, which is indicative of the presence of hierarchical mesopores.

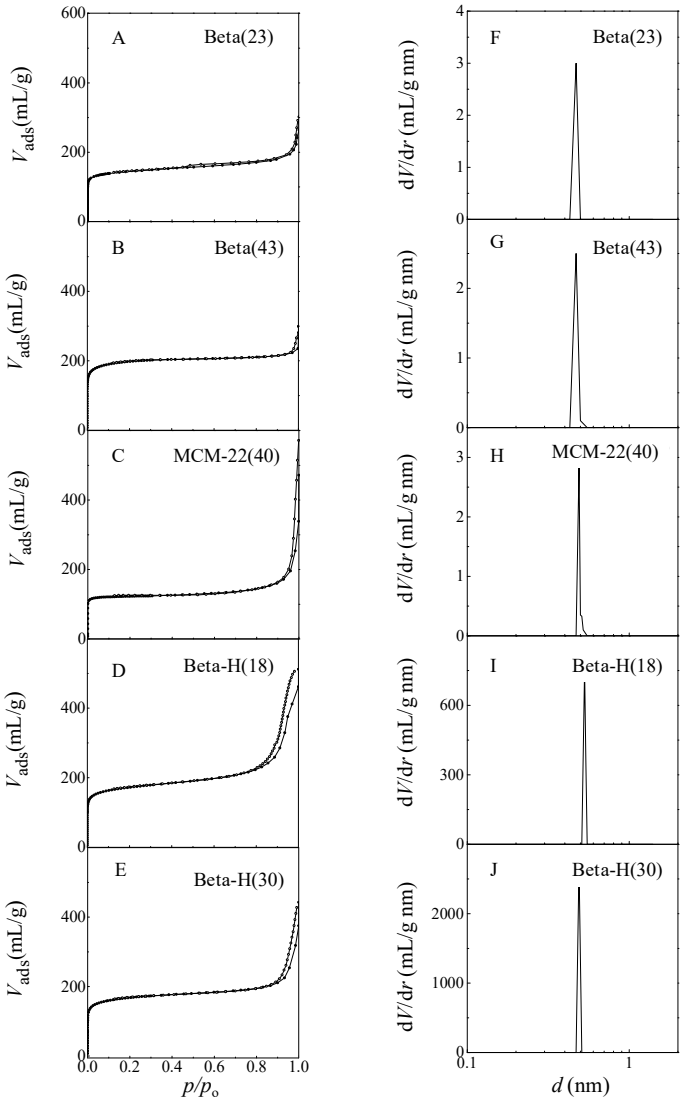

Figure 4.9. Nitrogen physisorption isotherms (**A-E**) and micropore size distribution plots (**F-J**) for Beta, MCM-22 and Beta-H zeolites.

In Table 4.2, data show that their formation, as a consequence of the addition of the cationic polymers during the synthesis [33], occurs without sacrificing the microporosity, which is comparable to that of the conventional microporous MCM-22 and Beta zeolites. The contributions to pore volume from mesopores (V_{meso}) and micropores (V_{micro}) are in the ratio of 2.6:1 and 1.2:1 for Beta-H(18) and Beta-H(30), respectively (Table 4.2). The mesopore size-distribution plots revealed the presence of pores in the range of 5-40 nm, with a dominant contribution to the mesopore volume from pores of *ca.* 30 nm.

Table 4.2. Textural properties of MCM-22, Beta, and Beta-H zeolites.

Sample	SA[a] (m^2/g)	V_{micro}[b] (mL/g)	V_{meso}[c] (mL/g)	D_{micro}[d] (nm)	D_{meso}[e] (nm)
Beta(23)	605	0.18		0.50	
Beta(43)	837	0.29		0.47	
MCM-22(40)	537	0.17		0.49	
Beta-H(18)	537	0.21	0.55	0.53	6.0-18.0-30.0
Beta-H(30)	516	0.22	0.26	0.49	30.1
Al-SBA(3)	479		0.86		6.5
Al-SBA(22)	519		0.80		6.4
Al-SBA(73)	678		1.02		6.1

[a]Specific surface area (Dubinin-Radushkevich and BET methods).
[b]Micropore volume (calculated from the t-plot by the Harkins-Jura equation).
[c]Mesopore volume (calculated by the BJH method).
[d]Micropore diameter (Horvath-Kawazoe method).
[e]Mesopore diameter (BJH method).

The nitrogen adsorption-desorption isotherms of the Al-SBA-15 catalysts, reported in Fig. 4.10A-C, can be classified as type IV and exhibit an H1-type hysteresis loop at high relative pressure, which are typical features for mesoporous materials with cylindrical

channels open at both ends. The pore size-distribution plot, shown in Fig. 4.10D-F, indicate for each sample a monomodal, narrow distribution centred at 6.5, 6.1, and 6.4 nm for Al-SBA(3), Al-SBA(22) and Al-SBA(73), respectively. Surface area values of 479, 519, and 638 m^2/g, and pore volume values of 0.86, 0.80, and 1.02 mL/g were calculated for the samples with Si/Al = 3, 22 and 73, respectively.

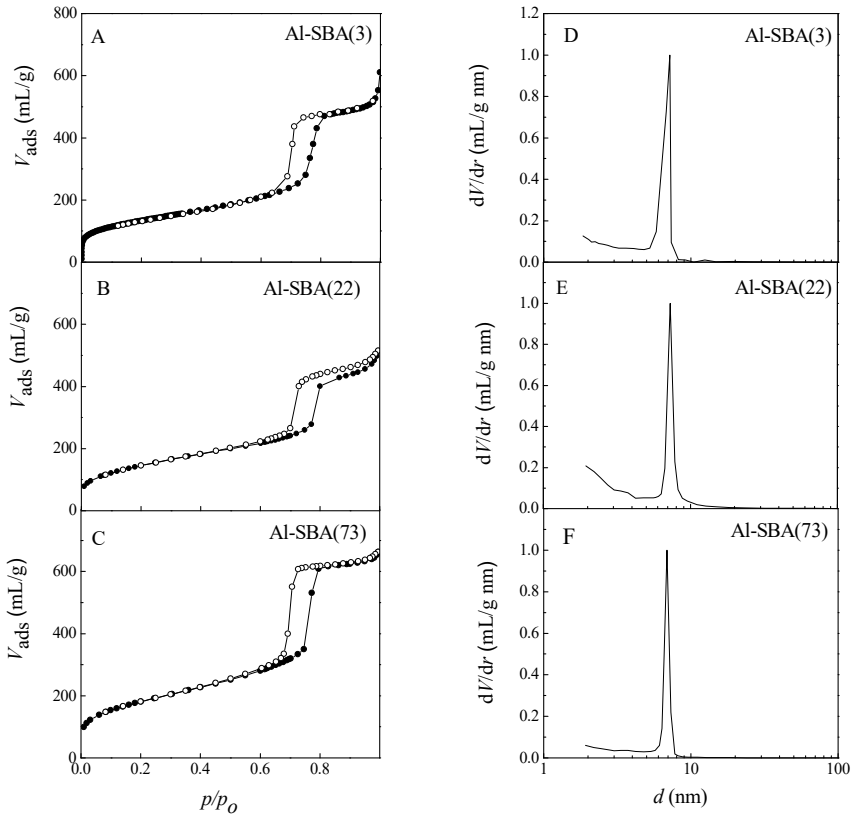

Figure 4.10. Nitrogen physisorption isotherms (**A-C**) and micropore size-distribution plots (**D-F**) for Al-SBA-15 samples.

4.2.3. Adsorption microcalorimetry characterization of the catalysts

The calorimetric results for all the samples are summarized in Fig. 4.11, where the differential heat of adsorption, Q_{diff}, is plotted *versus* the ammonia uptake. The presence of strong acid sites is revealed on all the samples by their initial Q_{diff} values, which are in the range 136-185 kJ/mol. The differential heat decreases for all the catalysts as the ammonia uptake increases, thus indicating heterogeneity of the sites. Based on previous ammonia

adsorption experiments on SBA-15 (Fig. 4.11 C), and on pure silica samples [37,38], it can be assumed that a differential heat of *ca.* 65 kJ/mol represents the boundary between chemical and physical adsorption. Accordingly, the fraction of ammonia uptake in Fig. 4.11 corresponding to differential heats below these value was ascribed to non-specific hydrogen bonding and/or physical adsorption on the silica part of the sample and neglected in calculating the acid site concentration, n_A.

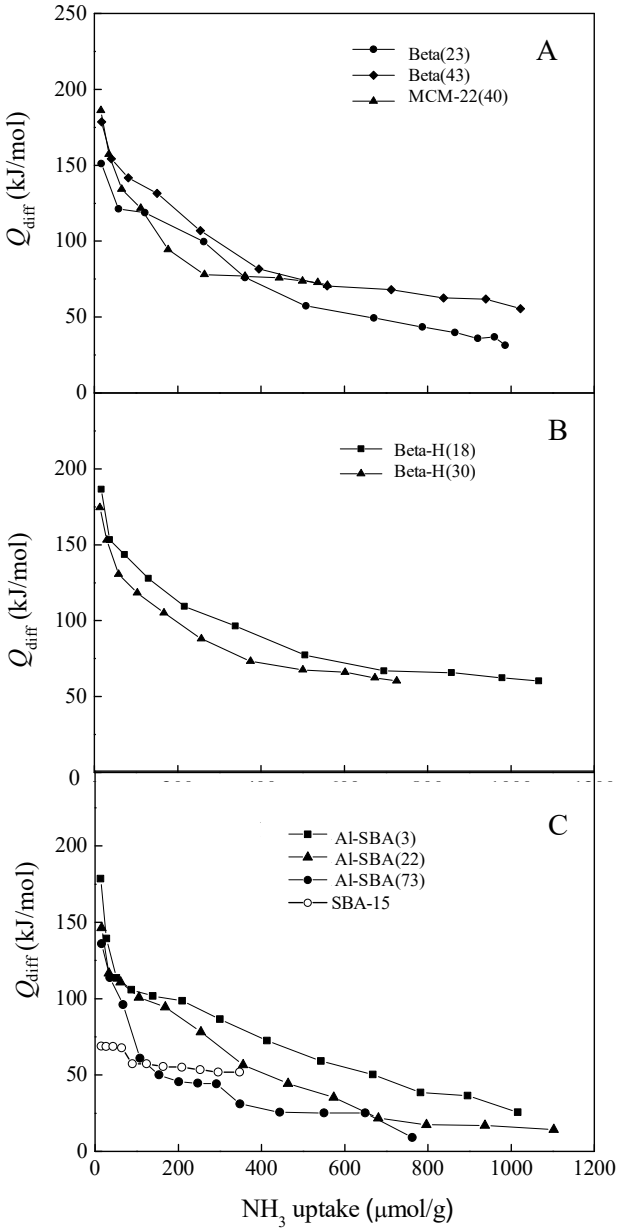

Figure 4.11. Differential heats versus ammonia uptake at 80 °C for microporous MCM-22 and Beta zeolites (**A**), micro/mesoporous hierarchical Beta-H zeolites (**B**), and Al-SBA-15 samples (**C**).

The n_A values for all the samples are given in Table 2, where the concentration of acid sites able to adsorb ammonia irreversibly, $n_{A,irr}$, calculated from the volumetric isotherms, is also given. From the curves of the differential heat in Fig. 4.11, it is possible to evaluate $Q_{diff,irr}$ values at which the adsorption shifts from irreversible to reversible. It can be seen in Table 2, where such $Q_{diff,irr}$ values are listed, that the acid sites able to adsorb ammonia irreversibly are those which release an adsorption heat higher than *ca*. 100 kJ/mol for microporous Beta and MCM-22, and for hierarchical Beta-H zeolites. These values are different for Al-SBA-15 samples, which have an adsorption heat higher than 70 kJ/mol. The differences are probably due to the different nature of the samples, the Al-SBA-15 samples are amorphous silica-aluminas while the zeolites are crystalline allumino-silicates.

Table 4.2. The concentration of total (n_A) and irreversible acid sites ($n_{A,irr}$), and the differential heat corresponding to the shift from irreversible to reversible adsorption ($Q_{diff,irr}$) for all the samples.

Sample	n_A (µmol/g)	$n_{A,irr}$ (µmol/g)	$Q_{diff,irr}$ (kJ/mol)
Beta(23)	408	378	≥ 105
Beta(43)	569	256	≥ 97
MCM-22(40)	568	120	≥ 111
Beta-H(18)	635	380	≥ 102
Beta-H(30)	442	247	≥ 100
Al-SBA(3)	439	408	≥ 72
Al-SBA(22)	294	274	≥ 73
Al-SBA(73)	98	91	≥ 77

4.2.4. Transesterification of soybean oil

The catalytic results for the soybean oil conversion into FAMEs over all the samples are summarized in Fig. 4.12, where the FAMEs yield is reported versus the reaction time. Over the conventional zeolites, a significant yield (22-40 mol%) is attained with a reaction time of 24 h (Fig. 4.12A).

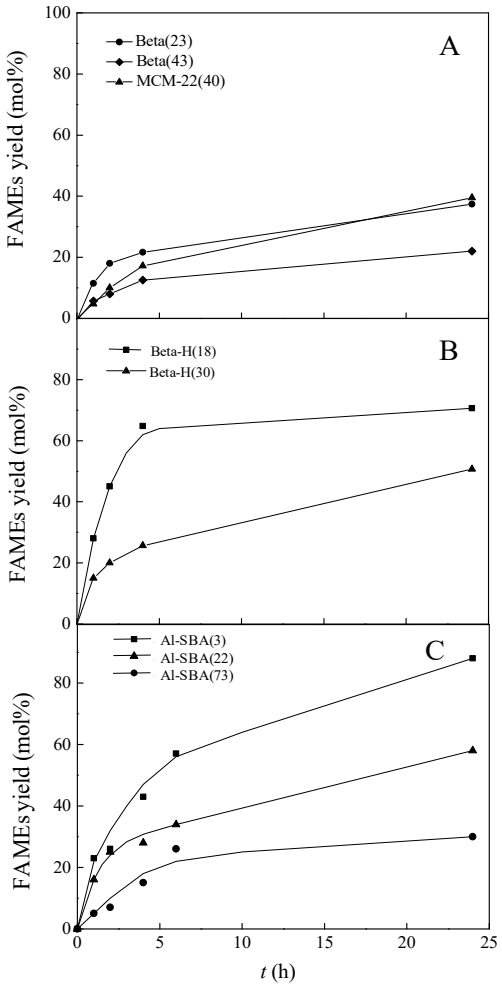

Figure 4.12. FAMEs yield *vs.* reaction time for soybean oil transesterification at 180 °C and 4 MPa, and CH_3OH/oil molar ratio of 12 using MCM-22 and Beta zeolites (**A**), hierarchical Beta-H zeolites (**B**) and Al-SBA-15 samples (**C**).

The superior behaviour of the hierarchical Beta zeolites is manifest from the much higher yields attained at 24 h (50-70 mol%, Fig. 4.12B). Beta-H(18) appears remarkably active, a FAMEs yield as high as 65 mol% being obtained with a reaction time of 4 h. All the Al-SBA-15 catalysts are active for the oil conversion while no reaction was observed over an Al-free SBA-15 sample. The catalytic results for the Al-SBA-15 samples are comparable to that of the hierarchical Beta zeolites and this supports the view that in both cases the favoured transport of the reactants inside the mesopore system is quite an important factor, among others, for the good performance of the catalysts. Among all the tested catalysts the best

performance is observed for Al-SBA(3), on which *ca.* 90 mol% methyl esters yield is attained at a reaction time of 24 h.

Besides glycerol and methyl esters, by far the most abundant products, also free fatty acids, whose content in the soybean oil feed is negligible (0.10 wt% of FFAs), were found to form. The FFAs content in the soybean oil at a reaction time of 24 h was of 6-11.9 wt% using classical and hierarchical zeolites samples, while values of 2.45-3.52 wt% were reached at 24 h with Al-SBA-15 samples. The presence of increasingly high amounts of FFAs in the soybean oil reaction mixture along with reaction time and the findings on the nature of the organic material retained by the catalysts suggest the simultaneous occurrence, besides transesterification, of several secondary reactions. In Fig. 4.13 is represented a scheme of the all hypothesized reactions.

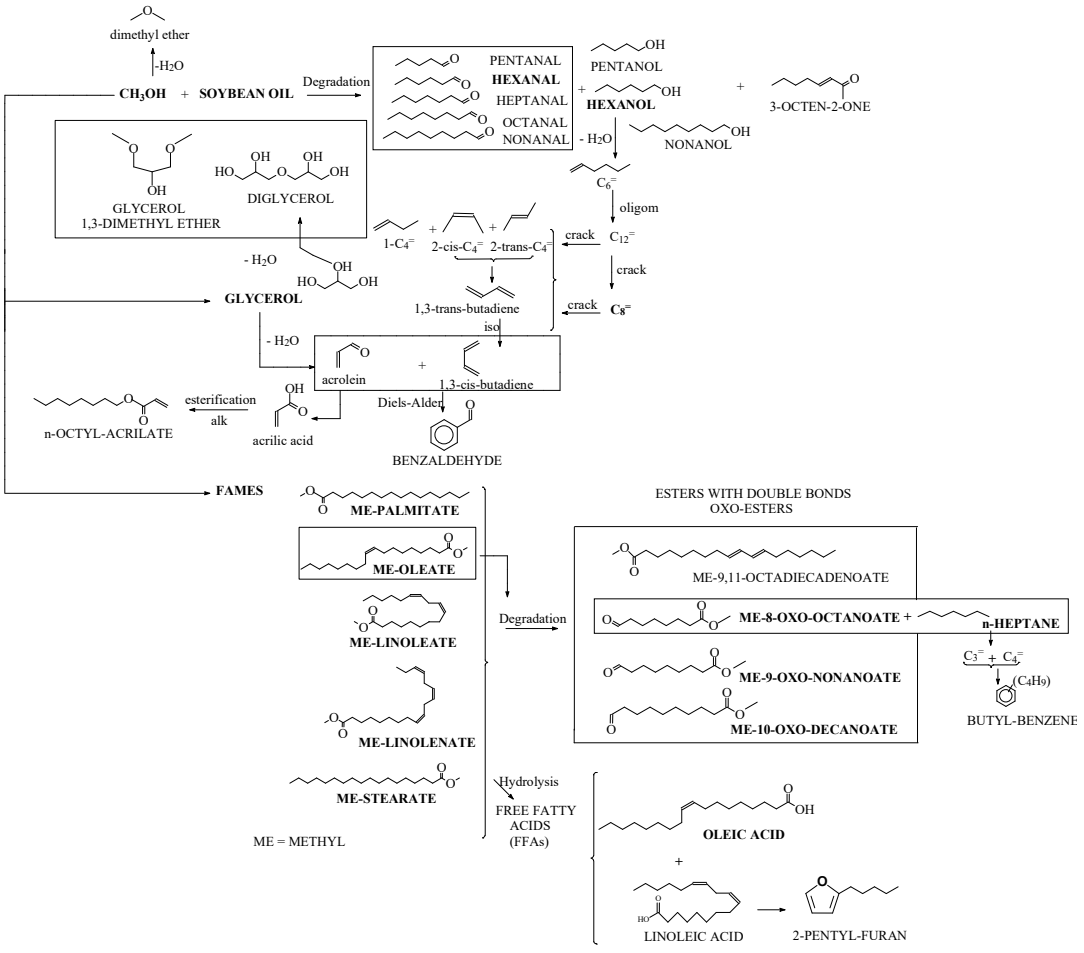

Figure 4.13. Scheme of the all reactions which is assumed to take place during the conversion of soybean oil, on the basis of the organic compounds retained by the catalysts during the reactions. The compounds actually identified by GC-MS are reported in capital, the most abundant in bold.

The FFAs content in the soybean oil at a reaction time of 24 h was of 6-11.9 wt% using classical and hierarchical zeolites samples, while values of 2.45-3.52 wt% were reached at 24 h with Al-SBA-15 samples. The presence of increasingly high amounts of FFAs in the soybean oil reaction mixture along with reaction time and the findings on the nature of the organic material retained by the catalysts suggest the simultaneous occurrence, besides transesterification, of several secondary reactions. The organic material adsorbed/retained in the catalysts during the reaction resulted completely soluble in methylene chloride and was found to contain, besides FAMEs, glycerol, and FFAs, also diglycerol, benzaldehyde, several aliphatic aldehydes and alcohols, 3-octen-2-one, C_8 olefins, dienes, fatty acids, esters with double bonds and oxo-esters. Plausible pathways for the transformations undergone by soybean oil are sketched in Fig. 4.13, where the products actually detected in the reaction mixture or in the organic material retained by the catalyst are indicated in bold characters.

The reliability of the scheme represented in Fig. 4.13 is supported by specific findings of other authors in reaction contexts different from transesterification [9,28,39-48]. FFAs would be originated through the acid-catalyzed FAMEs hydrolysis by the water resulting from either methanol dehydration to dimethyl ether and glycerol double dehydration to acrolein. The reactant alcohol dehydration has been reported to occur at 100-140 °C [28,39] and is hence plausible also in the present case. According to the patent literature on acrolein production [44], also glycerol double dehydration can take place under mild condition, though quite high temperatures (> 250 °C) would be required for its occurrence to a high extent [9,28,40]. In agreement with Refs (41-43), the observed formation of products such as methyl-9,11-octadecadienoate, methyl-8-oxo-octanonate, methyl-9-oxo-octanonate, and methyl-10 oxo-octanonate would occur through the thermal decomposition of FAMEs. Aldehydes (C_5-C_9) and alcohols (C_5, C_6, and C_9), among which hexanal and 1-hexanol are the main compounds, would be originated by the thermal decomposition of soybean oil, in agreement with Refs (45,46). The C_8 olefins (3,5 octadiene and *n*-octene) detected in the material extracted from the catalysts would form through the acid-catalyzed transformation of hexanol to hexene, followed by oligomerization to C_{12} olefins, which would then crack to C_4 and C_8 alkenes. This is suggested by literature results showing that: (i) 1-, 2-, and 3-hexene can be obtained from 1-hexanol over acidic resins and beta zeolites in liquid phase at 150-190 °C [47]; (ii) at 200 °C and 5 MPa, HZSM-5 zeolites, as well as Al-MCM-41 and Al-SBA-15

mesostructured silica-aluminas, are able to catalyze the formation of oligomers from C_6 olefins and their cracking to C_4 and C_8 alkenes [48]. Concerning the presence of benzaldehyde among the products retained by the catalysts, it would be the result of a Dies-Alder reaction involving 1,3-*cis*-butadiene originating through the hexane oligomerization-cracking pathway and acrolein coming from the acid-catalyzed glycerol double dehydration.

In spite of the deposition on the catalyst of the above described organic material during the reaction, the spent catalyst can be reused after a simple treatment consisting in washing with *n*-heptane and methanol, followed by calcination at 550 °C for 12 h. This is shown in Fig. 4.14, where the FAMEs yield *versus* reaction time of the Beta-H(30) (Fig. 4.14A) and the Al-SBA(3) samples (Fig. 4.14B) recovered after 24 h on-run and treated in this way are compared with that observed for a fresh sample.

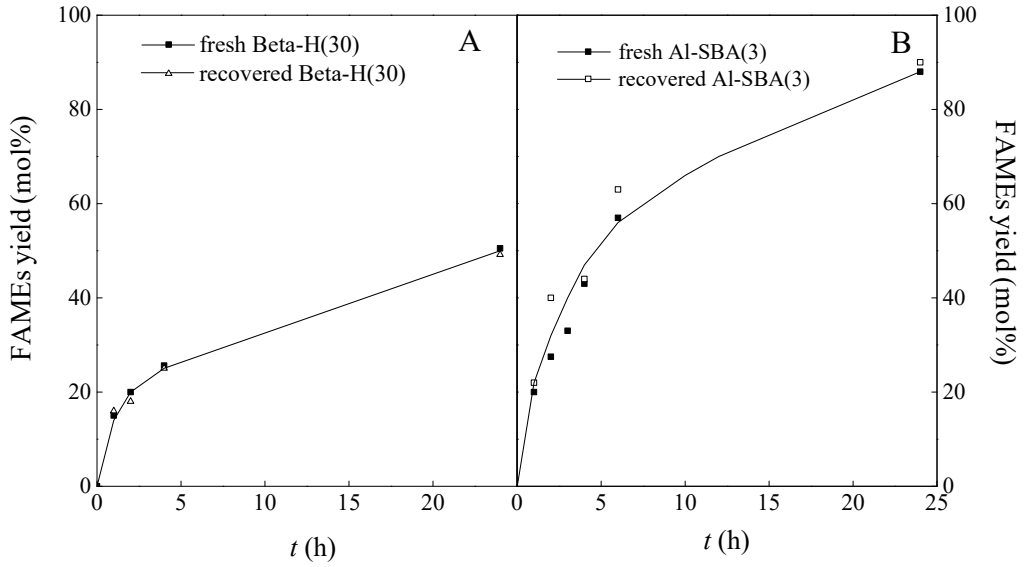

Figure 4.14. FAMEs yield *vs*. reaction time for soybean oil transesterification at 180 °C, 4 MPa, and CH_3OH/oil molar ratio of 12 on fresh and regenerated Beta-H(30) (**A**) and on fresh and regenerate Al-SBA(3) (**B**).

4.2.4.1. Influence of the methanol/oil ratio

Fresh Al-SBA(3) samples were also used for exploring the influence of the methanol to oil molar ratio. As shown in Fig. 4.15, increasing the methanol/oil ratio from 12 to 30

mol/mol results in an increased catalyst performance at 180 °C, 100 mol% FAMEs yield being early (6 h) obtained.

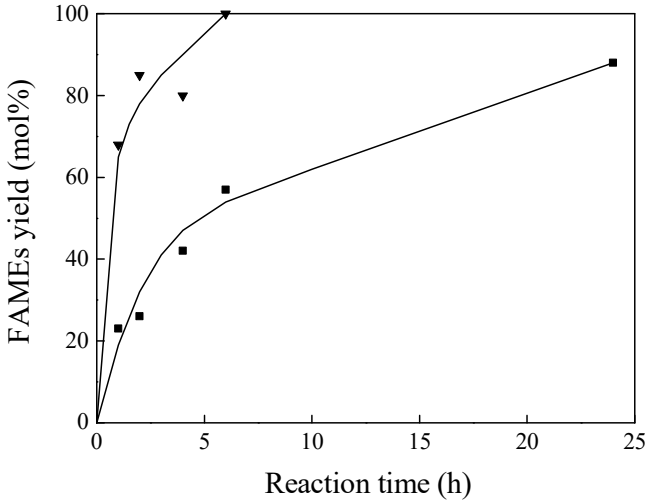

Figure 4.15. FAMEs yield *vs.* reaction time for soybean oil transesterification at 180 °C, 4 MPa, and CH_3OH/oil molar ratio of 12 (■) and 30 (▾) over Al-SBA(3).

4.2.4.2. Influence of the temperature

The influence of the temperature on the soybean oil transesterification was investigated in runs carried out on Al-SBA(3) in the 70-250 °C with a CH_3OH/oil ratio of 12 mol/mol. The pertinent FAMEs yield *vs*. reaction time curves are shown in Fig. 4.16.

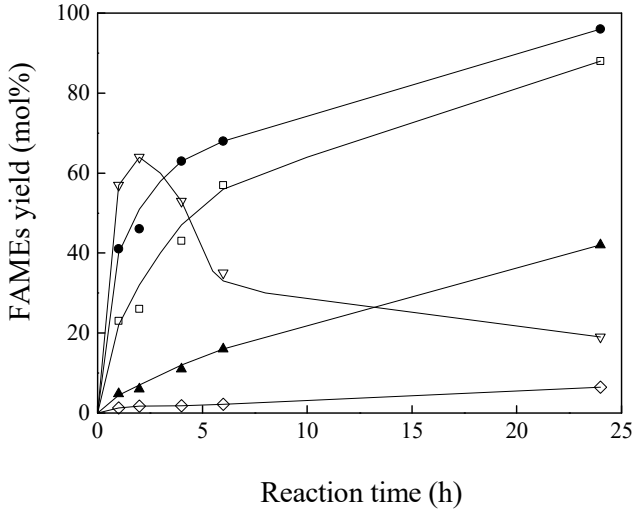

Figure 4.16. FAMEs yield *vs*. reaction time for soybean oil transesterification at 4 MPa, and CH_3OH/oil molar ratio of 12 at 70 °C (◇), 150 °C (▲), 180 °C (□), 200 °C (●), and 250 °C (▽) on Al-SBA(3).

A remarkable increase in the methyl esters yield is observed at a reaction time of 1 h as the reaction temperature is raised from 70 °C (FAMEs yield 1 mol%) to 250 °C (FAMEs yield 64 mol%). Whatever the reaction temperature, the FAMEs yield *vs.* reaction time curves monotonically increase, except for the run at 250 °C, whose curve dramatically grows to a maximum (64 mol% at 2 h) and then decreases (19 mol% at 24 h). This indicates that at such temperature the FAMEs resulting from the transesterification reaction rapidly undergo consecutive transformations to other products. Interestingly, after 1 h of reaction at 250 °C an FFAs content of 2.02 wt% was measured in the reaction mixture and a value as high as 24.03 wt% was determined after 24 h, whereas acidity values of 0.91-3.79 wt% were measured at 24 h for the runs at 70-200 °C. This suggests that at 250 °C free fatty acids may form to a remarkable extent through the consecutive transformation of the primary products of transesterification. Based on Fig. 4.13, the peculiar issues of the soybean oil transformation at 250 °C in comparison with those of the runs in the 70-200 °C range (monotonic increase of FAMEs yield and very low FFAs formation during the run) can be tentatively explained. The FAMEs obtained as primary products from transesterification undergo consecutive transformation through thermal degradation and hydrolysis, which occur in parallel. As far as the soybean oil is processed at low temperatures, thermal degradation is expected to occur to a limited extent. As to hydrolysis, it is dependent on the water forming through double dehydration of glycerol to acrolein, a reaction that, according to the patent literature on acrolein production [44], takes place to a limited extent under mild conditions. This is supported by the finding that FFAs, which are virtually absent in the feed, actually form when soybean oil is processed at 70-200 °C, but their amount remains low (0.9-3.8 wt% at 24 h). Though the rate of FAMEs formation from TGs is bound to decrease with the reaction time while the rate of FAMEs consumption through thermal degradation and hydrolysis is bound to increase, at 70-200 °C the former would remain higher than the latter over the whole duration of the run. As a result, the FAMEs yield is seen to increase monotonically with reaction time with a decreasing slope. By converse, at 250 °C the extent of double dehydration of glycerol to acrolein becomes quite high, as known from the literature on acrolein production [9,28,40], thus enhancing FAMEs hydrolysis. (An increase in the FFAs content up to 24 wt% at 24 h is actually observed). Also the FAMEs thermal degradation would be reasonably enhanced at 250 °C. Apparently, the decrease in the rate of FAMEs

formation and the simultaneous increase in the rate of FAMEs consumption would be such that there would be a point during the run at which the two rates become identical, appearing as a maximum in the FAMEs yield *vs*. reaction time curve.

The initial rate (r_i) of the transesterification reaction, expressed as mol% FAMEs yield/(h × $g_{catalyst}$), was calculated from the slope at zero reaction time of the curves in Fig. 4.16 and used for obtaining the Arrhenius plot shown in Fig. 4.17, which gives an activation energy of 59 kJ/mol. Though low, such value is somewhat higher than the activation energy reported for the transesterification of triacetin with methanol [49] in sulphuric acid (46.1 kJ/mol) and Nafion SAC-13 (48.5 kJ/mol), which are the only activation energy data available in the literature on the acid-catalyzed transesterification reaction.

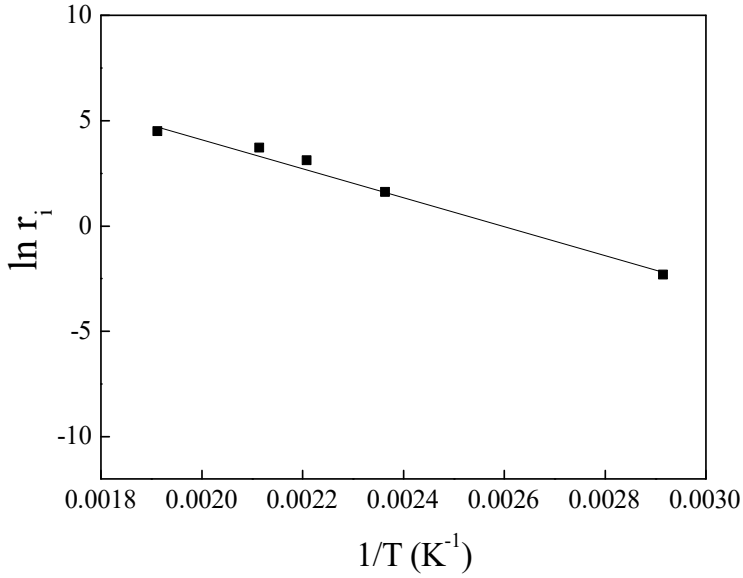

Figure 4.17. Arrhenius plot for soybean oil transesterification at 4 MPa, and CH_3OH/oil molar ratio of 12 on Al-SBA(3).

4.2.4.3. Influence of the acid properties

The initial FAMEs yields (so that the undesired reactions do not influence significantly the transesterification reaction) were plotted *versus* the population of sites with different strength in Fig. 4.18.

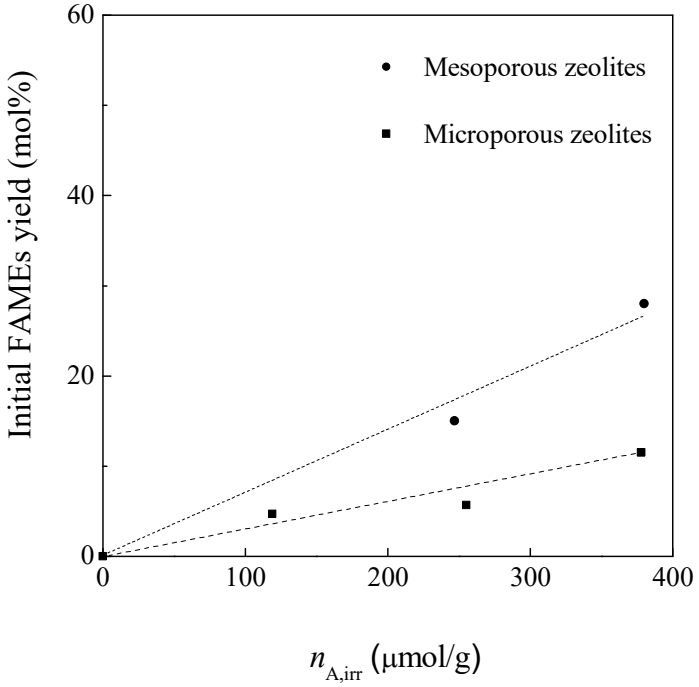

Figure 4.18. Initial (1 h of reaction) FAMEs yield for soybean oil transesterification at 180 °C 4 MPa, and CH_3OH/oil molar ratio of 12 *versus* concentration of the irreversible acid sites ($n_{A,irr}$) for microporous (full squares) and mesoporous zeolites (full circles).

In the case of microporous and mesoporous zeolites a linear correlation (represented in Fig. 4.18) was found between the initial yield to FAMEs and the concentration of the irreversible acid sites, which correspond to the sites stronger than 100-110 kJ/mol. It can be seen that hierarchical Beta-H zeolites, thanks to the combination of the characteristics of microporous zeolite (highly active acid sites) and mesoporous material (fast mass transport, due to mesopores with a high diameter up to 30 nm), have a catalytic performances of about twice or three times higher than that of the microporous solids of the same acidity.

Also in the case of the Al-SBA-15 the best correlation (R = 0.9996) was found between the initial FAMEs yield and the concentration of the irreversible acid sites, as shown in Fig. 4.19. However, at variance of the zeolites, the calculated limit between reversible and irreversible adsorption of ammonia is around 70 kJ/mol instead of around 100 kJ/mol.

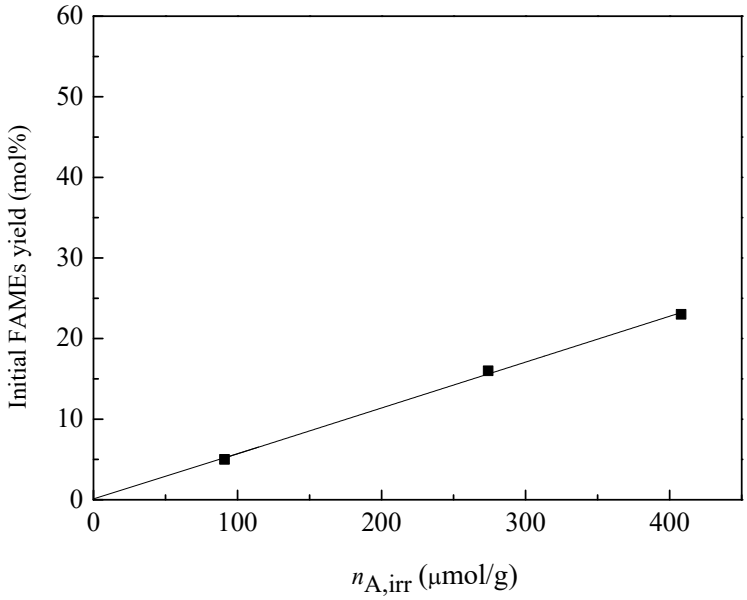

Figure 4.19. Initial FAMEs yield for soybean oil transesterification at 180 °C 4 MPa, and CH_3OH/oil molar ratio of 12 *vs.* concentration of the irreversible acid sites ($n_{A,irr}$) for Al-SBA-15 samples.

The FAMEs production by Triglycerides transesterification with methanol occurs through a stepwise pathway in which the triglyceride molecule is first converted to diglyceride, then to monoglyceride and finally to glycerol, a molecule of methyl ester being released in each step. The acid-catalyzed reaction is initiated by the interaction of the acid with a carbonyl group of the triglyceride, which results in an increased positive charge on the carbonyl carbon and makes it prone to the nucleophilic attack by the alcohol [50,51]. According to the literature [50 and literature therein], both Brønsted and Lewis acids are able to catalyze the reaction. It is stated that a requirement for a good solid acid catalyst is an appropriate site strength [28] and by analogy with the catalysis operated by sulphuric acid in homogeneous medium it is inferred that the acid sites should be quite strong. However, a clear-cut distinction between good catalysts with strong acid sites on the one hand and poor catalysts with weak acid sites on the other hand is probably an oversimplification. For instance, too high a strength of the acid sites is reported as detrimental in the case of heterogeneous Lewis acid catalysts, due to the disfavoured desorption of the new ester formed after the nucleophilic attack step [50 and literature therein]. Concerning the nature of the active sites, though adsorption microcalorimetry is unable to discriminate between Brønsted

and Lewis acidity, some clues can be obtained by the NMR results (reported in Fig. 4.8). These indicate that on the Al-SBA-15 catalysts bridging hydroxyl groups, Al–O(H)–Si, associated to Al_{IV} atoms [53] and acting as Brønsted sites, are by far the most abundant. Al species in which Al atoms are in octahedral coordination (Al oxides and/or Al oxohydroxides), acting as Lewis and/or Brønsted sites, account for *ca.* 10 % of the total Al content. The conclusion can be drawn that the contribution of Lewis sites to the overall acidity of the Al-SBA-15 catalysts is very low. Accordingly, if the Lewis sites were the only sites able to catalyze the soybean oil transesterification, a very low FAMEs yield would be observed, even assuming that all the Lewis sites were of appropriate strength. This is in contrast with the experimental evidence, which shows that even the Al-SBA-15 catalyst with the highest Si/Al ratio is able to catalyse the transesterification reaction to a significant extent. It hence seems that the major role in promoting soybean oil transesterification over the Al-SBA-15 catalysts is played by Brønsted sites.

4.2.5. Transesterification of Jatropha curcas oil

The extensive use of edible oils for the production of biodiesel is a problem because of they are far too expensive to be used as fuel at present and may cause significant problems such as starvation in developing countries [26]. Non-edible plant oils such as *Jatropha curcas*, *Pongamia pinnata*, *Madhuca indica*, and *Azadirachta indica* oils have been found to be promising crude oils for the production of biodiesel. Among them *Jatropha curcas* seems to be the most promising for producing biodiesel [26-28,43,54]. For this reason the Al-SBA-15 samples were tested also for the transesterification of *Jatropha curcas* oil with methanol.

In Fig. 4.20 are represented the results obtained by feeding *Jatropha* oil with methanol in a molar ratio of 1:12 over the Al-SBA-15 catalysts at 180 °C and 4 MPa. The FAMEs yield vs. reaction time data reported clearly show that there are no significant differences in the performance of the three catalysts, over which a FAMEs yield of (or very close to) 100 mol% is obtained at a reaction time of 24 h. The evolution of the free fatty acids, whose content in the *Jatropha* oil feed is 5.49 wt%, was also monitored and a residual amount of only 0.78-1.02 wt% of FFAs was detected in the reaction mixture at a reaction time of 24 h, suggesting the occurrence of their esterification by methanol.

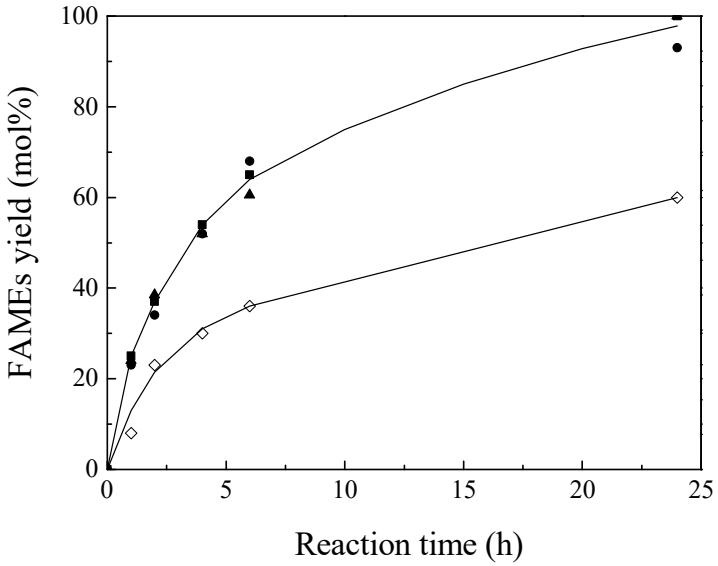

Figure 4.20. FAMEs yield *vs*. reaction time for *Jatropha curcas* oil transesterification at 180 °C, 4 MPa, and CH_3OH/oil molar ratio of 12 on Al-SBA(3) (■), Al-SBA(22) (▲), Al-SBA(73) (●), and in the absence of a catalyst (◇).

An important feature of *Jatropha* oil is that it undergoes transformation also in the absence of a catalyst. This is shown in the same Fig. 4.20, where it can be seen that at 180 °C the FAMEs yield in the absence of a catalyst is significant (8 mol%) already at a reaction time of 1 h and becomes remarkable (60 mol%) after 24 h. Runs at 120 and 100 °C were also carried out, showing that in the absence of a catalyst the oil transformation was remarkably depressed at 120 °C (FAMEs yield = 1 and 13 mol% at a reaction time of 1 and 24 h, respectively) and no more occurred at 100 °C. At such temperature the Al-SBA-15 catalysts were found only slightly active, the FAMEs yield being only 10, 8 and 6 mol% over Al-SBA(3), Al-SBA(22), and Al-SBA(73), respectively, at a reaction time as high as 24 h.

Soybean oil was subjected to the same test of *Jatropha* oil, at 180 °C and 4 MPa in the absence of the catalyst and, unlike what has been observed with *Jatropha* oil, were not detected FAMEs even after 24 hours. So, it is manifest that even carboxylic acids of such a weak acidic strength as the FFAs are able to catalyze, besides their own esterification, also triglycerides transesterification (the FAMEs yield grows up to the remarkable value of 60 mol% after 24 h, Fig. 4.20). The conclusion can hence be drawn that all the acid sites present on the catalysts are involved in the soybean oil transesterification, whatever their strength. Autocatalytic effects arising from the weak acidity of the carboxylic acids themselves have

been discussed for the esterification of acetic acid with methanol in Ref. 55. Acetic acid can in principle catalyze its own esterification either by directly attacking a second acid molecule or by releasing protons which then attack a CH_3COOH molecule. In either case, the protonated species undergoes nucleophilic attack by methanol, with formation of a tetrahedral intermediate which then disproportionates giving the ester. Undissociated acid protolysis is probably the dominating route in the case of the FFAs present in the *Jatropha* oil, in view of the lack of water in the feed and the weak dissociation of the acids in pure methanol. Concerning the influence of the feed acidity on the transesterification reaction, FAMEs formation in the absence of a catalyst has been reported during crude palm kernel and coconut oils processing [56]. Both the oils are acidic (FFAs content = 1.05 and 2.25 wt% as lauric acid, respectively) and FAMEs yields as high as 30 and 41 wt%, respectively, were observed with a reaction time of 4 h at 200 °C, 5 MPa and methanol to oil ratio of 6 mol/mol. Upon addition of a solid catalyst (zirconia, zinc oxide, sulphated tin oxide, or sulphated zirconia; 3 wt%, based on the oil mass), an increase in the FAMEs yield to *ca.* 65-95 wt% and *ca*. 49-86 wt% for palm kernel oil and coconut oil, respectively, was observed at a reaction time of 4 h. Accordingly, the catalyst performance was evaluated by subtracting the results for the blank run from those of the solid-catalyzed run. For *Jatropha* oil, a remarkable increase in the FAMEs yield in the presence of Al-SBA-15 catalysts is also observed, as a result of the occurrence of the reaction also on the acid sites of the solid.

Several other reactions also occur during the *Jatropha* oil processing, as schematized in Fig. 4.21, by the composition of the organic material retained by the catalysts: diglycerol, several aliphatic aldehydes and alcohols, 3-octen-2-one, esters with double bonds and oxo-esters were detected besides larger amounts of FAMEs and glycerol and traces of FFAs. Typical issues of the *Jatropha* oil in comparison with soybean oil are (i) the above-discussed occurrence of FFAs esterification in parallel to TGs transesterification and (ii) the lack of both glycerol double dehydration to acrolein and olefins formation from hexanol, highlighted by the absence of benzaldehyde among the products extracted from the exhaust catalysts. The reasons underlying the (ii) finding remain undisclosed.

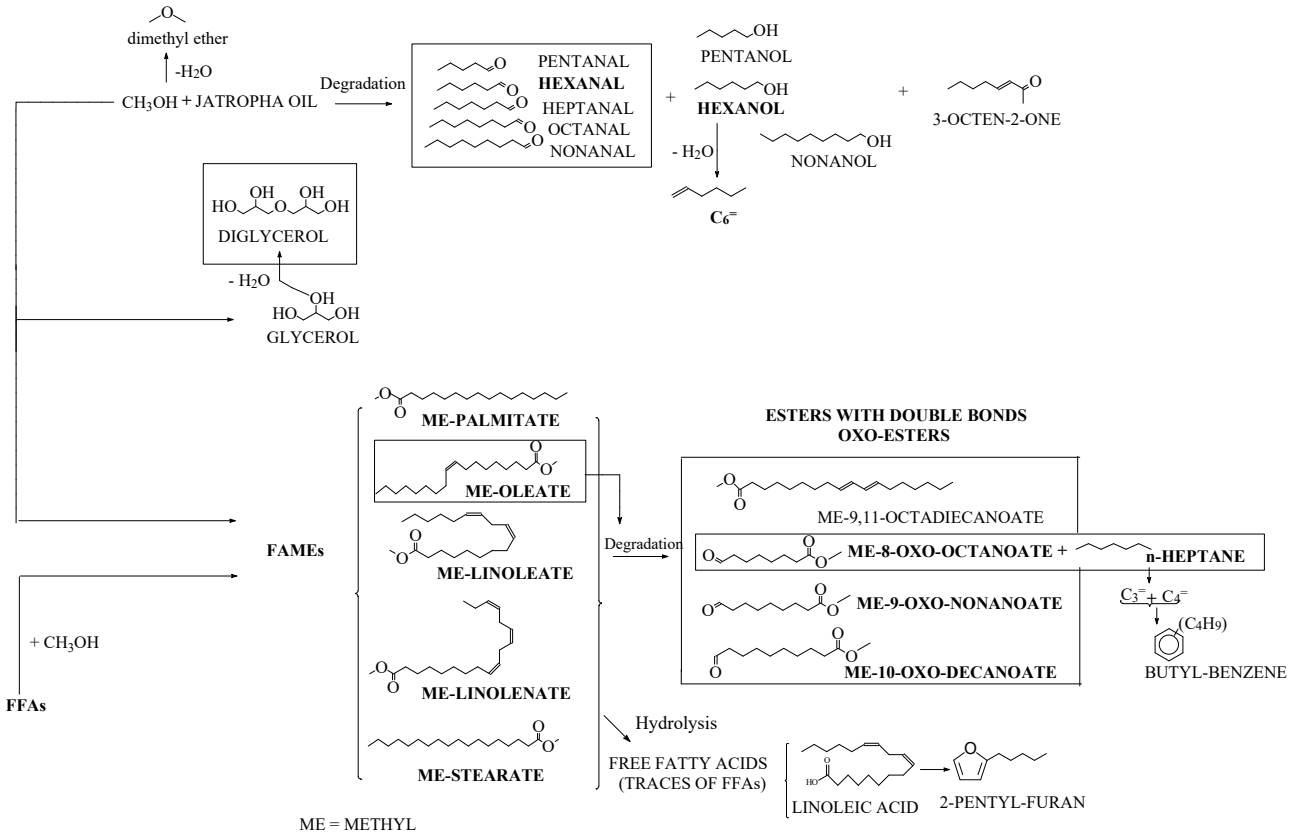

Figure 4.21. Scheme of the all reactions which is assumed to take place during the conversion of *Jatropha* oil, on the basis of the organic compounds retained by the catalysts during the reactions. The compounds actually identified by GC-MS are reported in capital, the most abundant in bold.

4.2.5.1. Influence of the acid properties

An interesting point is that the performance of the three Al-SBA-15 catalysts is virtually the same (Fig. 4.20), in spite of their remarkable differences in terms of both concentration and strength distribution of the acid sites. It is worthy of note that for soybean oil, whose FFAs content is negligible, the differences in the acid features of the three Al-SBA-15 catalysts are clearly reflected in their different transesterification performance (Fig. 4.12). Apparently, in the case of *Jatropha* oil, the catalytic effect stemming from the presence of FFAs and that originated by the acid sites of the solid are not simply additive. Rather, they seem involved in a complex (undisclosed) interplay, which levels out the catalyst performance. It is also worthy of note that when the homogeneously catalyzed reaction is

completely suppressed, *i.e*. at 100 °C, the solid-catalyzed reaction is depressed to such an extent (FAMEs yields at 24 h are 10, 8 and 6 mol% for Al-SBA(3), Al-SBA(22) and Al-SBA(73), respectively) that any performance-based comparison of the catalysts is unreliable.

4.3. Conclusions

Both protonic hierarchical Beta zeolites and Al-SBA-15 are active catalysts in the conversion of soybean oil into FAMEs at 4 MPa and 180 °C, higher FAMEs yields being obtained over these micro/mesoporous materials than over conventional Beta and MCM-22 zeolites. The low FAMEs yield observed over the conventional zeolites can be related to the restricted diffusion of the cumbersome trygliceride reactants inside the micropores of the Beta and MCM-22 zeolites. Besides porosity, also the acidity of the catalysts governs the transesterification reaction. The acid sites responsible for the transesterification of the soybean oil over the hierarchical Beta, the conventional Beta and MCM-22 zeolites, and the Al-SBA-15 are those whose interaction with ammonia is irreversible. For zeolites these sites are stronger than *ca.* 100 kJ/mol while for Al-SBA-15 they are stronger than *ca.* 70 kJ/mol.

The apparent activation energy for the soybean oil transesterification over the Al-SBA-15 catalyst with Si/Al = 3 is 59 kJ/mol. Such catalyst is the best-performing one: a FAMEs yield as high as 90 mol% being achieved at a reaction time of 24 h with a methanol to oil ratio of 12, and 100 mol% FAMEs yield being much earlier (6 h) obtained with a methanol to oil ratio of 30. It is also better than other heterogeneous acidic catalysts so far reported in the literature. Besides transesterification, soybean oil undergoes several secondary reactions during the run. These include acid-catalyzed FAMEs hydrolysis to FFAs (by the water resulting from methanol dehydration and glycerol double dehydration), thermal decomposition of FAMEs to esters with double bonds and oxo-esters, thermal degradation of soybean oil to aldehydes and alcohols, followed by acid-catalyzed alkene formation, oligomerization and cracking, and Dies-Alder benzaldehyde formation.

Very high FAMEs yields (*ca.* 100 mol% at a reaction time of 24 h, with methanol to oil ratio of 12) are obtained by reacting *Jatropha* oil over the three Al-SBA-15 catalysts. Their performance is virtually identical, in spite of the remarkable differences in terms of both

concentration and strength distribution of the acid sites. The esterification of the FFAs present in the feed occurs in parallel to TGs transesterification. Besides the acid sites of the catalyst, also the free fatty acids present in the feed catalyze both reactions, autocatalytic FFAs esterification and TGs transesterification being observed also in absence of the solid catalysts. Apparently, the homogeneous and heterogeneous catalytic effects are not simply additive; rather, they seem to combine in such a way to level out the catalyst performance. The underlying reasons remain undisclosed. The homogeneous reactions can be suppressed by decreasing the reaction temperature to 100 °C, a temperature at which, however, the solid catalyzed reaction is depressed to such an extent (FAMEs yields at 24 h, 10-6 mol%) that any performance-based comparison of the catalysts is unreliable. Several secondary reactions occur also during the transformation of *Jatropha* oil, the difference with soybean oil being the lack of both glycerol double dehydration and olefins formation.

References

[1] B.R. Moser, *Vitr. Cell. Dev. Biol*. 45 (2009) 229.

[2] M.K. Lam, K.T. Lee, A.R. Mohamed, *Biotechnol. Adv*. 28 (2010) 500.

[3] J. Sheehan, V. Camobreco, J. Duffield, M. Graboski, H. Shapouri, *Life Cycle Inventory of Biodiesel and Petroleum Diesel for Use in an Urban Bus*. Final Report, 1998.

[4] M. Canakci, J. Van Gerpen, *Trans. ASAE* 44 (2001) 1429.

[5] J. Van Gerpen, *Fuel Process. Technol*. 86 (2005) 1097.

[6] C.A.G. Quispe, C.J.R. Coronado, J.A. Carvalho, *Renew. Sustain. Energy Rev*. 27 (2013) 475.

[7] J.A. Kenar, *Lipid Technol.* 19 (2007) 249.

[8] H.W. Tan, A.R. Abdul Aziz, M.K. Aroua, *Renew. Sustain. Energy Rev*. 27 (2013) 118.

[9] B. Katryniok, S. Paul, V. Bellière-Baca, P. Rey, F. Dumeignil, *Green Chem*. 12 (2010) 2079.

[10] E.C.G. Aguieiras, E.D. Cavalcanti-Oliveira, D.M.G. Freire, *Fuel* 159 (2015) 52.

[11] A.S. Ramadhas, S. Jayaraj, C. Muraleedharan, *Fuel* 84 (2005) 335.

[12] A. Abbaszaadeh, B. Ghobadian, M.R. Omidkhah, G. Najafi, *Energy Convers. Manag.* 63 (2012) 138.

[13] A. Islam, Y.H. Taufiq-Yap, E.S. Chan, M. Moniruzzaman, S. Islam, M.N. Nabi, *Energy Convers. Manag*. 88 (2014) 1200.

[14] A.L. Cardoso, S.C.G. Neves, M.J. da Silva, *Energies* 1 (2008) 79.

[15] S.C.M. Dos Reis, E.R. Lachter, R.S. V. Nascimento, J. A. Rodrigues, M.G. Reid, *J. Am. Oil Chem. Soc*. 82 (2005) 661.

[16] L. Guerreiro, J.E. Castanheiro, I.M. Fonseca, R.M. Martin-Aranda, A.M. Ramos, *J. Vital, Catal. Today* 118 (2006) 166.

[17] C.M. Garcia, S. Teixeira, L.L. Marciniuk, U. Schuchardt, *Bioresour. Technol*. 99 (2008) 6608.

[18] G. Sunita, B.M. Devassy, A. Vinu, D.P. Sawant, V. V. Balasubramanian, S.B. Halligudi, *Catal. Commun.* 9 (2008) 696.

[19] Q. Shu, B. Yang, H. Yuan, S. Qing, G. Zhu, *Catal. Commun*. 8 (2007) 2159.

[20] D.Y.C. Leung, X. Wu, M.K.H. Leung, *Appl. Energy* 87 (2010) 1083.

[21] A.F. Lee, J. a Bennett, J.C. Manayil, K. Wilson, *Chem. Soc. Rev*. 43 (2014) 7887.

[22] J.C. Escobar, E.S. Lora, O.J. Venturini, E.E. Yáñez, E.F. Castillo, O. Almazan, *Renew. Sustain. Energy Rev.* 13 (2009) 1275.

[23] A.J. Yuste, M.P. Dorado, *Energy & Fuels* 20 (2006) 399.

[24] A.F. Clarens, E.P. Ressureccion, M. a White, L.M. Colosi, *Environ. Sci. Technol*. 44 (2009) 1813.

[25] M.K. Lam, K.T. Lee, *Biotechnol. Adv.* 30 (2012) 673.

[26] M. Balat, *Energy Convers. Manag*. 52 (2011) 1479.

[27] D. Pimentel, *Biofuels, Solar and Wind as Renewable Energy Systems*, Springer, (New York), 2008.

[28] J.C.J. Bart, N. Palmeri, S. Cavallaro, *Biodiesel Science and Technology. From Soil to Oil*, CRC Press (Boca Raton), 2010.

[29] C. Delitala, M.D. Alba, A. I. Becerro, D. Delpiano, D. Meloni, E. Musu, I. Ferino, *Micropor. Mesopor. Mater.* 118 (2009) 1.

[30] C. Delitala, E. Cadoni, D. Delpiano, D. Meloni, S. Melis, I. Ferino, *Micropor. Mesopor. Mater*. 110 (2008) 197.

[31] M.M.J. Treacy, J.B. Higgins, *Collection of Simulated XRD Powder Patterns for Zeolites*, Elsevier, (Amsterdam), 2001.

[32] K. Möller, B. Yilmaz, R.M. Jacubinas, U. Müller, T. Bein, *J. Am. Chem. Soc.* 133 (2011) 5284.

[33] L. Wang, Z. Zhang, C. Yin, Z. Shan, F.S. Xiao, *Micropor. Mesopor. Mater*. 131 (2010) 58.

[34] R.B. Borade, A. Clearfield, *Catal. Letters* 31 (1995) 267.

[35] K.R. Kloetstra, H.W. Zandbergen, H. van Bekkum, *Catal. Letters* 33 (1995) 157.

[36] F. Rouquerol, J. Rouquerol, K.S.W. Sing, P. Llewellyn, G. Maurin, A*dsorption by Powders and Porous Solids, Principles, Methodology and Applications*, Second Edition, Elsevier (Amsterdam), 2014.

[37] N. Cardona-Martínez, J.A. Dumesic, *J. Catal*. 125 (1990) 427.

[38] G. Colón, I. Ferino, E. Rombi, E. Selli, L. Forni, P. Magnoux, M. Guisnet, *Appl. Catal. A Gen.* 168 (1998) 81.

[39] P.M. Ejikeme, I.D. Anyaogu, C.L. Ejikeme, N.P. Nwafor, C.A.C. Egbuonu, K. Ukogu, J.A. Ibemesi, *E-Journal Chem.* 7 (2010) 1120.

[40] A. Corma, G. Huber, L. Sauvanaud, P. Oconnor, *J. Catal*. 257 (2008) 163.

[41] S. Bax, M.H. Hakka, P.A. Glaude, O. Herbinet, F. Battin-Leclerc, *Combust. Flame* 157 (2010) 1220.

[42] M.H. Hakka, P.-A. Glaude, O. Herbinet, F. Battin-Leclerc, *Combust. Flame* 156 (2009) 2129.

[43] E.S. Silva, M.M. Conceição, E.H.S. Cavalcanti, V.J. Fernandes, A.C.D. Medeiros, A.G. Souza, *J. Therm. Anal. Calorim.* 113 (2013) 437.

[44] A. Neher, T. Haas, D. Arntz, H. Klenk, W. Girke, *US Patent* 5,387,720, 1995.

[45] E.N. Frankel, *Prog. Lipid Res*. 22 (1983) 1.

[46] Q. Zhang, A.S.M. Saleh, J. Chen, P. Sun, Q. Shen, *J. Therm. Anal. Calorim*. 115 (2014) 19.

[47] E. Medina, R. Bringué, J. Tejero, M. Iborra, C. Fité, *Appl. Catal. A Gen*. 374 (2010) 41.

[48] R. van Grieken, J.M. Escola, J. Moreno, R. Rodríguez, *Appl. Catal. A Gen*. 305 (2006) 176.

[49] D.E. López, J.G. Goodwin, D.A. Bruce, E. Lotero, *Appl. Catal. A Gen.* 295 (2005) 97.

[50] E. Lotero, Y. Liu, D.E. Lopez, K. Suwannakarn, D.A. Bruce, J.G. Goodwin, *Ind. Eng. Chem. Res.* 44 (2005) 5353.

[51] I.K. Mbaraka, B.H. Shanks, *J. Am. Oil Chem. Soc*. 83 (2006) 79.

[52] M. Di Serio, R. Tesser, L. Pengmei, E. Santacesaria, *Energy and Fuels* 22 (2008) 207.

[53] M. Trombetta, G. Busca, M. Lenarda, L. Storaro, M. Pavan, *Appl. Catal. A Gen.* 182 (1999) 225.

[54] H.J. Berchmans, S. Hirata, *Bioresour. Technol*. 99 (2008) 1716.

[55] Y. Liu, E. Lotero, J.G. Goodwin, *J. Mol. Catal. A Chem*. 245 (2006) 132.

[56] J. Jitputti, B. Kitiyanan, P. Rangsunvigit, K. Bunyakiat, L. Attanatho, P. Jenvanitpanjakul, *Chem. Eng. J.* 116 (2006) 61.

Chapter V

Conversion of dihydroxyacetone to methyl lactate

5.1. Introduction

5.1.1. Lactic acid and lactates

Lactic acid (2-hydroxypropanoic acid) is an organic molecule highly widespread in nature. The presence of two functional groups, a hydroxyl group adjacent to a carboxylic group, in a three carbon molecule gives it a high chemical reactivity [1]. It has a wide variety of applications in food, pharmaceutical, textile, leather and chemical industry. In the last two decades world lactic acid production has expanded 10 folds, in large part due to the increased demand for green products, including ethyl lactate and polylactic acid (PLA) [1-3]. Ethyl lactate finds application in particular as green solvent, representing an interesting alternative existing hazardous solvents [4]. PLA is a polymer considered a green alternative to petroleum derived plastic due to its biodegradability and reduced carbon footprint [5]. Due to its chemical features lactic acid could be a valuable platform molecule. It can be converted into different potentially useful chemicals, as shown in Fig. 5.1, such as acrylic acid, acetaldehyde, 2,3-pentanedione, pyruvic acid, 1,2-propanediol, and lactates [1].

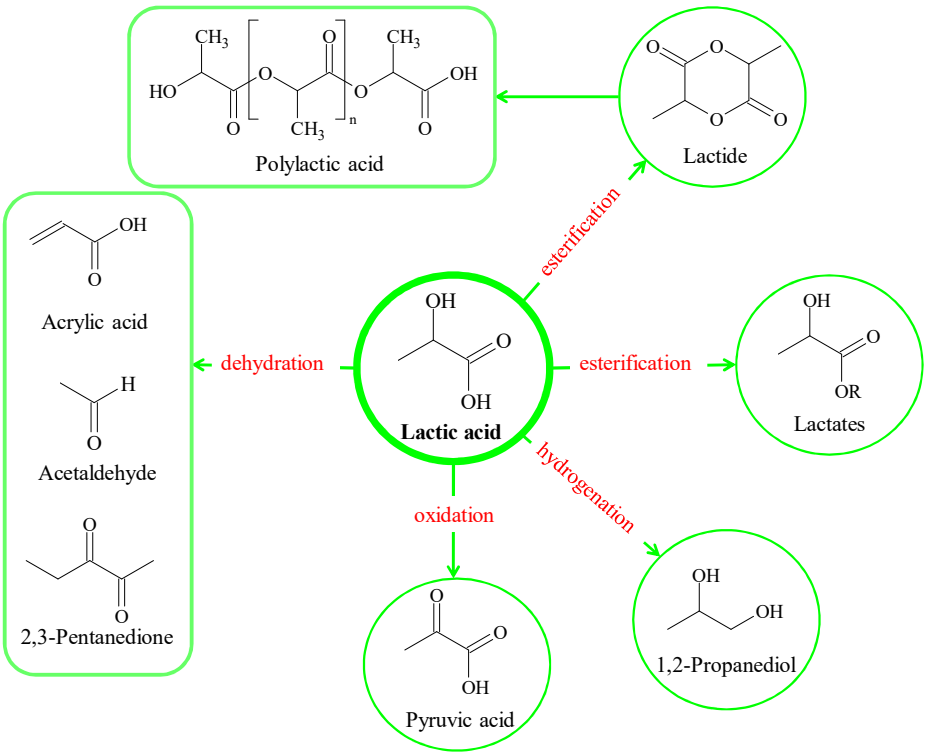

Figure 5.1. Potential applications for lactic acid.

5.1.2. Traditional production processes of lactic acid and methyl lactate

Lactic acid production can be achieved either by chemical synthesis routes or by fermentative production routes. Chemical synthesis is based on petrochemical feedstock because it involves the hydrolysis of lactonitrile, an intermediate formed by reacting acetaldehyde (originating from fossil derived ethylene) with hydrogen cyanide. This synthetic route has many limitations which include limited capacity and high manufacturing costs [6]. For these reasons it was prevalent until about 1990 when a more economic fermentation approach was developed [5]. Currently, over 90 % of the commercial production of lactic acid is performed *via* fermentation of sugars [1]. In Fig. 5.2 is represented a scheme of the fermentation process.

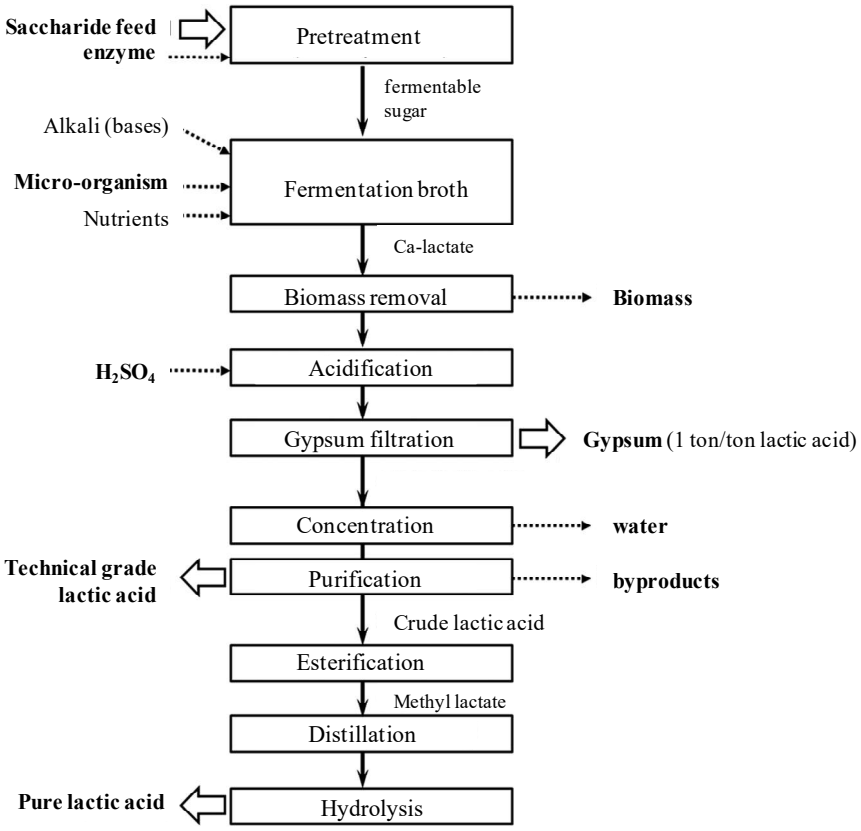

Figure 5.2. Block scheme of the fermentative production of lactic acid [1].

Lactic fermentation is relatively fast, has high yields and can lead, selectively, to one of the two stereoisomers of lactic acid or to their racemic mixture [2]. The main starting resources are glucose and sucrose derived from corn syrup, molasses, or starches [1]. The

fermentation is performed under anaerobic conditions using various *lactobacillus* strains [7]. The overall process is far from ideal, since it has some inherent disadvantages which add to the cost of lactic acid. The process typically requires 2-4 days to complete and is performed batch-wise. The bacterial strains do not survive in an acidic environment, so it is necessary to neutralize the lactic acid as it is formed by a stoichiometric amount of base (commonly calcium hydroxide). The subsequent step (Fig 5.2) is an acidification with sulphuric acid in order to have newly crude lactic acid. Approximately 1 ton of crude gypsum, $CaSO_4$, is produced and needs to be disposed as waste byproduct. Despite the recent progress, the separation, acidification, and purification steps have made large-scale production by this conventional route economically and ecologically unattractive [1,6].

5.1.3. An alternative synthetic way for lactic acid and alkyl lactate

Because of the difficulties of the lactic acid production by fermentation many researchers have focused on novel chemo-catalytic methods for directly converting sugars and other compounds into lactic acid and its esters [8,9].

A promising synthetic way starts from trioses, dihydroxyacetone and glyceraldehydes, which represent a convenient feedstock for this reaction. Indeed both trioses can be obtained by catalytic selective oxidation of one of the three alcoholic functions of glycerol [10]. The conversion of trioses can be performed in water or in alcohol. If it is carried out using an alcohol as a solvent it leads to the corresponding alkyl lactate, while lactic acid is obtained if water is the solvent. The one-pot formation of alkyl lactate using an alcohol as a solvent offers an important advantage over the lactic acid synthesis, since the purification of technical-grade lactic acid is always performed by esterification with methanol or ethanol followed by distillation of the alkyl ester and hydrolysis to release pure high-grade lactic acid [6].

Various mechanism have been proposed to explain the conversion of dihydroxyacetone and glyceraldehyde to alkyl lactates. The generally accepted reaction mechanism consists of two steps (shown in Fig. 5.3): a first dehydration step where a molecule of triose is converted into piruvaldehyde and a second step where water or alcohol nucleophilically attacks piruvaldehyde to give the hydrated form or the hemiacetal, that by a 1,2-hydride shift gives lactic acid or alkyl lactate. When the reaction is carried out in alcohol,

another molecule of alcohol can nucleophilically attack the intermediate hemiacetal, giving the piruvaldehyde alkyl acetal, which can further react with alcohol to form 1,1,2,2-tetraalkoxypropane [1,11,12].

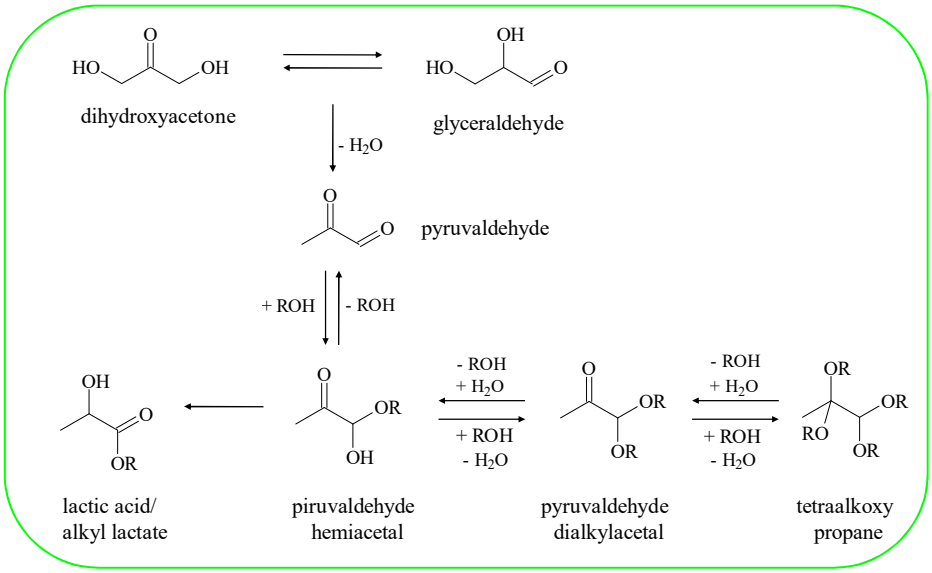

Figure 5.3. The mechanism of trioses conversion where R = H or alkyl. Pyruvaldehyde diacetal and tetraalkoxypropane can be produced only when R = Alkyl.

The lactic acid/methyl lactate synthesis from trioses is catalyzed by acidic catalysts. Among the homogeneous catalysts tested for alkyl lactate production, particular interest has been aroused by the tin compounds. Hayashi et al. [13] tested different tin halides showing fast and selective conversion of trioses to alkyl lactate while other salts had little or no activity in the reaction in alcoholic media.

The most active heterogeneous catalysts are materials with both Lewis and weak Brønsted acid sites [14,15]. The dehydration step is proposed to be catalyzed by the weak Brønsted acid sites while the Lewis acid sites would be active in the last step of the reaction from pyruvaldehyde into methyl lactate, assisting the final 1,2-hydride shift [14-18]. Among the zeolites, H-USY [16] has proved to be the best catalyst, leading to 75 mol% methyl lactate yield at the first hour of reaction at 115 °C. Other zeolites with lower Lewis acid sites concentrations have shown a low methyl lactate selectivity [17,18]. Another class of materials constituted by silicon-based materials containing tin have been tested in the conversion of

trioses to lactic acid or methyl lactate. Sn-MCM-41, Sn-Beta, Sn-montmorillonite, Sn-CSM [16-21] have proved to be excellent catalysts. It was shown that tin is active only when it is in the silica framework, tin dioxide and tin grafted to MCM-41 being not active [17,18,20].

5.2. Results and discussion

The conversion of dihydroxyacetone to methyl lactate was studied on three samples of MCM-22 zeolite catalysts either after thermal treatment of the catalyst or without any thermal treatment.

5.2.1. Structural and textural characterization of the catalysts

The ICP-AES results for all the samples gave total Si/Al molar ratio in agreement with the gel compositions, indicating the efficiency of the preparation procedures. The samples were denoted writing in brackets, next to the name of the catalysts, the corresponding Si/Al molar ratio as MCM-22(19), MCM-22(30), and MCM-22(46). The temperature of the thermal treatment were annotated at subscript of the sample name, also indicating if the thermal treatment was in vacuum. For example a sample treated at 500 °C in air is named MCM-22(x)$_{500}$ while, if the sample is treated at 500 °C under vacuum the name is MCM-22(x)$_{500V}$.

The XRD patterns of the samples are shown in Fig. 5.4. They can be identified as crystalline MCM-22 by comparison with the XRD pattern reported in the literature [13].

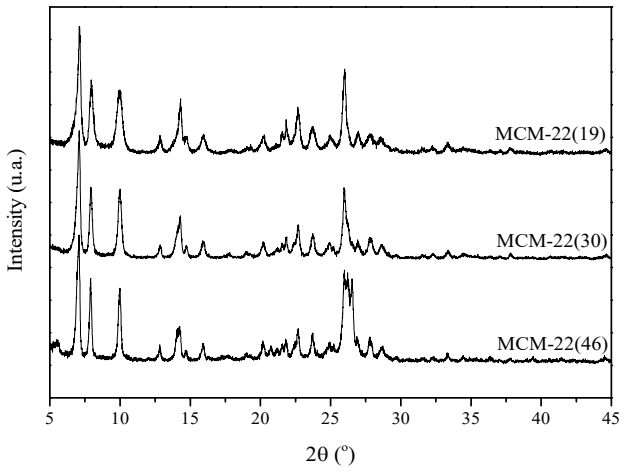

Figure 5.4. XRD patterns of the MCM-22 samples.

The nitrogen adsorption/desorption measurements were performed after evacuating the samples at 80, 250 or 400 °C. In Fig. 5.5 the results obtained on the samples evacuated at 250 °C are shown, no significant differences being observed after treatment at different temperatures. The features of the isotherms are typical of microporous materials, in which a sudden increase in the amount of nitrogen adsorbed is observed at very low p/p_0 values. At very high p/p_0 values a very narrow hysteresis loop can be observed, which is originated from the interstructural meso-macroporosity, associated with the aggregation of the particles.

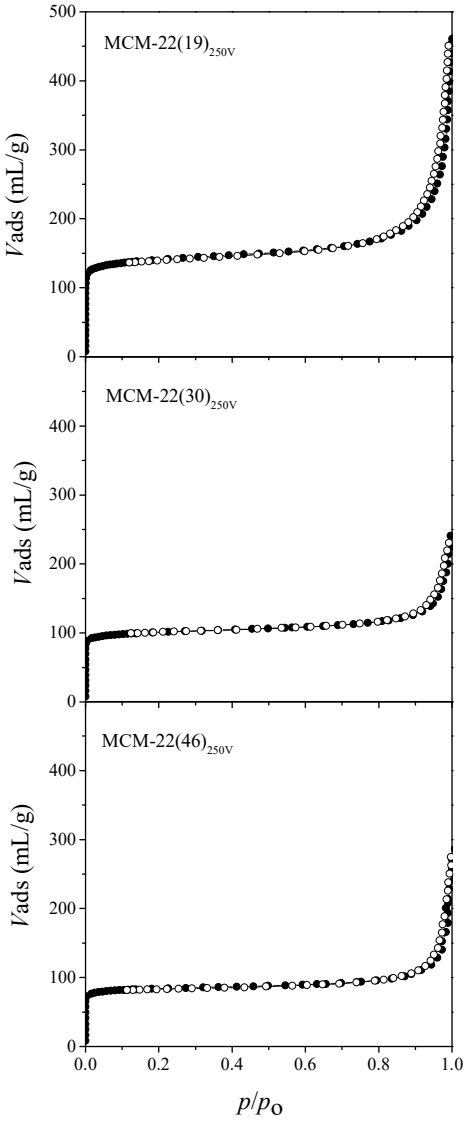

Figure 5.5. Nitrogen adsorption (full symbols) and desorption (open symbols) isotherms at -196 °C for the three samples evacuated at 250 °C.

The textural properties of the samples are summarized in table 5.1. Both the specific surface area and the microporous volume increase with the aluminium content.

Table 5.1. Textural properties of the samples treated at 250 °C under vacuum.

Sample	S_{DR} [a] (m^2/g)	V_{DR} [b] (mL/g)	D_{micro} [c] (nm)
MCM-22(19)$_{250V}$	592	0.21	0.50
MCM-22(30)$_{250V}$	429	0.15	0.54
MCM-22(46)$_{250V}$	357	0.13	0.53

[a]Specific surface area, determined by the Dubinin-Raduskevitch method.
[b]Total microporous volume, determined by the Dubinin-Raduskevitch method.
[c]Microporous diameter, determined by the Horvath-Kawazoe method.

5.2.2. Acid properties and influence of the thermal treatment

5.2.2.1. Adsorption microcalorimetry

Ammonia adsorption microcalorimetric experiments were carried out with the purpose of getting information on the acid sites strength and concentration of the samples treated at increasing temperatures. The microcalorimetric measurements were performed after heating the samples at 80 °C, 250 °C, and 400 °C under vacuum. The results are reported in Fig. 5.6 where the differential heat of adsorption, Q_{diff}, is plotted *versus* the ammonia uptake, n_A. The curves of the samples treated at 80 °C are not shown because they are practically identical to those of the samples treated at 250 °C, with the exception of a slightly lower ammonia adsorption due to a not completely cleaned surface at 80 °C. The curves of the samples treated at 250 °C are less steep, stop at not very low differential heat (about 65 kJ/mol), and conclude the adsorption with a plateau. This plateau, that defines a family of acid sites, ranges at about 65-75 kJ/mol of differential heat of adsorption. It disappears for the samples treated at 400 °C for which differential heat decreases until values lower than 50 kJ/mol. Such low values of Q_{diff} are so close to the liquefaction heat of ammonia (20 kJ/mol at 80 °C, calculated by the Watson relation [14]), that the corresponding ammonia uptake cannot be ascribed to interactions with surface sites; rather, it would be related to condensation-like phenomena occurring on the solid surface.

Fig. 5.6 also shows the negative inverse of the first derivative of the differential heat with respect of the amount adsorbed *vs.* the differential heat. It is used to emphasize the differences in the strength distribution of acid sites among the samples activated at 250 and 400 °C. For all the samples activated at 250 °C the derivative curve has a well defined peak centred at about 65 kJ/mol of differential heat that is a clear evidence of a numerous family of weak acid sites. The derivative curves shape of the samples activated at 400 °C do not show any intense peak, thus confirming that temperatures higher than 250 °C cause changes in the strength distribution of the acid sites and are not observed acid site families.

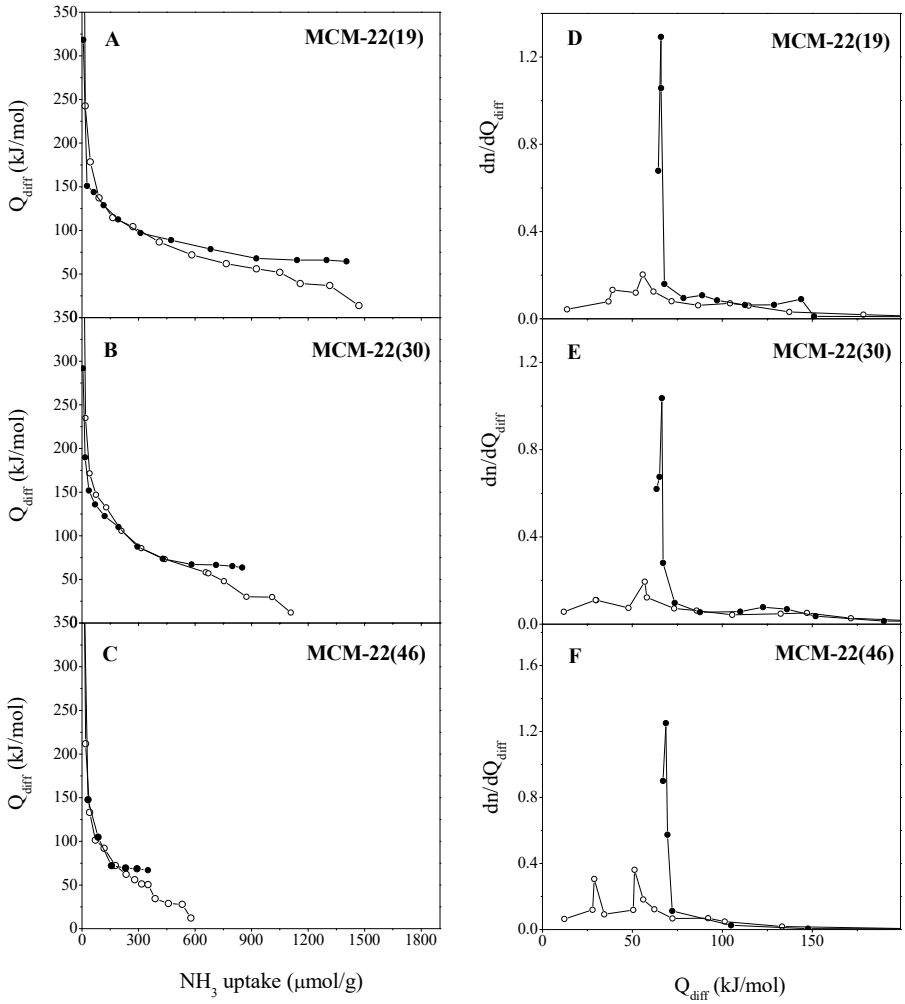

Figure 5.6. Calorimetric plots of the differential heat of adsorption (kJ/mol) *vs.* the ammonia uptake (μmol/g) (**A-C**); derivative curves represented as the negative inverse of the first derivative of the differential heat respect the amount adsorbed *vs*. the differential heat (kJ/mol) (**D-F**). The full symbols represent the samples thermal treated at 250 °C, while the open symbols represent the samples treated at 400 °C.

In Table 5.2 are summarized the calorimetric results for the samples thermally treated at 250 °C and 400 °C. The total acid sites concentration is determined taking the value of 65 kJ/mol as limit for the differential heat of adsorption between chemical and physical adsorption. The corresponding total acid sites concentration is higher for the samples treated at lower temperature. Above values of 75 kJ/mol (as shown in Fig. 5.6) the curves of Q_{diff} *versus* ammonia uptake for the samples thermal treated at 250 °C and 400 °C are almost identical. So the lower total acidity for the samples treated at 400 °C is mainly due to the disappearance of the weak acid sites to which correspond a Q_{diff} comprised between 65 and 75 kJ/mol.

Table 5.2. Acid sites distribution for the samples thermally-treated in vacuum at 250 °C and 400 °C.

Sample	Total acid sites (µmol/g)[a]	Weak acid sites (µmol/g)[b]	Weak acid sites %[c]
MCM-22(19)$_{400V}$	706	160	23
MCM-22(19)$_{250V}$	1215	455	37
MCM-22(30)$_{400V}$	558	138	25
MCM-22(30)$_{250V}$	802	387	48
MCM-22(46)$_{400V}$	219	49	22
MCM-22(46)$_{250V}$	350	200	57

[a]starting from $Q_{diff} \geq$ 65 kJ/mol; [b]corresponding to Q_{diff} = 65-75 kJ/mol; [c]calculated respect the total acid sites amount.

5.2.2.2. FTIR spectroscopy

The influence of the thermal treatment on the nature of the surface hydroxyl groups was investigated by FTIR spectroscopy. The measurements were carried out on all the samples after evacuation at different temperatures from 100 °C to 480 °C. In the following the results for the MCM-22 sample with Si/Al = 19 mol/mol are shown, those obtained on the

other samples being practically the same. In Fig. 5.7 are reported the FTIR spectra registered after evacuation of the MCM-22(19) sample in the ν(O–H) vibration region (3800-3000 cm^{-1}).

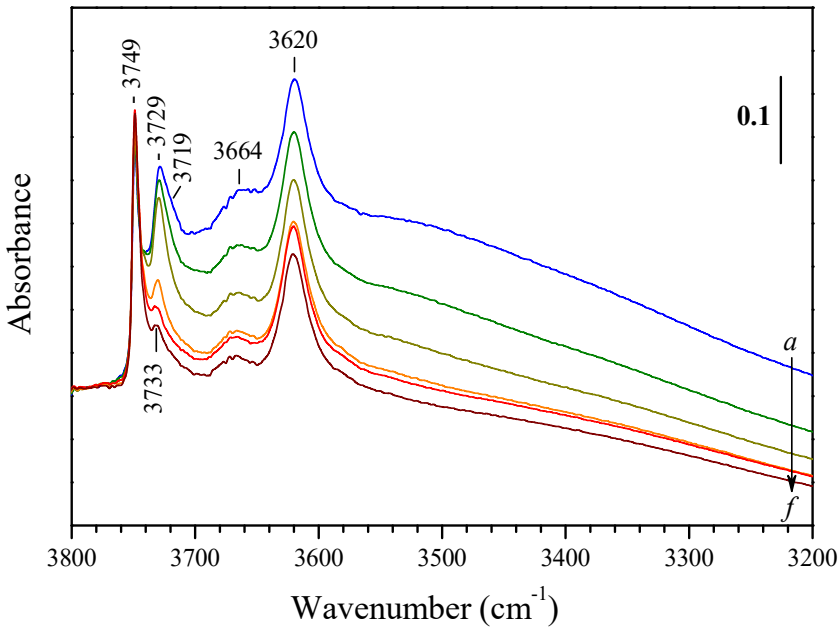

Figure 5.7. Background FTIR spectra of MCM-22(19) after evacuation at 100 (a), 200 (b), 300 (c), 400 (d), 450 (e) and 480 °C (f).

The spectrum of the sample evacuated at 100 °C (Fig. 5.7, spectrum a) displays a series of bands in the OH region with maxima at 3749, 3729, 3719 (shoulder), 3664 and 3620 cm^{-1}. A broad absorbance centred around 3550 cm^{-1} is also well distinguished. The band at 3749 cm^{-1} is attributed to isolated silanol groups. The lower frequency bands at 3664 and 3620 cm^{-1} are attributed to Al–OH and bridging hydroxyls, respectively. The broad absorbance around 3550 cm^{-1} is typical of H-bonded hydroxyls and most probably related to silanol nests. In the literature [15] it is reported that this band is usually accompanied by a higher frequency band (3720-3700 cm^{-1}) due to hydroxyls terminating the "non-perfect" nests. Therefore, the shoulder at 3719 cm^{-1} can be assigned to such silanol groups. Noteworhty, in this case the OH frequency is lowered as compared to free silanols due to involvement of the oxygen atom of the hydroxyl group in H-bonding. The band at 3729 cm^{-1} is rarely observed on zeolites but is quite typical of MCM-22 samples treated at low temperatures. However, there is no consensus on the assignment of this band. Cejka et al. [16]

attributed the band to perturbed Si–OH groups interacting with other hydroxyl groups. Onida et al. [17] hesitated between assignment to terminal Si–OH species located in framework defects or Al–OH species in Al_2O_3 particles. More recently Gil et al. [18] assigned the band to geminal silanols. The position of the band clearly indicates that the hydroxyls (if they are silanols) are involved in weak H-bonding.

After evacuation at 200 °C (Fig. 5.7, spectrum b) the band at 3729 cm^{-1} is slightly reduced in intensity and slightly blue-shifted to 3730 cm^{-1}, whereas the shoulder at 3719 cm^{-1} almost completely disappears. Simultaneously, the broad band at about 3550 cm^{-1}, representing H-bonded silanols, decreases in intensity.

With the further increase in the evacuation temperature to 300 °C (Fig. 5.7, spectrum c) these changes become more pronounced. Evacuation at 400 °C (Fig. 5.7, spectrum d) leads to an almost twofold decrease in intensity of the band at *ca.* 3730 cm^{-1}; simultaneously, its maximum continues to shift to higher wavenumbers. The broad absorbance at 3550 cm^{-1} almost disappears.

The last two spectra in Fig. 5.7 show the changes in the MCM-22(19) sample after increasing the evacuation temperature to 450 and 480 °C, respectively (Fig. 5.7, spectra e, f). The main change observed is the additional reduction in intensity of the 3730 cm^{-1} band (the maximum being at 3733 cm^{-1}).

Other FTIR measures carried out after leaving the MCM-22(19)$_{450V}$ and MCM-22(46)$_{450V}$ samples in 100 Pa water vapour showed that the disappearance of the silanols is not reversible even after more than 150 h in 100 Pa water vapour (these results are reported in Fig. 5.8 for the sample MCM-22(19)).

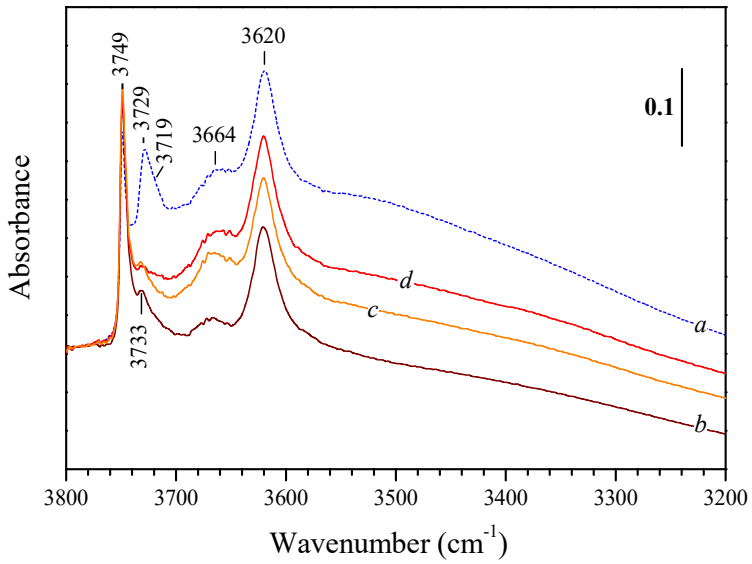

Figure 5.8. FTIR spectra of MCM-22(19) after evacuation of the sample at 100 (a) and 480 °C (b), and spectra of the sample MCM-22(19)$_{450V}$ after staying in 100 Pa water vapour for 18 h (c) and for 189 h (d), followed by evacuation at 100 °C.

5.2.2.3. CO adsorption FTIR

To get information on the Lewis and Brønsted acid sites of the MCM-22 samples, FTIR analysis was performed after adsorption of CO. The use of different probe molecules in microcalorimetry and FTIR spectroscopy is due to the different methods used for getting information on the acidity of the samples. While in microcalorimetry the quantitative information on the overall acidity needs a strong basic probe molecule such as ammonia, in FTIR spectroscopy the information on the nature and the strength of the surface acid sites is usually obtained by the so-called "H-bond method", in which a weakly basic probe molecule, such as CO, interacts very weakly with the surface active sites.

The adsorption FTIR experiments were carried out at -173 °C for two reasons:

- to get information on all the sites on the surface (CO is a weak base and at room temperature it can be adsorbed only on strong Lewis acid sites);
- to get information on the surface OH groups (at room temperatures CO cannot coordinate to surface OH groups).

In the following the results for the MCM-22 sample with Si/Al = 19 mol/mol are shown, those obtained on the other samples being practically the same.

Low-temperature (-173 °C) adsorption of CO (200 Pa equilibrium pressure) on the MCM-22(19) sample treated under vacuum at 100 °C leads to the appearance, in the CO region (2183-2045 cm^{-1}), of several bands with maxima at 2173, 2156, 2138 and 2092 cm^{-1} (Fig. 5.9A, spectrum a). A shoulder at 2166 cm^{-1} can also be distinguished. The weak band at 2092 cm^{-1} can be attributed to ^{13}CO satellite of this band arising from ^{13}C natural abundance. The band at 2138 cm^{-1} is unambiguously assigned to physically adsorbed CO. The band at 2156 cm^{-1} is related to CO adsorbed on silanols while the band at 2173 cm^{-1} is due to the CO adsorbed on bridging hydroxyls. The absence of bands at 2250-2200 cm^{-1} indicates the absence of c.u.s. cations, which are the Lewis acid sites.

The evacuation of the adsorbed CO is useful for understanding the strength of the adsorption. CO desorption (at -173 °C) results in a fast decrease of the band at 2138 cm^{-1} and a weaker decrease of all the other bands in the CO absorption region (Fig. 5.9A, spectra b-k).

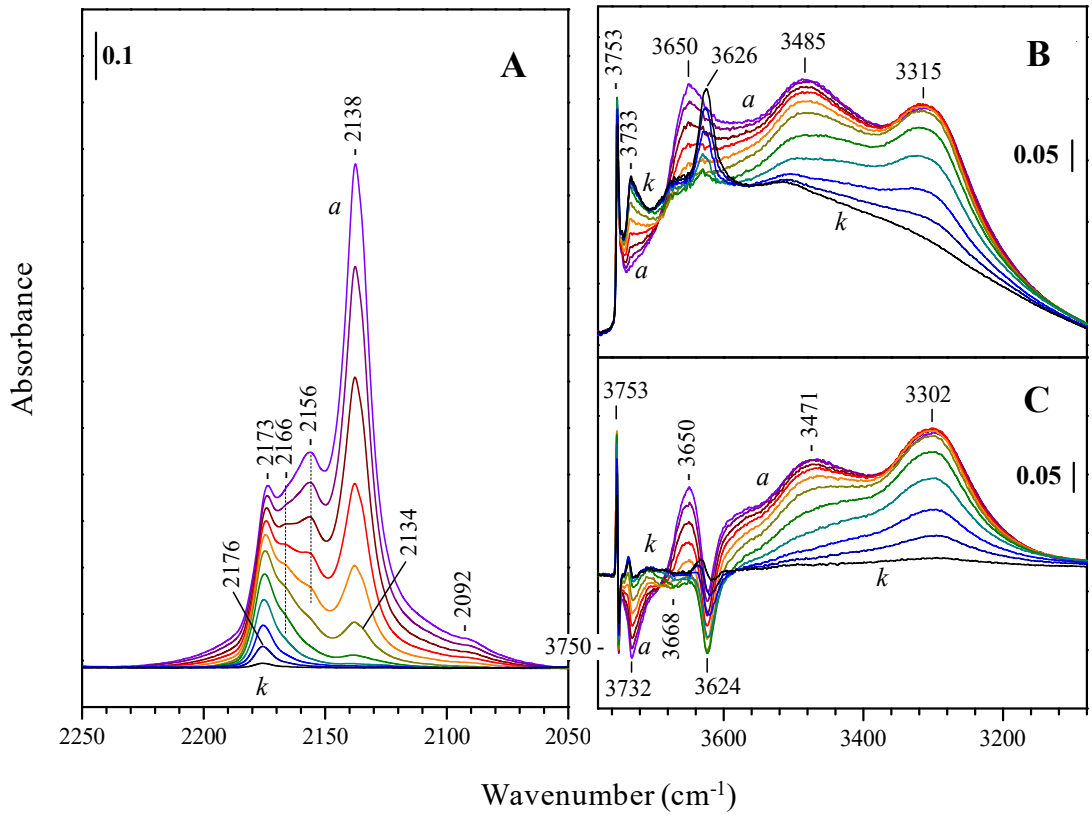

Figure 5.9. FTIR spectra of CO (200 Pa equilibrium pressure) adsorbed at -173 °C on MCM-22(19)$_{100V}$ (a) and evolution of the spectra during CO desorption at -173 °C (b-k). Spectra of the CO vibration modes region are reported in (**A**), while spectra of the OH region are reported in (**B**) and (**C**). Spectra in (**A**) and (**C**) are background and CO gas-phase corrected.

In Fig. 5.9B are reported the spectra of the CO in the OH region. These spectra are useful because, as a result of the interaction of the OH groups with CO, the O–H stretching modes undergo a red shift. The higher is the acidity of the OH group, the more pronounced is the shift. In principle, also the position of the carbonyl vibration (Fig. 5.9A) could be used for estimation of the acidity of the OH groups, but it is much less sensitive than the shift of the ν(OH) bands [19]. A way to simplify the spectrum and better display the changes due to the CO adsorption, is the use of difference spectroscopy, which permits to eliminate bands that have not been altered [20]. So, by subtraction of the background and CO gas-phase are obtained the spectra reported in Fig. 5.9C. Comparing these spectra with the spectra in Fig. 5.7, adsorption of CO results in the development of a series of negative (3750, 3732, 3668 and 3624 cm^{-1}) and positive (3753, 3650, 3471 and 3302 cm^{-1}) bands in the ν(OH) region (Fig. 5.9C, spectrum a). In Fig. 5.9C the band at 3650 cm^{-1} decreases in concert and the band at 3732 cm^{-1} is simultaneously restored. The band at 2156 in Fig. 5.9A can be assigned to CO polarized by the 3732 cm^{-1} silanol groups (Fig. 5.9B). The CO-induced shift of the OH modes, Δν(OH), is -82 cm^{-1} (3732 - 3650) which is similar to the shift reported for surface silanols. However, Δν(OH) of hydroxyls that have already been involved in weak H-bonding is not a real measure for their acidity. Therefore, if the stretching modes of isolated silanols are taken as reference values, the acidity would be higher (Δν(OH) = 103 cm^{-1}). In any case the acidity of these silanols is very weak. In the region of isolated silanols (Fig. 5.9C), a weak sharp and negative band at 3750 cm^{-1} and another positive band at 3753 cm^{-1} are detected. This band has often been observed and is most probably due to temperature effect (decrease of temperature as a result of increase in thermal conductivity in the presence of a gas in the cell). The band that in Fig. 5.7 is centred at 3664 cm^{-1}, undergoes a shift to 3485 cm^{-1} (Δν(OH) = 183 cm^{-1}). This is consistent with literature data on acidity of Al–OH groups in zeolites. The most stable carbonyl band with maximum at 2173 cm^{-1} (shifted to 2176 cm^{-1} at low coverages), in the Fig. 5.9A, is due to CO adsorbed on the bridging hydroxyls of the sample. In this case the shift of the 3624 cm^{-1} band is -309 cm^{-1}, indicating a strong acidity of the hydroxyls.

FTIR spectra were collected applying the same adsorption procedure on the MCM-22(19)$_{450V}$ sample. After low-temperature adsorption of CO (200 Pa equilibrium pressure), the already described bands at 2174 cm^{-1} (CO adsorbed on the bridging hydroxyls),

2167 cm^{-1} (CO coordinated to Al–OH groups), 2138 cm^{-1} with a shoulder at 2134 cm^{-1} (physically adsorbed CO) and 2092 cm^{-1} (^{13}CO from the ^{13}C natural abundance) were detected (Fig. 5.10A, spectrum a). The behaviour of all these bands as a result of the CO desorption at -173 °C (Fig. 5.10A, spectra b-h) was similar to that observed for the sample evacuated at 100 °C. No significant difference was noticed in the OH region as well (Fig. 5.10B and C). The main difference, as compared with the evacuation at 100 °C, is that the band at 2156 cm^{-1} that arouses from CO adsorbed on H-bonded silanols cannot be resolved. This is easy explicable because the fraction of these hydroxyls is strongly reduced after increase of the evacuation temperature to 450 °C.

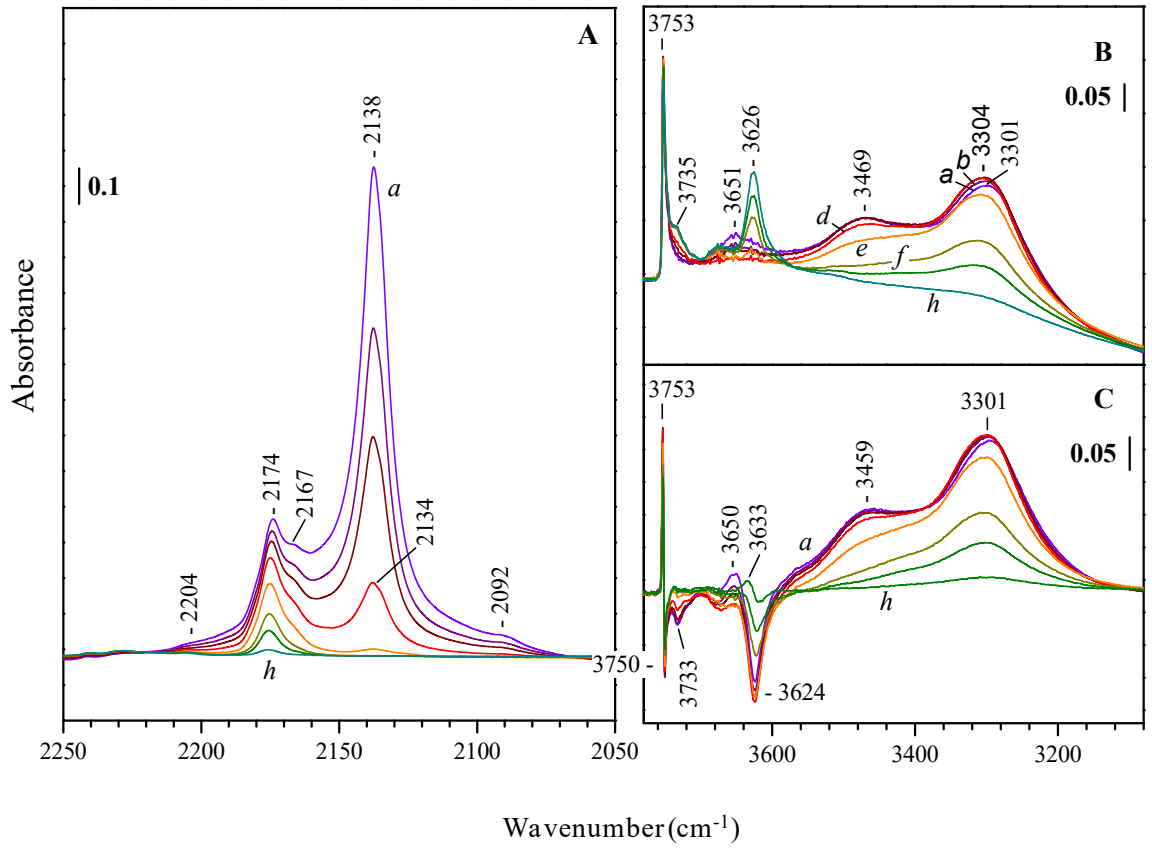

Figure 5.10. FTIR spectra of CO (200 Pa equilibrium pressure) adsorbed at -173 °C on MCM-22(19)$_{450V}$ (a) and evolution of the spectra during CO desorption at -173 °C (b-h). Spectra of the CO vibration modes region are reported in (**A**), while spectra of the OH region are reported in (**B**) and (**C**). Spectra in (**A**) and (**C**) are background and CO gas-phase corrected.

The results of FTIR and CO adsorption FTIR indicate the destruction of H-bonded silanols with the increase of the temperature. H-bonded hydroxyls are often detected (although not always discussed) in various types of zeolites and are related to defects usually due to the extraction of a T atom (T = Al or Si) [21]. This disappearance of the H-bonded hydroxyls band with the increasing of the evacuation temperature, could be related to the well known [15,22] dehydroxylation process, in which the hydrogen-bonded hydroxyls disappear through elimination of water and formation of Si–O–Si bridges. The temperature at which the H-bonded silanols band (3730 cm^{-1} in Fig. 5.7) decreases very sharply in intensity is 400 °C evacuation, meaning that temperatures higher than 300 °C constitute the limit temperatures for the H-bonded sylanols. Combining FTIR, CO adsorption FTIR and NH_3 adsorption microcalorimetric results, the family of weak acid sites, with Q_{diff} in the range 65-75 kJ/mol, should correspond to the H-bonded silanols that disappear in the FTIR spectra of the sample treated at temperatures higher than 300 °C (Fig. 5.7, band at 3729-3733 cm^{-1}).

5.2.3 Catalysis

Each sample was tested either without any preliminary thermal treatment or after a thermal treatment at 500 °C for 12 h in air. In Fig. 5.11 the evolution with time of the %yields to the three main products - methyl lactate, pyruvaldehyde dimethyl acetal, and tetramethoxypropane - is reported. Other products (such as pyruvaldehyde, pyruvaldehyde hemiacetal) are present only in traces.

The methyl lactate yield during the first two hours increases very fast, slowing down until the 24th hour. The trend is different for the pyruvaldehyde dimethylacetal where a value is reached after the first hours and remains approximately constant. The tetramethoxypropane yield reaches a maximum within the first three hours and decreases until almost zero after six hours. The trend is in agreement with the proposed mechanism shown in Fig. 5.3, where the formation of pyruvaldehyde dimethylacetal and tetramethoxypropane is reversible.

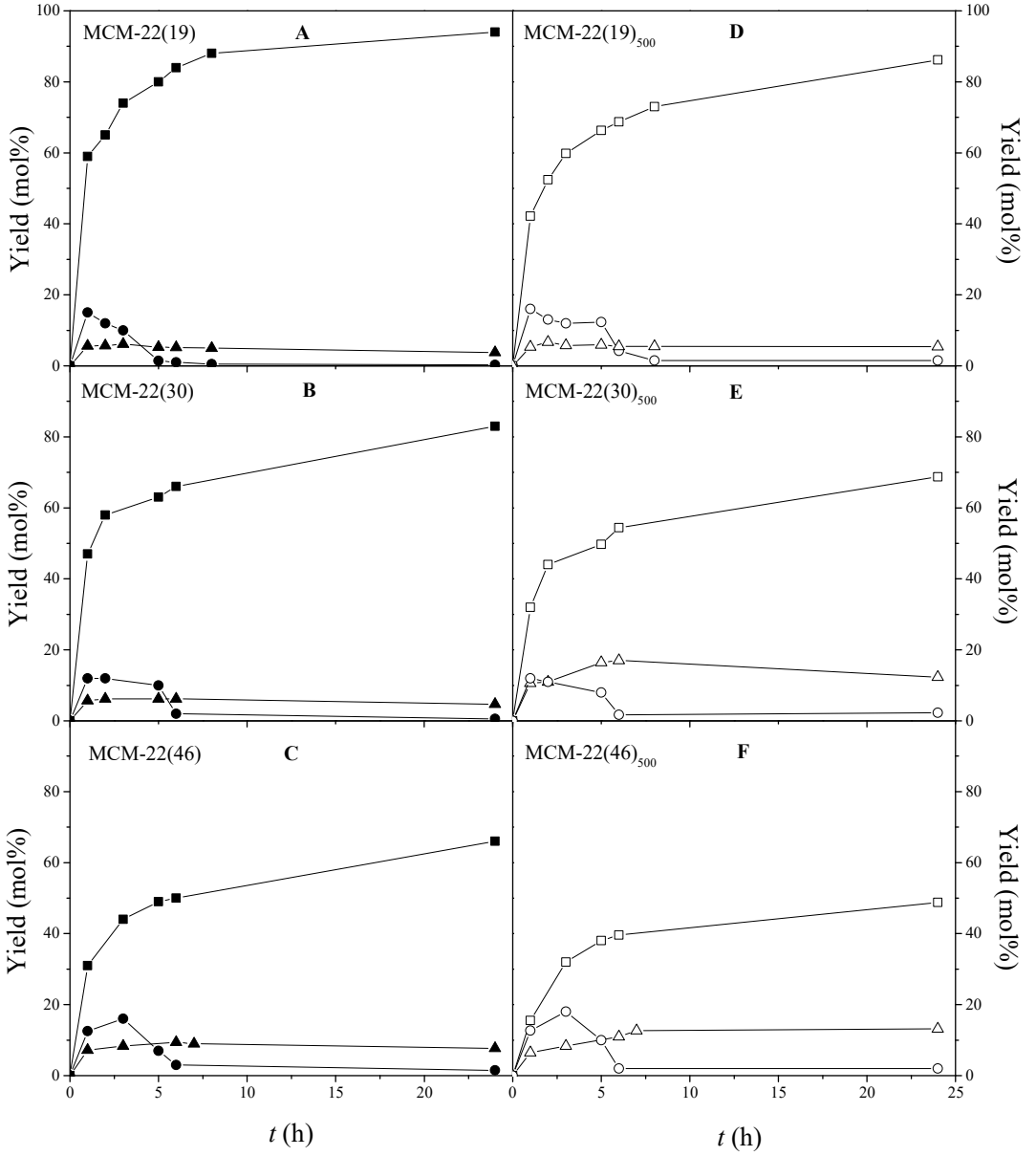

Figure 5.11. Methyl lactate yields (square), tetramethoxypropane yields (circle) and pyruvaldehyde dimethylacetal yields (triangle) *versus* reaction time. The catalytic results of the samples without any preliminary thermal treatment are shown in (**A-C**). The catalytic results of the samples thermal treated are reported in (**D-F**).

In Fig. 5.11 is possible to note that for the two series of samples (thermally treated and untreated) the increase in the conversion is mainly due to the increase in the methyl lactate yield rather than in the other products. The samples with lower Si/Al are more selective to

methyl lactate. This can be well visible in Table 5.3 where are summarized the conversions and the methyl lactate yields at the first hour of the reaction time.

Table 5.3. Conversions and yields at the first hour for all the samples.

Sample	Conversion (mol%)[a]	Yield (mol%)[b]
MCM-22(19)$_{500}$	64	42
MCM-22(19)	80	58
MCM-22(30)$_{500}$	55	32
MCM-22(30)	65	47
MCM-22(46)$_{500}$	34	15
MCM-22(46)	50	31

[a]calculated as sum of the main products yields;

5.2.3.1. Influence of the acid properties

The samples with the highest total acid sites concentration are the most effective samples as can be observed by comparing the microcalorimetric results reported in Table 5.2 with the catalytic results shown in Fig. 5.11. So apparently all the acid sites play an important role in the conversion of dihydroxyacetone to methyl lactate.

The initial FAMEs yields were plotted both *versus* the population of weak sites with Q_{diff} = 65-75 kJ/mol and *versus* the total concentration of acid sites in Fig. 5.12. There is not a very good linearity but can be observed a trend. The slope of the fitting line for the plot of the initial methyl lactate yield versus the weak acid sites concentration is three times higher than that for the total acid sites concentration. This result means that weak acid sites (mainly silanols) play a more important role in the formation of methyl lactate than all the other acid sites of the sample.

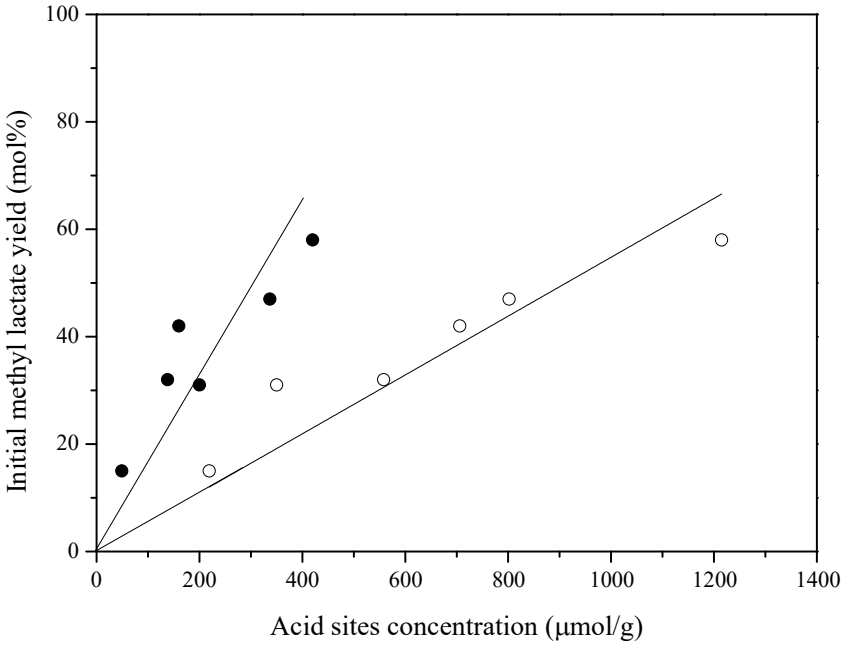

Fig. 5.12. Initial methyl lactate yield (mol%) *versus* total acid sites concentration (open circles) and weak acid sites concentration (full circles) (μmol/g).

In literature is supposed that a combination of Lewis and mild Brønsted acid sites is necessary for an effective catalyst in the conversion of trioses to alkyl lactate [1,8,10,23]. Mild Brønsted acidity is considered helpful in catalyzing the dehydration of dihydroxyacetone to pyruvaldehyde (Fig. 5.3), while Lewis acidity is required to efficiently convert the pyruvaldehyde to alkyl lactate (Fig. 5.3). The formation of dialkyl acetal is supposed to be catalyzed by strong Brønsted acid sites [1].

The CO adsorption FTIR measurements have shown that the acidic MCM-22 samples have not Lewis acid sites. Despite the presence of only Brønsted acidity (also strong) the thermally untreated MCM-22(19), the most effective catalyst, has catalytic performances similar or only slightly lower than those of the best samples in literature [1,8,10,11,23,24].

5.3. Conclusions

Three acidic MCM-22 samples with Si/Al molar ratios of 19, 30 and 46 have been successfully synthesized. The acidity of these samples has been investigated after having thermally treated the samples at various temperatures. The investigation through ammonia adsorption microcalorimetry has shown that the total acidity of the samples decreased after

the samples were thermally treated at 400 °C. The decrease in acidity was mainly due to the disappearance of a well defined family of weak acid sites (with an acid strength expressed in terms of differential heat of adsorption of 65-75 kJ/mol). The nature of these acid sites was investigated by FTIR and carbon monoxide FTIR spectroscopy. It has been found that these sites are H-bonded silanol, which may be irreversibly disappeared through dehydroxylation forming water and Si–O–Si bridges. The role of these sites was investigated in the conversion of dihydroxyacetone to methyl lactate, an important alternative reaction for the methyl lactate. It has been observed that the thermally untreated samples were the best catalysts, giving higher conversions than that of the thermally treated samples, mainly due to the higher yields in methyl lactate. The key role played by silanols in the reaction has been highlighted comparing the influence of these weak acid sites on the methyl lactate yield at the first hours with that of the total acid sites concentration. The importance of these weak Brønsted acid sites in the conversion of trioses to methyl lactate was already supposed in the literature, but in combination with Lewis acid sites, that in these MCM-22 samples are not present as shown by CO adsorption FTIR spectroscopy. Despite this the most active sample has catalytic performances similar to the best samples in the literature [1,8,10,11,23,24].

References

[1] M. Dusselier, P. Van Wouwe, A. Dewaele, E. Makshina, B.F. Sels, *Energy Environ. Sci*. 6 (2013) 1415.

[2] F.A. Castillo Martinez, E.M. Balciunas, J.M. Salgado, J.M. Domínguez González, A. Converti, R.P.D.S. Oliveira, *Trends Food Sci. Technol*. 30 (2013) 70.

[3] C. Miller, A. Fosmer, B. Rush, T. Mcmullin, D. Beacom, P. Suominen, Industrial *Production of Lactic Acid, Comprehensive Biotechnology*, Second Edition, Elsevier, (Amsterdam), 2011.

[4] C.S.M. Pereira, V.M.T.M. Silva, A.E. Rodrigues, *Green Chem.* 13 (2011) 2658.

[5] B. Gupta, N. Revagade, J. Hilborn, *Prog. Polym. Sci.* 32 (2007) 455.

[6] R. Datta, M. Henry, *J. Chem. Technol. Biotechnol*. 81 (2006) 1119.

[7] M.A. Abdel-Rahman, Y. Tashiro, K. Sonomoto, *Biotechnol. Adv.* 31 (2013) 877.

[8] F. De Clippel, M. Dusselier, R. Van Rompaey, P. Vanelderen, J. Dijkmans, E. Makshina, L. Giebeler, S. Oswald, G. V. Baron, J.F.M. Denayer, P.P. Pescarmona, P. A. Jacobs, B.F. Sels, *J. Am. Chem. Soc*. 134 (2012) 10089.

[9] M.S. Holm, S. Saravanamurugan, E. Taarning, *Science* 328 (2010) 602.

[10] L. Li, C. Stroobants, K. Lin, P. A. Jacobs, B.F. Sels, P.P. Pescarmona, *Green Chem*. 13 (2011) 1175.

[11] E. Taarning, S. Saravanamurugan, M.S. Holm, J. Xiong, R.M. West, C.H. Christensen, *ChemSusChem* 2 (2009) 625.

[12] J. Wang, Y. Masui, M. Onaka, *Appl. Catal. B Environ*. 107 (2011) 135.

[13] D. Meloni, R. Monaci, E. Rombi, C. Guimon, H. Martinez, I. Fechete, E. Dumitriu, *Stud. Surf. Sci. Catal*. 142 (2002) 167.

[14] B.E. Poling, J.M. Prausnitz, J.P. O'Connel, *The Properties of Gases and Liquids*, Third Edition, McGraw-Hil, (New York), 1977.

[15] S. Bordiga, P. Ugliengo, a Damin, C. Lamberti, G. Spoto, A. Zecchina, G. Spanò, R. Buzzoni, L. Dalloro, F. Rivetti, *Top. Catal*. 15 (2001) 43.

[16] J. Cejka, A. Krejčí, N. Ilková, J. Kotrla, S. Ernst, A. Weber, *Micropor. Mesopor. Mater.* 53 (2002) 121.

[17] B. Onida, F. Geobaldo, F. Testa, F. Crea, E. Garrone, *Micropor. Mesopor. Mater*. 30 (1999) 119.

[18] B. Gil, B. Marszałek, A. Micek-Ilnicka, Z. Olejniczak, *Top. Catal*. 53 (2010) 1340.

[19] K.I. Hadjiivanov, G.N. Vayssilov, *Adv. Catal.* 47 (2002) 307.

[20] J. Grdadolnik, *Vib. Spectrosc*. 31 (2003) 279.

[21] K. Hadjiivanov, *Adv. Catal.* 57 (2014) 99.

[22] D.W. Fickel, A.M. Shough, D.J. Doren, R.F. Lobo, *Micropor. Mesopor. Mater*. 129 (2010) 156.

[23] L. Li, X. Collard, A. Bertrand, B.F. Sels, P.P. Pescarmona, C. Aprile, *J. Catal.* 314 (2014) 56.

[24] R.M. West, M.S. Holm, S. Saravanamurugan, J. Xiong, Z. Beversdorf, E. Taarning, C.H. Christensen, *J. Catal*. 269 (2010) 122.